ACOUSTIC EMISSION
INVESTIGATION OF MARINE
CORROSION-INDUCED AND
EXTERNAL LOAD-INDUCED
CRACKING OF CONCRETE

R. N. SAILAPPAN

ACOUSTIC EMISSION INVESTIGATION OF MARINE CORROSION- INDUCED AND EXTERNAL LOAD-INDUCED CRACKING OF CONCRETE

BY

R. N. SAILAPPAN

A Thesis Submitted to the Faculty of the

College of Engineering

in Partial Fulfillment of the Requirements for the Degree of

Master of Science in Engineering

Florida Atlantic University

Boca Raton, Florida

April, 1991

ACOUSTIC EMISSION INVESTIGATION OF MARINE CORROSION-INDUCED AND EXTERNAL LOAD-INDUCED CRACKING OF CONCRETE
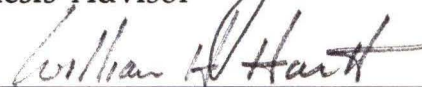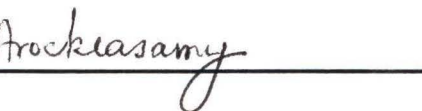
by

R. N. SAILAPPAN

This thesis was prepared under the direction of the candidate's thesis advisor, Dr. D. V. Reddy, Department of Ocean Engineering. It was submitted to the faculty of the college of engineering and was accepted in partial fulfillment of the requirement for the degree of Master of Science in Engineering.

SUPERVISORY COMMITTEE
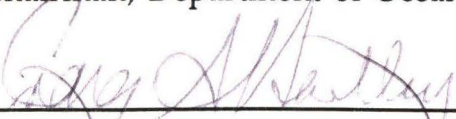
D. V. Reddy
Thesis Advisor

William H. Hart

Mrockeasamy
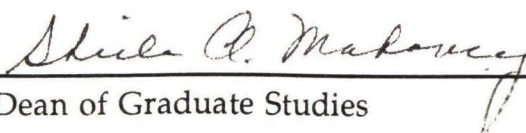
_____
Chairman, Department of Ocean Engineering

_____
Dean, College of Engineering

Shila A. Mahoney   4/8/91
Dean of Graduate Studies   Date

ii

ACKNOWLEDGEMENT

DEDICATED TO

My Parents

ABSTRACT

AUTHOR:	R.N.Sailappan
TITLE:	Acoustic Emission Investigation of Marine Corrosion-Induced and External Load-Induced Cracking of Concrete.
INSTITUTION:	Florida Atlantic University
THESIS ADVISOR:	Dr. D. V. Reddy
DEGREE:	M.S.
YEAR:	1991

The acoustic emission investigations reported herein are divided into two experimental sets. In the first, the concrete specimens were stressed internally, and the resulting acoustic emissions were monitored. In the second, specimens were subjected to fracture mechanics tests and simultaneously studied for AE signals. For both sets, two kinds of concrete were studied - regular concrete and concrete containing fly ash. The specimens were stressed internally by subjecting them to an accelerated state of corrosion in a marine environment. The corroded specimens were then tested for impact and flexural strengths to study the effect of fly ash replacement on rebar corrosion in a marine environment, and to ascertain any correlation between the monitored AE signals and residual strength. Furthermore, an attempt was made to predict the remaining life of the specimens. For the externally stressed specimens, AE was used to determine the load at initiation of unstable crack propagation terms of ultimate load. These tests have immediate and relevant applications to field problems.

TABLE OF CONTENTS

LIST OF TABLES

LIST OF FIGURES

xi

Current practices in the concrete industry use U.S. customary units. Hence, U.S. customary units have been used in this thesis as well. However, to facilitate readers familiar with the SI units, a conversion table has been given below.

Conversion factors—U.S. customary to SI

To convert from	To	Multiply by
in	m	*0.025 400*
ft	m	0.304 800
in^2	mm^2	645.160 000
ft^2	m^2	0.092 903
in^3	m^3	$16.387\,064 \times 10^{-6}$
ft^3	m^3	*$28.316\,847 \times 10^{-3}$*
quart (U.S. liquid)	liter (1000 mm^3)	0.946 353
gallon (U.S. liquid)	m^3	$3.785\,412 \times 10^{-3}$
in^4	cm^4	41.623 143
cm^4	m^4	$1.000\,000 \times 10^{-8}$
ft^4	m^4	$8.630\,975 \times 10^{-3}$
gram	dyne	980.665 000
kg (force or mass)	N	*9.806 650*
lb (mass)	kg (mass)	0.453 592
kips (1000 lbs)	kN	*4.448 222*
kip/ft	kN/m	14.593 898
lb/ft	kg/m	1.488 164
kg/m^2	N/m^2 (pascal)	9.806 650
kg/cm^2	kN/m^2 (kPa)	98.066 500
kip/ft^2	kN/m^2	*47.880 260*
lb/in^2 (psi)	kN/m^2	6.894 757
lb · in (torque)	N · m	0.112 985
lb · ft	N · m	1.355 818
kip · ft	kN · m	*1.355 818*
lb · ft (energy of work)	joule	1.355 818
cal · g (International value)	joule	4.186 800
lb/ft^3	kg/m^3	16.018 460
kip/ft^3	kN/m^3	*157.087 477*
g/cm^3	lb/ft^3	62.427 900
g/cm^3	kN/m^3	9.806 650

Chapter 1

INTRODUCTION

In recent years there has been an accelerating interest in the development of new and improved methods of assessing the integrity of structures. Current field practices are largely based on visual inspection. This is viable only when the crack erupts at the surface. By then, most of the damage has already been done. Hence, there is a growing emphasis on 'Non-Destructive Evaluation' (NDE) at an early stage. One of the many NDE techniques for early detection is acoustic measurement. In acoustic measurement there are two (2) principal modes of testing:

i) Ultrasonic waves are passed into the subject structure. The reflected/ refracted waves are studied in conjunction with the transmission time to give an idea of the flaws, their location and size.

ii) When cracks occur, the noise emitted by the structure is picked up by sensitive transducers and the data analyzed to obtain the flaw parameters.

The latter, called 'Acoustic Emission Monitoring' (AE) is one of the fastest developing non-destructive evaluation tools. This is a relatively new technique with tremendous potential that enables one to not only detect crack initiation but also crack growth and thereby provides the rare opportunity of being employed as an on-line monitoring system. The mechanics of AE and its evaluation modes will be discussed in detail in the next chapter.

1

1.1 OBJECTIVES

This study forms part of a Sea Grant Project 'Strength and Durability of Fly Ash Modified Concrete in Coastal Construction' (Grant # R/C-D-15). This study is a continuation of two earlier Sea Grants. The objectives were:

i) To assess the improvement in the resistance of fly ash modified concrete in the marine environment by acoustic emission monitoring of accelerated corrosion-induced cracking of seawater-submerged specimens.

ii) To determine the structural integrity of seawater-exposed fly ash modified concrete in terms of flexural strength, impact and fracture.

1.2 BACKGROUND

Fly ash or Pulverized Fuel Ash (PFA) is a by-product generated at thermal power plants where coal is burnt as fuel. It is composed of mainly silica, alumina and iron, and is one of the best artificial pozzolans. The ACI (Committee 226 - 1987) defines a pozzolan as a siliceous or siliceous and aluminous material, which in itself possesses little or no cementitious properties but, in finely divided form and in the presense of moisture, chemically reacts with calcium hydroxide at ordinary temperatures to form compounds possessing cementitious properties. Examples of pozzolans are volcanic ash, pumicite, burnt clay and fly ash.

Fly ash has many beneficial effects like improved strength and durability, water tightness, workability and pumpability, acid and sulphate resistance besides reducing bleeding, heat of hydration, creep deformation and drying shrinkage. More importantly, fly ash also has corrosion-inhibiting properties, since it reduces pore water besides decreasing the permeability of

the system, which makes it of special relevance to construction in marine environments. Not only does fly ash contribute to the economy by reducing the cement requirement but is also environment friendly in the sense that it makes use of a combustion waste product. An amazing sidelight is that in 1983, while approximately 52 million tons of flyash were produced in the U.S., only 3.6 million tons were utilized in the concrete industry! This gives one an idea of the large amount of readily avilable, cost saving, cheap, additive available to the industry but is currently going waste.

1.3 CONCRETE CORROSION

Concrete normally provides reinforcing steel with excellent corrosion protection since the high alkaline environment in concrete results in the formation of a tightly adhering film which passivates the steel thereby protecting it from corrosion. However, the corrosion of steel in concrete has received increasing attention in recent years due to its widespread occurence in certain types of structures and the high cost of repairs. The corrosion of steel reinforcement has mainly been observed in marine structures, chemical manufacturing plants, bridge decks, parking structures and quays. Chloride ions are considered to be the major cause of premature corrosion of steel reinforcement. Corrosion can also be caused by the carbonation of concrete resulting in the reduction of alkalinity thereby permitting corrosion of embedded steel.

The rate of corrosion of steel reinforcement in concrete is strongly influenced by environmental factors. Both oxygen and moisture must be present if electrochemical corrosion is to occur. Reinforced concrete with significant gradients in chloride ion content is vulnerable to macrocell

corrosion, especially if subjected to cycles of wetting and drying. Other factors which affect the rate and level of corrosion are heterogenities in the concrete and the steel, pH of the concrete pore water, carbonation of the cement paste, cracks in concrete, stray currents and galvanic effects due to contact between dissimilar metals.

Rebar corrosion in turn causes structural distress to occur either by loss of bond between the steel and concrete due to cracking and spalling or as a result of reduced steel cross-sectional area. This latter effect can be of special concern in structures containing high strength prestressing steel in which a small amount of metal loss could possibly induce tendon failure.

1.4 FRACTURE MECHANISM

The first experimental study of fracture mechanics in concrete was made by Kaplan (1983), who carried out bending tests using single-edge notched beams made of mortar and concrete, and calculated the critical strain energy release rate, G_c. In view of its heterogenous composition with inclusions, concrete has numerous microcracks in high stress zones, and consequently a fracture process zone (strain softening zone or plastic deformation zone) develops continuously until fracture occurs. This is important because LEFM (Linear Elastic Fracture Mechanics) parameters, obtained experimentally, are valid only if the fracture process zone is small compared to the specimen size. Studies show that while G_c is a function of notch depth and specimen volume, the fracture toughness, K_{IC}, is independent of the above parameters. There are some difficulties in performing stable fracture mechanics tests in concrete due to a) small deformations at rupture of concrete and b) extreme stiffness of concrete

specimens. However, reducing the notch angle greatly enhances the test stability.

1.5 LIFE PREDICTION

One of the fundamental assumptions is that damage in a specimen is cumulative and that a totally damaged specimen has zero strength left and hence its damage is one hundred percent. In other words, complete damage can be quantified as an unity. Therefore, no specimen can have a damage greater than 1. This concept was first put forward by Palmgren and Miner (Miner, 1945).

Based on strength tests of virgin beams and beams subjected to varying periods of accelerated corrosion, the complete loss in strength (damage = 1) of the beams can be predicted. Logarithmic extrapolation improves the accuracy.

Note: In this thesis the 'Principles of Acoustic Emission' are explained in chapter 2, before the 'Literature Survey' (chapter 3), in order to familiarize the reader with AE terminology.

Chapter 2

PRINCIPLES OF ACOUSTIC EMISSION

Acoustic emission is the characteristic and irreversible sound emitted by a material when it is deformed. In other words, when a solid is subjected to either mechanical or thermal stress at a sufficiently high level, sound is generated in the material and emitted in the form of an elastic wave. Almost all materials produce AE when they are stressed to failure. There are two kinds of acoustic emission - Continuous and Burst type. Continuous emission can be thought of as an inertial emission and does not relate to a stress-induced change in the physical structure of the specimen. Hence, while monitoring AE it is imperative to eliminate the continuous emission. Fortunately, it is a low energy emission and can be eliminated from the data acquisition system, along with other unwanted filter noises by setting an appropriate threshold.

The first practical use of AE occurred in about 6500 B. C. as pottery makers listened for the cracking sounds made by clay pots that had been allowed to cool too quickly. By experience the potters learned that cracked pots were structurally defective and would fail prematurely. However, the father of modern AE testing was Josef Kaiser of Germany. In 1950, Kaiser published his Ph. D. thesis, which was the first comprehensive investigation of AE. He made two important discoveries. The first was that materials emit minute pulses of energy when stressed. The second discovery was that once a given load is applied and the AE due to that load ceases, no further emission

would occur until the previous stress level is exceeded, even if the load is removed and later reapplied. In other words, AE activity is irreversible, ie., acoustic emissions are not generated until the stress level exceeds the previous high. This irreversible phenemenon has since become known as the 'Kaiser Effect' and can be time dependent for materials with elastic aging. This principle is used in present day AE proof testing of fiberglass and metallic pressure vessels.

Burst type emission can be mathematically described as a decaying sinusoid. AE sources, emitting elastic waves can be distinctly classified into four groups:

i) Dislocation movements

ii) Phase transformations

iii) Friction mechanisms

iv) Crack formation and extension

2.1 AE SIGNAL PARAMETERS

Fig. 2.1 shows a typical AE wave form and its characteristics. A single burst type emission wave form is called an AE event. An event consists of one to several counts. These counts, also called ringdown counts, can be detected by a transducer attached to the stressed structures. A typical AE signal has a short rise time and a long decay period. Data acquisition (DA) systems can also monitor the peak amplitude of the emission. The number of monitored counts is the number of times the signal crosses the set threshold, and is an indication of the magnitude of the emission. DA systems can also determine event duration, and with a multiple transducer
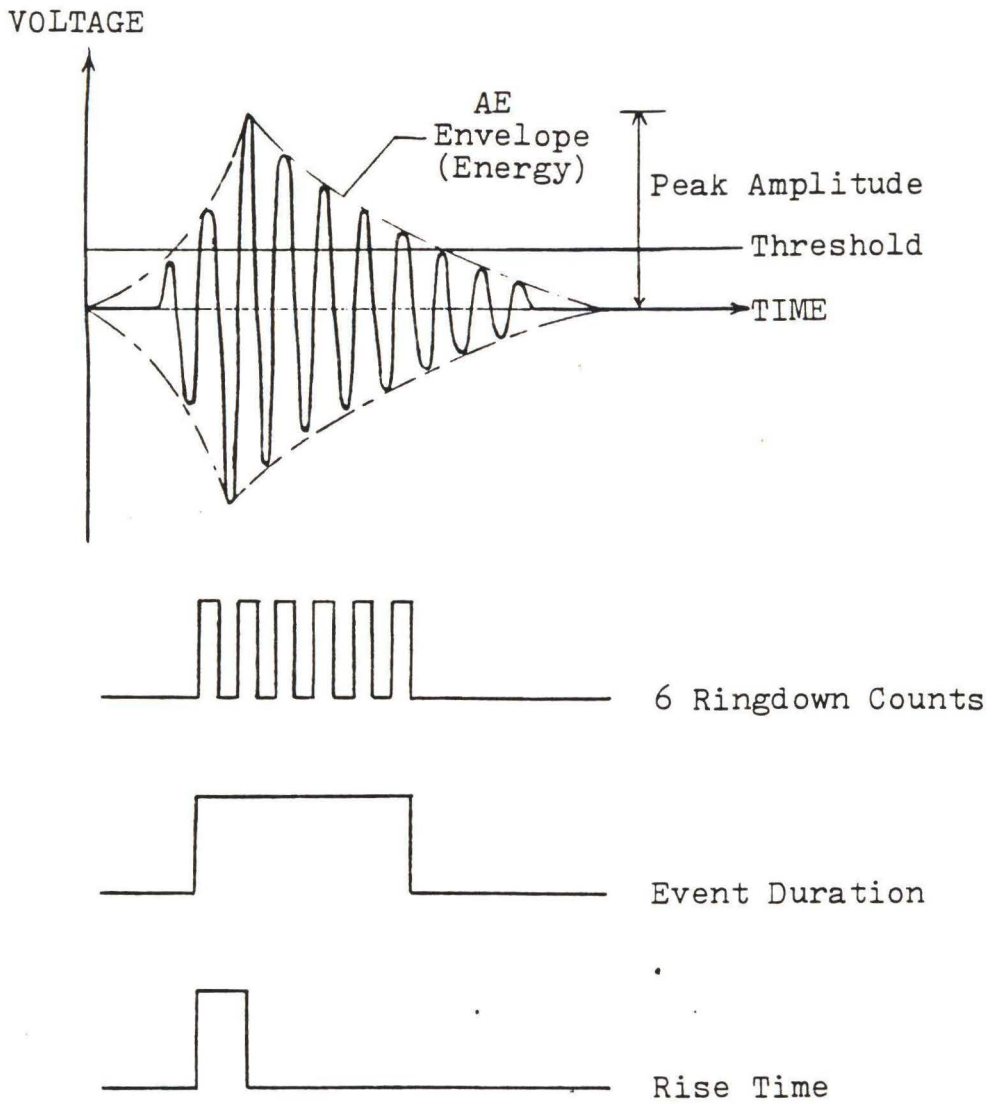
Fig. 2.1   Typical AE waveform and its characteristics.

8

arrangement, the difference in arrival times of the signal. The latter is used for source location. Fig. 2.2 gives the schematic of an AE monitoring setup.
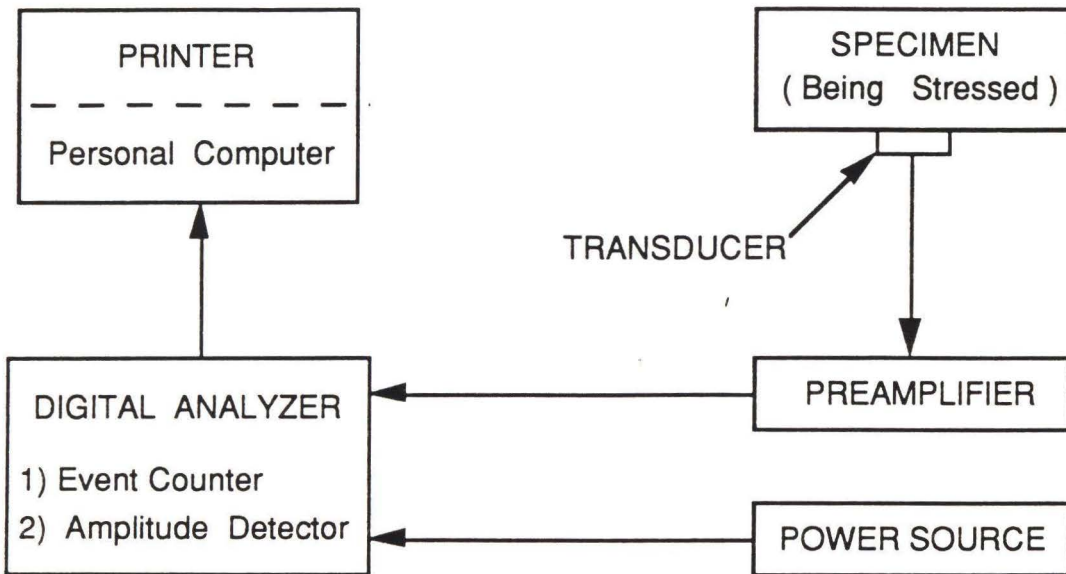
Fig. 2.2 - Schematic of an AE monitoring setup.

2.1.1 Ringdown Counts

Ringdown counting is the number of times the signal crosses a preset threshold level in a given event. For any given emission, the number of counts is a function of the threshold level 'v'. The number of counts per event and cumulatively over a period of time, as will be shown later, increases with the progression of the corrosion process.

2.1.2 Energy

AE energy is the area under the envelope and is defined as the square of the event amplitude in arbitrary units. The quantitative value of AE energy is a variable dependent on many parameters, and its attenuation in the material medium makes it extremely difficult to determine accurately

(Hutton, 1970). However, the enegy release in most applications is very small and generally AE falls within the frequency range 30 KHz to 30 MHz.

2.1.3 Rise Time & Event Duration

Rise time, usually measured in micro seconds, is the time elapsed from the moment of detection of the event by the DA system to the moment of maximum (peak) amplitude. The duration of an AE event, usually measured in milliseconds, is the time elapsed from the moment of detection of the event to the moment the signal dips below the threshold level.

2.1.4 Amplitude

AE amplitude is one of the most commonly studied features of AE signals. AE amplitude generally refers to the peak amplitude in an AE signal. The cumulative amplitude distribution, obtained by summing the distribution starting from the highest amplitude, is a significant characteristic of failure mechanisms (Dunegan, 1973).

One of the most useful mathematical models for analyzing cumulative AE amplitude distribution is the one proposed by Pollock (1980). Let the cumulative distribution function for AE amplitudes be F(v). Now, the number of events whose amplitude exceeds 'v' the threshold can be termed an exceedance (Note: This is different from ringdown counts). The relationship between the exceedance and cumulative distribution is given by

$$\text{Exceedance} = 1 - F(v) \tag{1}$$

The differential distribution function f(v) is given by

$$f(v) = \frac{dF(v)}{dv} \tag{2}$$

The conversion of the experimentally determined frequency (of occurrence) distribution function to a probability distribution requires multiplication by a normalizing factor. This normalizing factor is the reciprocal of the total number of AE events in the sample. The probability of an emission amplitude exceeding the threshold v is $\Phi(v)$, and is given by

$$\Phi(v) = \frac{f_i(v)}{\sum f_i(v)} \tag{3}$$

2.2 AE THEORY

In experiments, an AE event is normally recorded on an instrument such as an AE analyzer. In addition to the source frequency spectrum, the recorded wave form may contain the influence of the transducer frequency response and the effect of the system electronic frequency response. In order to conduct an accurate time study of AE changes in a structure relative to its deformation, all the undesirable frequency information has to be weeded out from the received signal data base. But first, let a simple AE source event be evaluated. A simple example of an AE source would be that of a microscopic event emitting acoustic energy into the surrounding medium. Studies show the microscopic events can be modeled closely by a point event with a step or square pulse time history. As a structure is loaded, due to the non-uniform nature of the material and presence of manufacturing defects and discontinuities, the stress distribution in the material is non-uniform. In regions where the loading stresses exceed the material critical strength, the crystal lattice bonds rupture (Robinson, 1977). While this provides stress

relief in the material, elastic energy is released in the process. Thus, the shape of the AE source function is dependent on two processes. The leading edge of the pulse is dependent on the fracture mechanism and the trailing edge on the mode of energy dispersal in the material medium.

The leading edge of an AE pulse can be mathematically modeled (Achenback, 1973) as follows:

$$A_1(t) = \sigma_{max} - \sigma_1 e^{\frac{-t}{\tau_1}} \tag{4}$$

where

A_1 = stress-energy function,

σ_1 = decrease in stresses,

σ_{max} = maximum stress,

and

τ_1 = time constant (an acoustic characteristic of the source and the material)

Once the stress level exceeds the tensile strength of the material, the material bonds are ruptured and this is followed by a stress relaxation period. The trailing edge of the pulse corresponds to the stress relaxation, and can be written as

$$A_2(t) = \sigma_2 e^{-t/\tau_2} - \sigma_{max} \tag{5}$$

The total pulse is, therefore, given by

$$A(t) = A_1(t) + A_2(t) \tag{6}$$

Equation 6 can be rewritten as

$$A(t) = \sigma_2 \, e^{-t/\tau_2} - \sigma_1 e^{-t/\tau_1} \qquad (7)$$

At regions immediately adjoining the point of discontinuity (rupture), $\sigma_1 = \sigma_2 = \sigma_{max}$ owing to stress relief. Hence Equation 7 reduces to

$$A(t) = \sigma_{max} \, (e^{-t/\tau_2} - \sigma_1 e^{-t/\tau_1}) \qquad (8)$$

This is plotted in Fig. 2.3. Fig. 2.3a shows a AE source function with a fast buildup of stored energy followed by a gradual release. Fig. 2.3b shows another AE source function where the builup is gradual but the release is sudden.

From the above discussion, it can be seen that a triangular displacement function would be a reasonable model of a microscopic AE source. Hence, an AE source can be described as having a pulse-like time dependency. However, after leaving the source, the AE wave propagates as a combination of P-waves (pressure), S-waves (shear), and Rayleigh waves or Lamb waves (Achenback, 1973). As a result, by the time the AE waveform is sensed by a transducer, the signal has lost its simple step function characteristics and has evolved into a more complex combination of ringing packets of vibration.

One of the more recently used AE theories is the generalized ray theory. This theory uses the concept of the time domain instead of the more difficult frequency domain analysis. Figure 2.4 illustrates the application of the generalized ray theory to a unit step function. An AE wave radiated into a
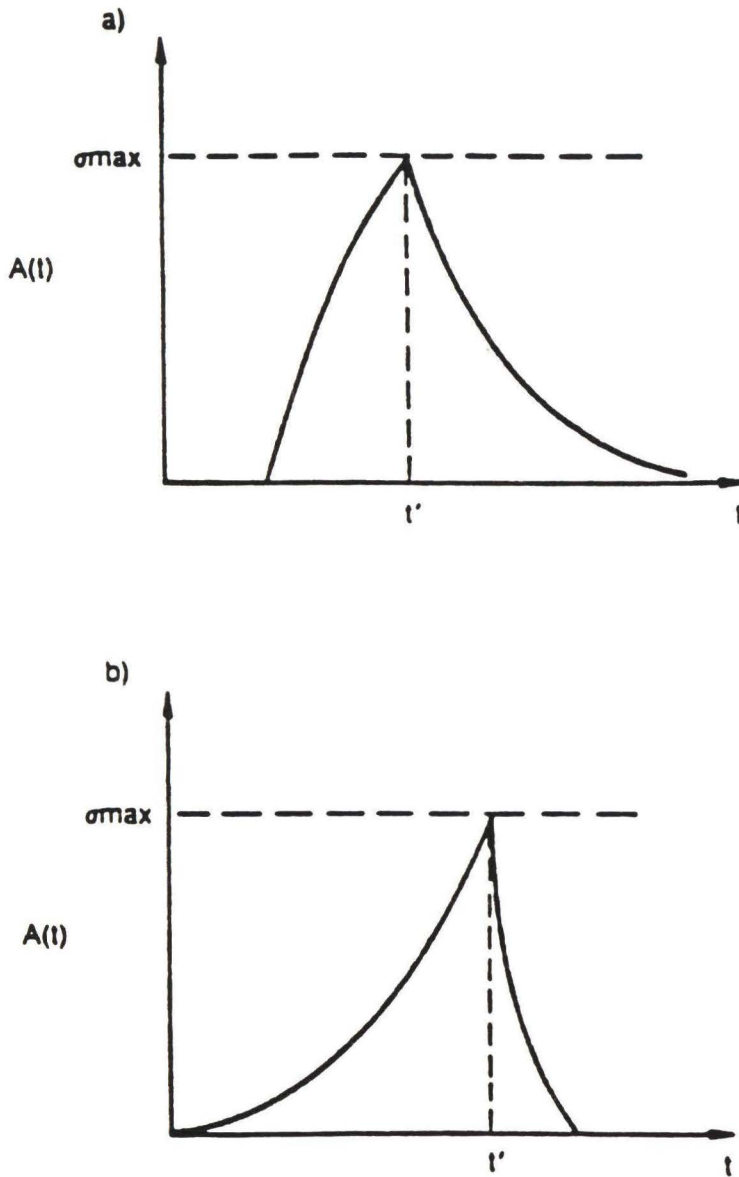
Fig. 2.3   AE source pulse function - a) Quick energy build-up to a peak and then a gradual release; b) A gradual energy build-up to a peak followed by a sudden release.

medium is influenced by many parameters, such as the geometry of the medium, its material composition and the travel distance. Due to multiple reflections and refractions, this signal travels along various ray paths before reaching the receiving transducer. Figure 2.4 illustrates this when the tranceiver is in

(a)   an infinite medium,

(b)   at the surface of an infinite half space,

and

(c)   at the surface of a plate.

A mathematical representation of the signal, as it travels along each ray path, is given by the ray integral U (1928):

$$U(r, z, t) = \sum_{j=1}^{\infty} H(t - t_j) \int_{t_j}^{t} \frac{df(t - t_j)}{dt} U_j H(r, z, t) \, dt$$

(9)

where

$U(r,z,t)$ = displacement in the system,

$H(t-t_j)$ = unit step time function for the j th ray of a point source,

and

t_j = arrival time of the j th ray.

In figure 2.4a the displacement due to the source is detected as a P-wave, while in Fig. 2.4b it is received as a Rayleigh wave. Fig. 2.4c shows the result of the event arriving at the receiver 'x' after the signals' many rays taking different paths and hence arrive as a complex wave form.
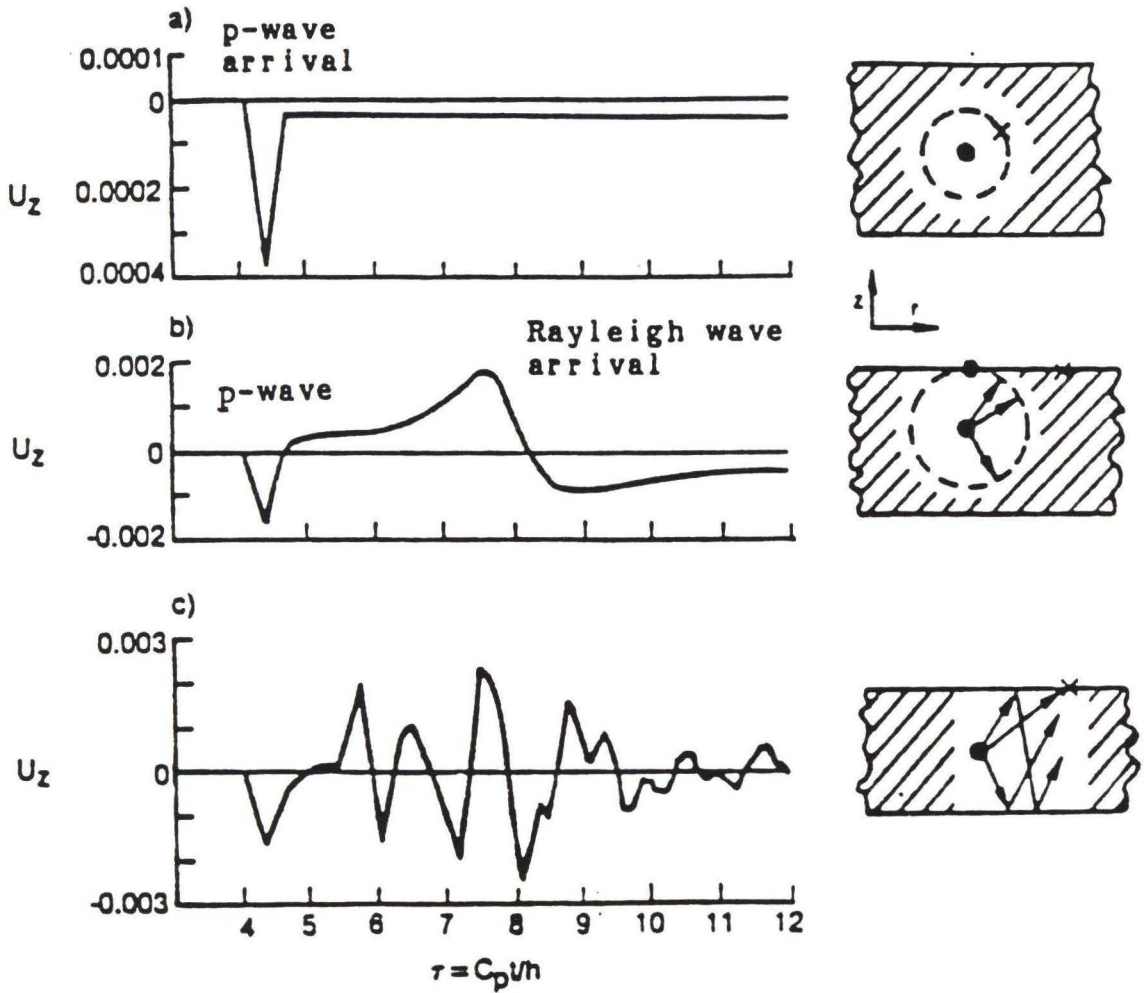
Fig. 2.4   AE displacement waveforms calculated from the generalized ray theory, assuming a unit step function at the center of dilation, with the center located: a) in an infinite space; b) at the surface of a half space; c) at the surface of a plate (Joffo, 1928).

Chapter 3

LITERATURE SURVEY

Acoustic emission is a relatively new field in the sense that most of its modern development has occurred in the second half of the twentieth century. Three basic ideas have fuelled the use of AE as a non-destructive testing method. They are as follows:

(i)   to monitor the rate of emission during stressing and observe any sudden changes in it, which may indicate the formation of new defects such as cracks,

(ii)   to use several detectors and timing circuits together with 3-D geometry to locate the source of AE, and the regions where stresses cause something to happen, such as crack propagation,

and

(iii)   to relate the rate of emission to the defect size and determine the remaining safe life of the structure.

Although the frequency content of acoustic emission signals is not well understood, they are generally thought to be broad band at source, extending from very low frequencies into the MHz range (Jax, 1973). The useful frequency range is determined by equipment sensitivity. For example, the Dunegan/Endevco equipment used in these tests contained band pass filters from 100-300 kHz. Maximum transducer response occured at the transducer's primary resonant frequency, 140 kHz. Attenuation in the medium is

frequency dependent as well; thus, transducer response and attenuation make it difficult to ascertain true frequencies associated with the source event.

Pollock and Stephens (1971) suggested that a simple visual inspection of the waveform can be informative as to the nature of the event. The pulse train of the one had a duration of 30 ms compared to 300 ms of the other. It was indicated that the former consisted of a single grain-sized microfracture, while the other may have consisted of a crack advancement across a dozen adjoining grains in succession. Since the signal duration and counts are related, it would be expected that this kind of analysis could be achieved by counting as well.

Primarily, investigators have used AE for monitoring structures made up of the following four material types:

(1)   metals,

(2)   fiber reinforced plastic composites,

(3)   soils,

and

(4)   concrete.

3.1 METALS

Early observations of AE in metals were made by tin smiths who noted 'tin cry' or twinning, during deformation of tin. However in the last two decades, the primary AE application as a NDE method has been in metal structures, discussed in detail, below.

3.1.1 Aircraft Structures

A program was initiated in September 1977 by Battelle Northwest to develop and apply an AE monitoring system to detect fatigue crack growth in fastner holes in the center section of the wing structure on a RAAF (Royal Australian Air Force) Macchi MB 326 jet trainer - Hutton et al., (1982). The capital AE monitoring system performed trouble-free for over 2 1/2 years of routine aircraft operation. The results provided extremely encouraging evidence that the valid AE recorded was directly related to fatigue crack growth. It was also found that most of the valid AE was generated during low level flying, with increased wing flexure, as a result of greater air turbulence.

In another interesting study, a program was conducted to determine the flaw detection sensitivity of acoustic emission relative to the critical flaw size that will cause rocket motor case failures - Corle (1973). Data from seven different metals tested to revealed that acoustic emission can detect flaws ranging from 10 percent of the critical size of electron beam welded 4335V steel to 100 percent for 6061-T6 aluminum. The program also demonstrated that acoustic emission can detect flaw instability in sufficient time to discontinue a hydro test prior to catastrophic failure. Moreover, a cursory evaluation of applying acoustic emission technology to verify rocket motor nozzle reliability was successful.

3.1.2 Nuclear Reactor Components

Prine and Clark (1974-75) developed real time NDE of nuclear power piping welds, by means of acoustic emission. The test results confirm the

feasibility of using AE for in-process inspection of nuclear reactor welding. It was also found that simple digital logic, in conjunction with frequency discrimination, could eliminate background noises encountered in a production environment. Possa (1982) described the varied use of AE as an on-line monitoring system for critical components of nuclear reactors to proof test various pressure components for leak detection (both hydraulic and pneumatic), loose part monitoring, and mechanism monitoring. AE was also used to investigate the pipe union zone of the Novovorenezh AES reactor's (VVER-1000) vessel surface, during hydraulic loading - Tripalin et al., (1982).

3.1.3 Steel Highway Bridges

Overall monitoring of a typical steel bridge would be extremely complicated due to the many riveted and bolted joints which severely interfere with AE signal propagation. A simple compact AE system for continuous monitoring of a selected area of a bridge structure developed by Battelle Northwest (Hutton et al., 1982) for the U.S. Federal Highway Administration during 1975-78. The monitoring system included several unique features. A zone isolation concept utilizes limits on time of signal arrival among various sensors to limit accepted signals to those originating from the area of interest. A large memory space and rechargeable batteries enabled continuous operation in the field, unattended for several weeks. The system recorded two parameters :

(1)   total AE count seen by one sensor,

and

(2)   Count of valid AE signals, classified as originating from the subject crack, by the zone isolation system.

The zone isolation system proved effective in separating AE produced in the area of interest from the background noise, and hence greatly reduced the field data to be analyzed.

3.1.4 Tanks, Pressure Vessels, etc.

While most studies have concentrated on detecting the occurrence of flaws, some have focused on locating the flaw. One procedure adopted to locate structural flaws in 105 in. diameter tanks was to divide the tank surface into many areas - Moskal and Fageol (1984). Each area was sectioned into 20 equilateral triangles that form an icosahedron. Twelve transducers were equally positioned on the tank surface at vertex of each triangle. The transducers monitored areas for flaws by detecting any increase in acoustical activity. .

In another study Miller (1990) performed Tank Bottom Leak Detection (TBLD) in above-ground storage tanks using AE. This technique involves setting up of 12 transducers at a height of about 15 in. above the tank bottom and spaced equidistantly along the perimeter of the tank wall as shown in Fig. 3.1a. The tank should be filled to capacity with no activity for a minimum of 24 hours prior to testing, to eliminate background noise associated with fluid swirling. Next, the transducers are affixed and calibrated. Once the test commences the AE data is accumulated through a DA system in a personal
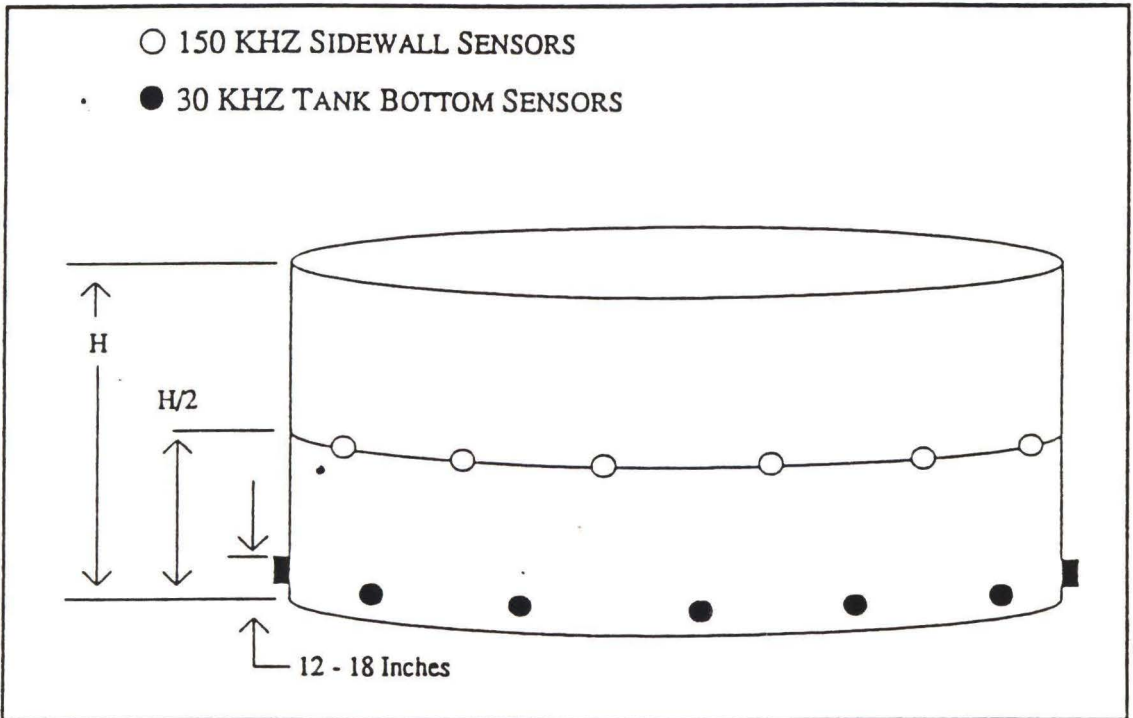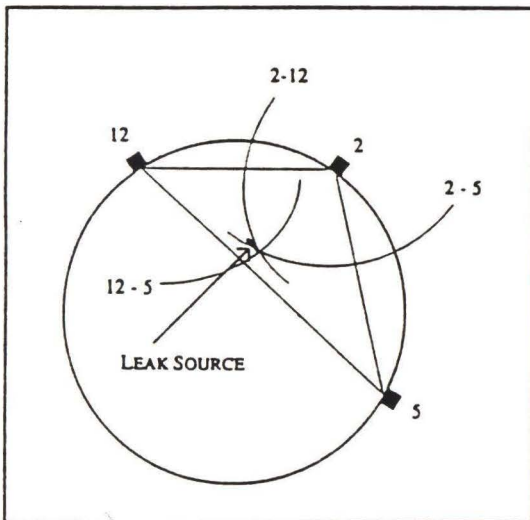
Fig. 3.1a — *Lower sensors used for leak detection.*
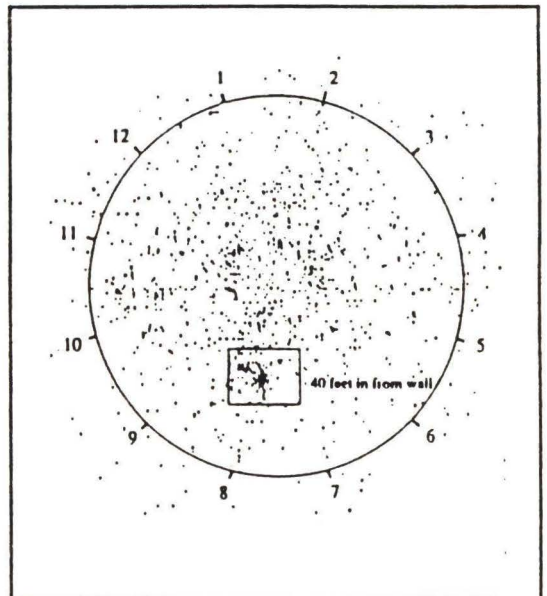

Fig. 3.1b — *Source location for ideal cause.*

Fig. 3.1c — *Leak indication on 150 ft (45.7 m) dia tank.*

computer. The test is terminated after 1 hour. Based on differential arrival times, each event is located. As the speed of sound in fluid is known, for a given event a hyperbola is drawn with the two transducers as the hyperbola's two foci. This hyperbola is given by the locus of a point at a distance of velocity multiplied by the arrival time from the given transducer. Any event picked up by three or more transducers would give two or more hyperbolas, and the intersection of the hyperbolas would be a likely event site as detailed in Fig. 3.1b. In this manner, all events are assigned locations and any cluster of events at a given location is a likely leak source. This is illustrated in Fig. 3.1c. Figures 3.1 a, b and c are from Miller (1990).

Acoustic pulses in a frequency range, which extends far into the ultrasonic region, are emitted in metals during plastic deformation. Measurement of the acoustic emission provides interesting information on the kinetics of the slip processes taking place during plastic deformation. Research has also been done to study the effect of metal irradiation on AE signal characteristics. It was found that generally AE counts were higher for irradiated specimens during tensile and wedge opening tests. Additional tests on welded steel pressure vessels demonstrate that incremental crack growth during pressurization can be accurately located and assessed.

3.1.5 Other Applications

Acoustic emission has been used to determine crack susceptibility of beryllium coupons - Drouillard et al. (1974), to detect phase transformation in steel. Other areas of application include low cycle high-stress-intensity fatigue, stress corrosion cracking and hydrogen embrittlement, strain-aging embrittlement, and weld cracking.

AE has also been used to monitor martensite formation during welding, which could lead to cold cracks. The 'click' that occurs during the formation of martensite in high-nickel steel was first reported by Forster and Scheil (1936). Until the early 70s, however , not much research was done on AE generated during phase transformations. Since then the research activity has considerably intensified.

During welding, martensite formation, porosity (defective weld), and the sound weld all generated intense AE signals. The pattern recognition technique, developed by Liu and Asibu (1990), provides a means by which positive signal sorting, classification and source identification can be obtained. The signals associated with martensite transformation are relatively small in amplitude compared with are noise during welding.

3.2 FRP COMPOSITES

Advanced states of AE monitoring are used in the evaluation of the structural integrity of fiber reinforced plastic (FRP) tanks, pipes, vessels, and manlift booms (Hutton et al, 1982). AE behavior of FRP composites is slightly different from that of other materials. There are four important AE parameters characterizing a FRP structure.

1) *Emissions under Constant Load*

A damaged specimen of FRP will continue to emit AE when held at constant load. In the damaged area, the resin matrix will be subjected to high local stresses and can result in fiber debonding, resin cracking, and fiber breakage.

2) *Felicity Effect*

The Kaiser Effect (Ch. 2), does not seem to hold good for FRP. The violation of the Kaiser Principle is called 'Felicity Effect'. The ratio of stress at onset of emission to the previous maximum stress, termed as the Felicity Ratio, is an indication of the severity of damage.

3) *Amplitude Distribution*

Low stresses in FRP will produce primarily low amplitude of AE. The population of high amplitude signals increases as the stress increases.

4) *True Mean Square (TMS)*

TMS is the squared value of the root mean square signal. TMS is a continuous function and will vary with time depending on the nature of the emissions and the value of the time constant. For FRP, the recommended time constant time would be 5-10 ms.

Further results from graphite-epoxy honeycomb structures indicate that AE is also a viable tool in detecting and locating impending failure in composite materials - Kelly et al. (1974).

3.3 SOILS

Obert and Duvall (1938) were carrying out sonic studies in a deep hard rock mine, when they discovered that a stressed rock pillar appeared to emit micro-level sounds. This phenomenon of acoustic emission is associated with microseismic activity in the earth. Hardy (1972) has written a comprehensive review of acoustic emission applications in rock mechanics. A bibliography of microseismic emission research in geological materials has

been prepared by Hardy and Leighton (1977). Traditionally, acoustic emission has been widely used for geological applications but recently these techniques are being applied to geotechnical engineering as well. Drnevich and Gray (1978), edited a series of papers dealing with acoustic emission in soil mechanics. Thus, acoustic emission applications have found widespread use as non-destructive evaluation tools. Applications include materials research, material characterization, and structural integrity evaluation.

Koerner et al. (1984) used AE to determine prestress in granular soils in a lab study. Remolded granular soils were loaded in a standard consolidometer, the prestress load was first released, and then reapplied in an incremental manner. AE was monitored during this reloading process. As the load equivalent to the originality applied preconsolidation pressure was exceeded, AE increased markedly. Thus, the original prestress was easily detectable. Tests were performed on five different granular soils, each at four different saturation levels, for four different prestress conditions (80 in all). Results obtained show that AE predicted the originally applied pre-consolidation pressure to within about 6% average error for each preconsolidation pressure, with the exception being the lowest pre-consolidation pressure where there was an error of 12.9%.

The mechanisms responsible for the shear strength of soils appear to be the basic generators of acoustic emissions in soils - Koerner et al. (1977). Well-graded soils, with a high coefficient of uniformity, produce large levels of AE counts, though angular non-spherical soils produced greater AE than soils consisting of rounded spherical particles.

AE monitoring of the seepage of water through soil has been carried out in the laboratory and correlated with a field study at the site of reservoir leakage beneath a small earth dam - Koerner et al. (1981). At comparable flow rates, turbid water produced higher AE than clear water. Another area of study with AE is soil stability - Koerner et al. (1978). Soil masses that generate very high levels of AE are those undergoing large deformations. They should be considered to be in a failure state and emergency precautions initiated.

3.4 CONCRETE

Compared to metals, relatively little research has been devoted to the study of acoustic emission phenomena associated with deformation mechanisms in concrete. However, acoustic emission has been used by several investigators to study concrete. Rusch (1960) examined the relationship between creep and microcracking using acoustic emission methods. Robinson (1977) discussed a number of methods for detecting microcrack formation and propagation in concrete, one of which was sound emission. Hawkins, Kobayashi, and Fourney (1979) used acoustic emission to study bond deterioration in reinforced concrete under seismic loading.

Stress wave emission data from cylindrical concrete specimens under compression have been used by Green (1970) to determine impending failure and previous loading extremes. There is limited correlation between stress wave emission and the modulus of concrete. Robinson (1977) conducted experiments on the elastic behavior of concrete. A significant increase in AE activity above a certain load, was noticed depending on aggregate size.

Izumi et al. (1988) studied the AE process corresponding to the fracture process zone in fracture mechanics tests of concrete using three-point bending and double cantilever beams. Based on the bilinear relationship between the energy release rate G and cumulative sum of AE energy, a parameter GAE was defined which is a stable LEFM value. Rossi et al. (1989) studied the physical mechanisms underlying AE during the cracking of concrete, and showed that it is possible to distinguish cracks at the matrix-inclusion interface and cracks propagating in the matrix during mechanical tests.

Research at Florida Atlantic University has focussed on the use of AE to detect and characterize

    i)   Corrosion of reinforced concrete,

    ii)   Crack growth/fracture of metal under fatigue,

and

    iii)   Linear location of AE sources in a corroding reinforced concrete slab.

Chapter 4

EXPERIMENTAL PROCEDURE

The work in this chapter is divided into three parts. The first part gives the material and specimen configuration. The second part deals with the specifications of the various testing equipment used. The third and last part deals with the experimental setup.

4.1 MATERIAL AND SPECIMEN CONFIGURATION

For corrosion testing 16 beams were used. Eight of these were made of regular concrete while the remaining eight were of flyash modified concrete.

The amount of fly ash replacement was determined by fly ash optimization, done in an earlier study based on a method developed by Popovics (1982) and by compressive strength versus fly ash percentage studies (Table 1). The Popovics formula for optimum fly ash content for a given concrete strength is

$$F_{opt} = 33.33 \frac{K_c}{K_c - K_p} - \sqrt{1111\left(\frac{K_c}{K_c - K_p}\right)^2 - 0.5556 f'_c - 902.8} \tag{10}$$

where K_c and K_p are the prices of 1 lb cement and fly ash respectively.

The results of the earlier study showed that 20 percent fly ash replacement (by weight) was ideal; hence this percentage was used for casting the fly ash modified beams.

The beams were made large enough to be capable of carrying loads of practical significance and magnitude and also to avoid criticism based on size effects. The reinforced beam details are shown on Fig. 4.1. Table 2 shows the number of beam specimens used in each test.
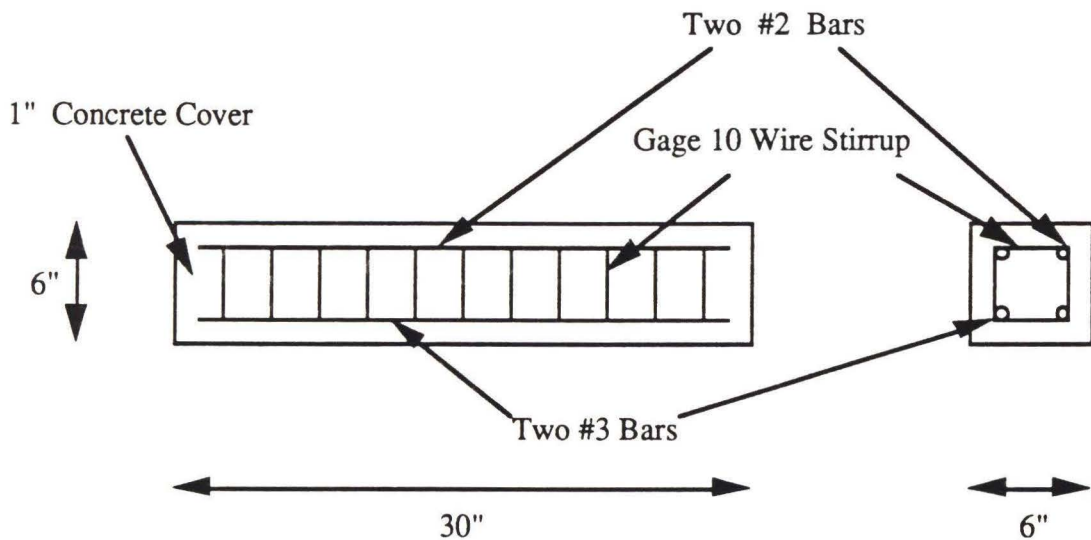
Fig. 4.1   Details of beam specimen used in corrosion tests.

The fracture mechanics specimens were non-reinforced and formed part of another study on marine durability. The types of specimens used were beams (4 x 4 x 18 in.), cubes (4 x 4 x 4 in.), and prisms (4 x 4 x 1.6 in.). Beam

Table 1 - Compressive strengths of various concrete mixes

Flyash Replacement %	Compressive Strength (psi)		
	7-day	28-day	90-day
0	4960	5710	6670
15	5760	6710	8350
25	4930	6090	7580
35	3100	4690	5580
15.4*	5730	6990	8520

* Blended

Table 2 - Corrosion specimens

CORROSION PERIOD	IMPACT		FLEXURE		TOTAL
	Flyash	Normal	Flyash	Normal	
1 Week	1	1	1	1	4
2 Weeks	1	1	2	2	6
3 Weeks	2	2	1	1	6
TOTAL	4	4	4	4	16

specimens were used for the single-edge notched bending test, cubes for the split-cube test and prisms for the wedge splitting test. Fig. 4.2 gives details of the fracture mechanics specimens.

4.2 EQUIPMENT SPECIFICATIONS

4.2.1 AE Signal Analyzer

The AE equipment used was a Dunegan Endevco AE analyzer. It consists of the Dunegan Module 950, which is a Computer Interface Module that can read information from any Dunegan module 303, 920, 922 or 934, and transfer it to a host computer. The AE analyzer used in this study had a total of nineteen data aquisition channels, of which four were devoted exclusively to monitoring ringdown counts and three to amplitude distribution.

In these experiments, the module 303 was used to monitor the AE counts, while the module 922 was used to monitor the amplitude distribution. An IBM PC was used to store the data. The data can be acquired both in a time driven and an event driven mode. The 950 has a buffer of 256 kilobyte RAM.

The transducers used were the Dunegan Endevco Model S9204 high sensitivity transducers, with very high signal to noise ratios. They are ceramic type transducers with a very low physical profile (0.89 in. diameter and 0.56 in. thick) aluminum casing. Their sensitivity range was between 50 kHz

33
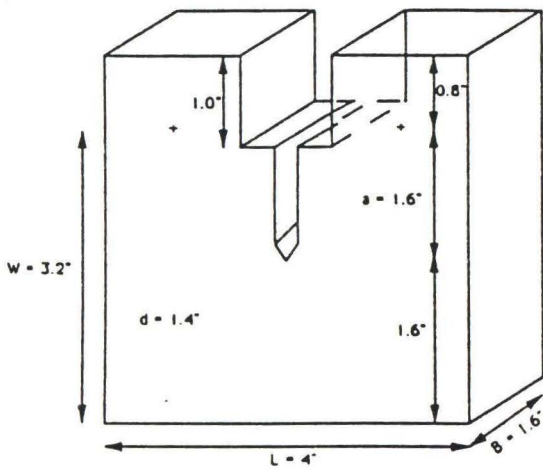
Fig.4.2 a) Wedge Splitting Test Specimen (a/W = 0.5)
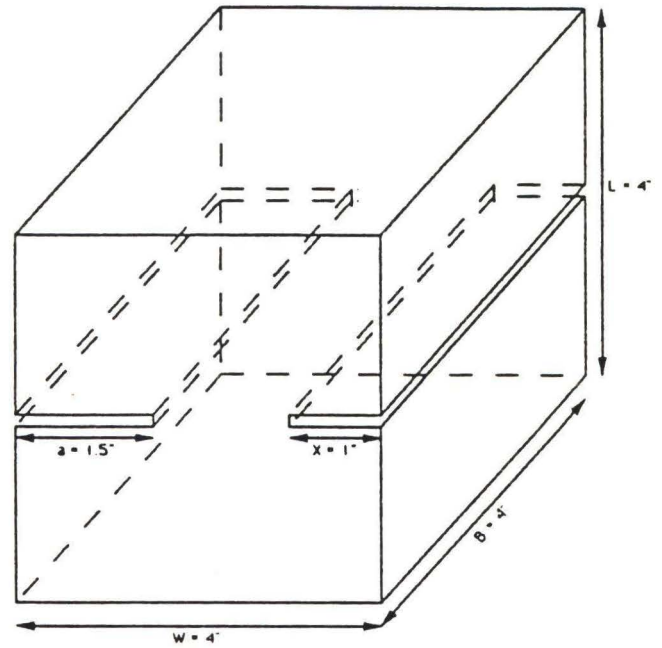
Fig. 4.2 b) Split-Cube Test Specimen
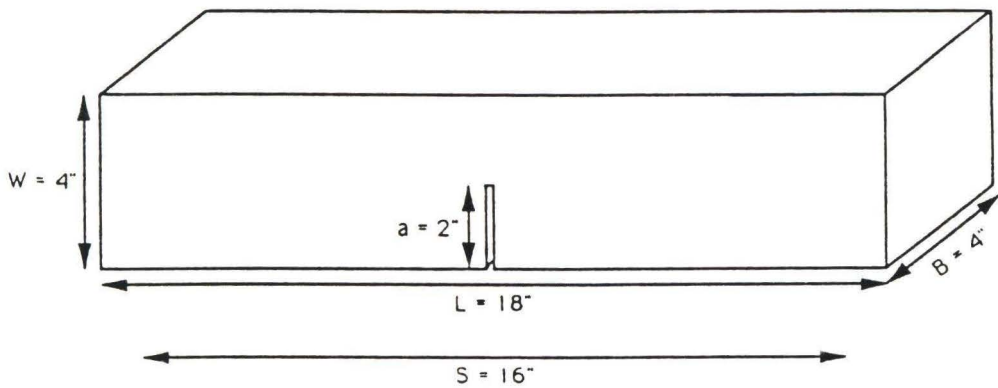
Fig. 4.2 c) Three-point bending test specimen   (a/W = 0.5)

and 425 kHz. However, their peak sensitivity (primary resonant frequency) was 140 kHz. The transducers were affixed to the specimens with silicone sealant and wired through a preamplifier to the DA system. The AE monitoring setup is shown in figure 4.3. The threshold used was 4 dB.

4.2.2 Impact Testing Apparatus

Drop weight	150 to 800 lb
Electromagnet	Model 110-150
Instrumented tup	Dynatup 8302
Oscilloscope	Tektronix 5113
Dynamic response module	Dynatup 500 DRM/AMPL
Velocity trigger system	Dynatup 400 VDM
Time base system	Model 5B10N

An electromagnet was used to raise and lower the dropweight. In this study, the weight and tup assembly together weighed 300 lb. The drop weight and electromagnet are provided with teflon sleeves which slide over precisely aligned vertical guides. The velocity trigger system has an infrared flag assembly for triggering of the oscilloscope signal. The tup measures the compressive load interaction between the tup and the specimen at the time of impact using two semiconductor strain gages. The dual trace oscilloscope has
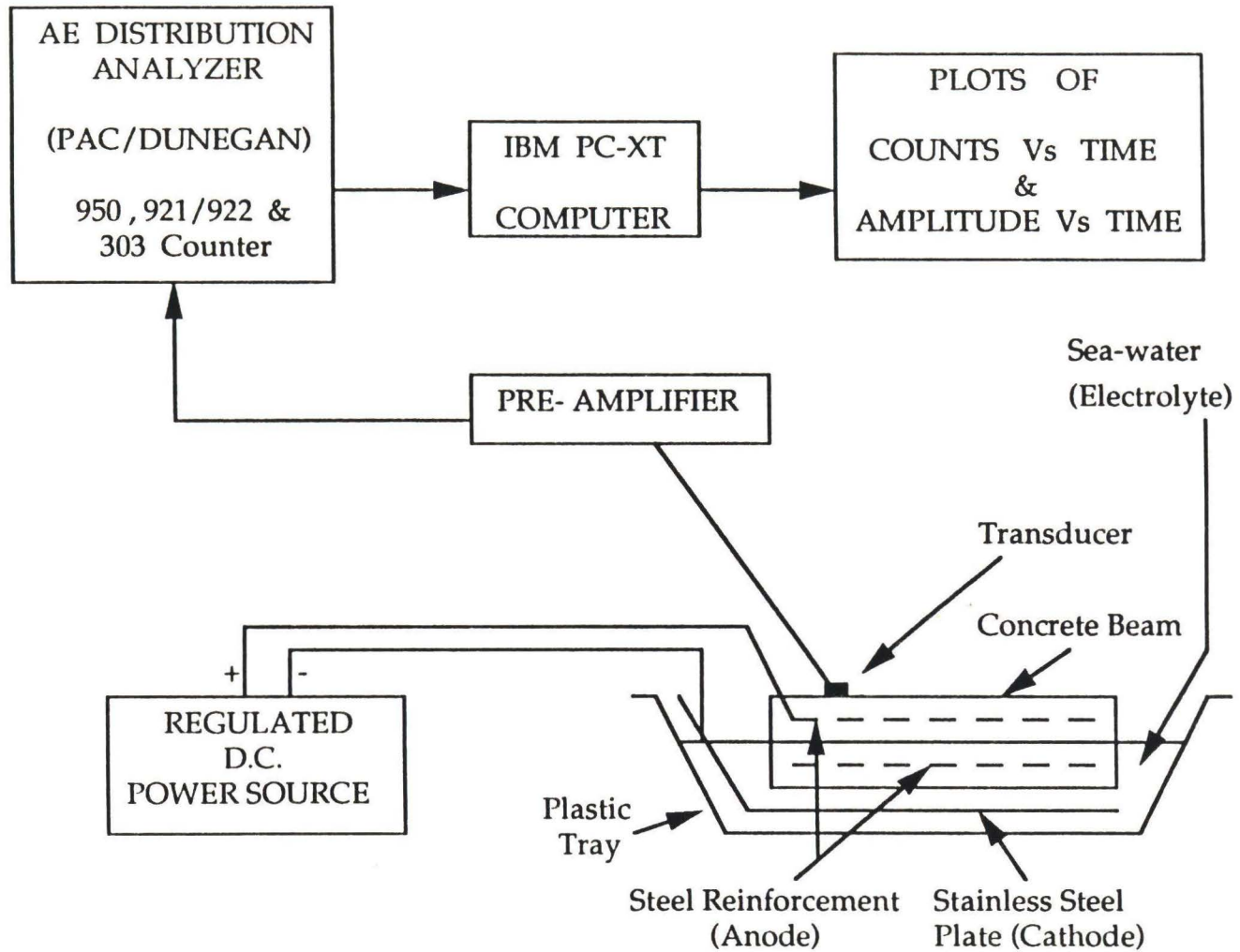
Fig. 4.3 Experimental setup for accelerated corrosion test.

a storage feature in which one signal trace records the load while the other records the energy absorbed. The energy absorbed is given by

$$E_{abs} = v_0 \int P \, dt \qquad (11)$$

where

v_0 = velocity at impact, and

P = load at any given time.

4.2.3 Flexure Testing Apparatus

The mode of flexure testing was four point bending with the loads at the third points of the span. The free body diagram is shown as Fig. 4.4. The testing machine used was a Forney model QC-150-DR, with a range of 300,000 lb. It has a dual range setting with low and high ranges. The low range has a peak load capacity of 30,000 lb. with a least count of 50 lb., and the high range 300,000 lb. with a least count of 500 lb. All the flexure tests done in this study were carried out on the low range.
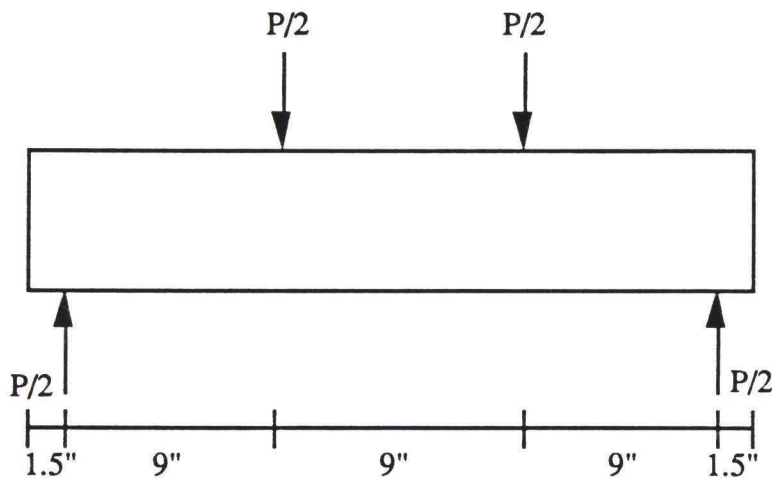
Fig. 4.4 Free body diagram of beam in flexure test.

4.2.4 Fracture Mechanics Test Apparatus

The equipment used for fracture mechanics tests was a Tinius-Olsen testing machine with a peak capacity of 30,000 lb. The loading rate used was 0.05 in. per min. and the deformations were measured by LVDTs (Linear Variable Deformation Transducers). All the specimens were prenotched. Table 3 gives the number and type of specimens used in fracture mechanics tests.

4.3 EXPERIMENTAL SET-UP

For the accelerated corrosion tests, one of the fundamental questions to be resolved was the mode of current application. Initially, a constant current application was considered. But then it was found that once the passive oxide film was ruptured, the electrical resistance of the beams was greatly reduced and the voltage dropped abruptly. In the passive stage (before passivity is overcome) the corrosion rate is not proportional to the applied current. Hence, it was decided to apply constant voltage.

In studies of concrete cracking in the sea water due to embedded metal corrosion by Grimes et al. (1979), it was found that an effective anodic current density of 0.75 mA/cm^2 on the steel caused cracking to occur in two days. From pilot runs on a control beam the applied voltage level was set as 12 V; this caused the average current to be 0.4 A, which combined with the effective anode area of about 520 cm^2, provided comparable stimulus for cracking.

Table 3 - Number and Type of Fracture Mechanics Specimens

Concrete Type	Mix Type	Batch #	Specimen Type				Total #
			Cylindrical (3"x6")	Beam (4"x4"x18")	Cube (4"x4"x4")	Cuboid (4"x4"x1.6")	
Air-entrained Concrete	Control (I)	1~2	16	4	4	4	28
	Blended (Ip)	3~5	24	6	6	6	42
	Flyash 25%	6~8	24	6	6	6	42
	Flyash 35%	8~11	24	6	6	6	42
Non Air-entrained Concrete	Control (I)	12	12	3	3	3	21
	Blended (Ip)	13	12	3	3	3	21
	Flyash 25%	14	12	3	3	3	21
	Flyash 35%	15	12	3	3	3	21
TOTAL			136	34	34	34	238
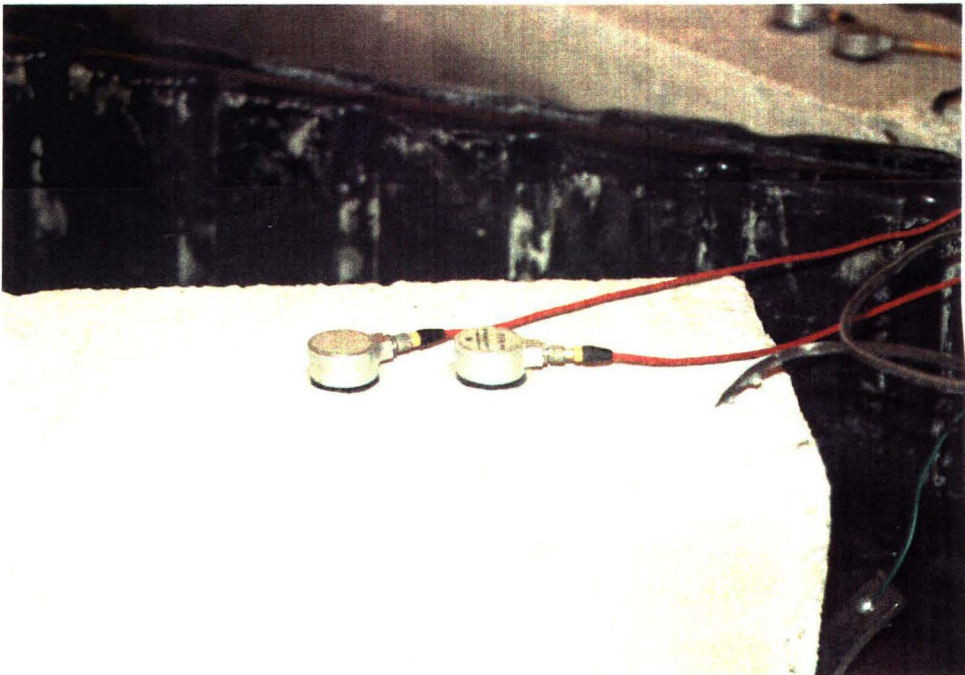
Fig 4.5   Photographs of accelerated corrosion test setup, and close-up view of transducers affixed to the beam specimen.
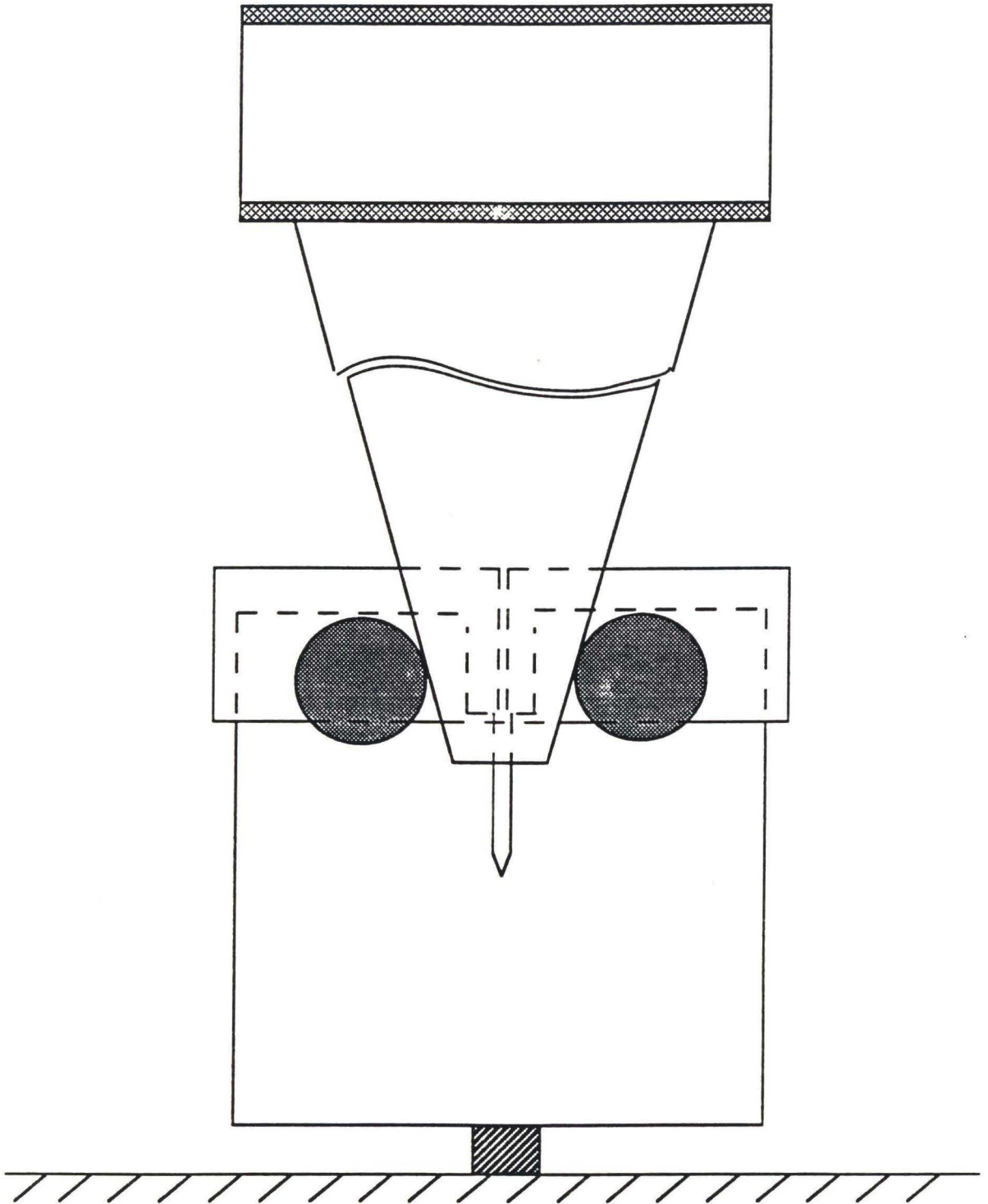
Fig. 4.6   Statical System of the Wedge Splitting Test
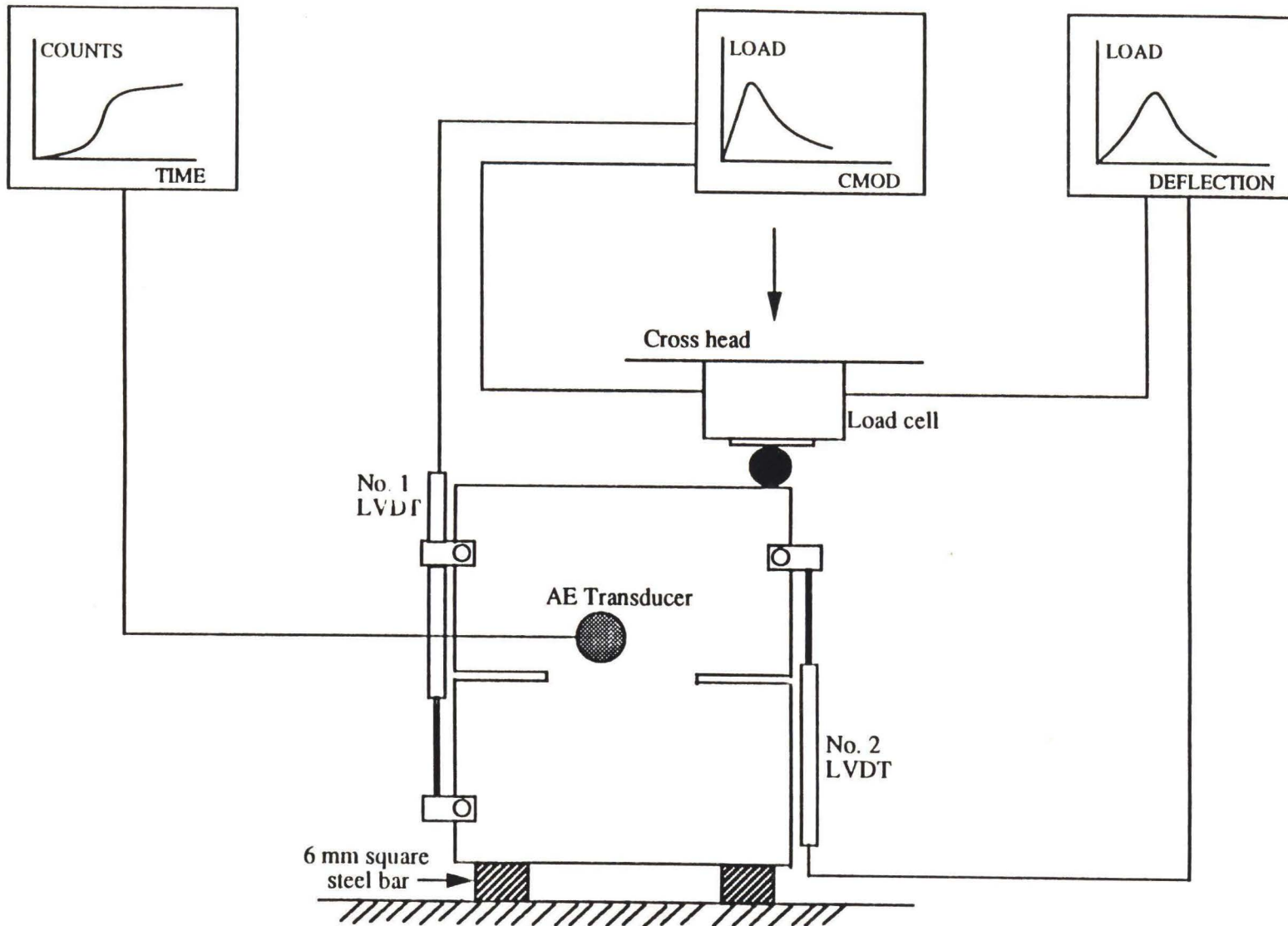
Fig. 4.7   Experimental setup for the split-cube compression test
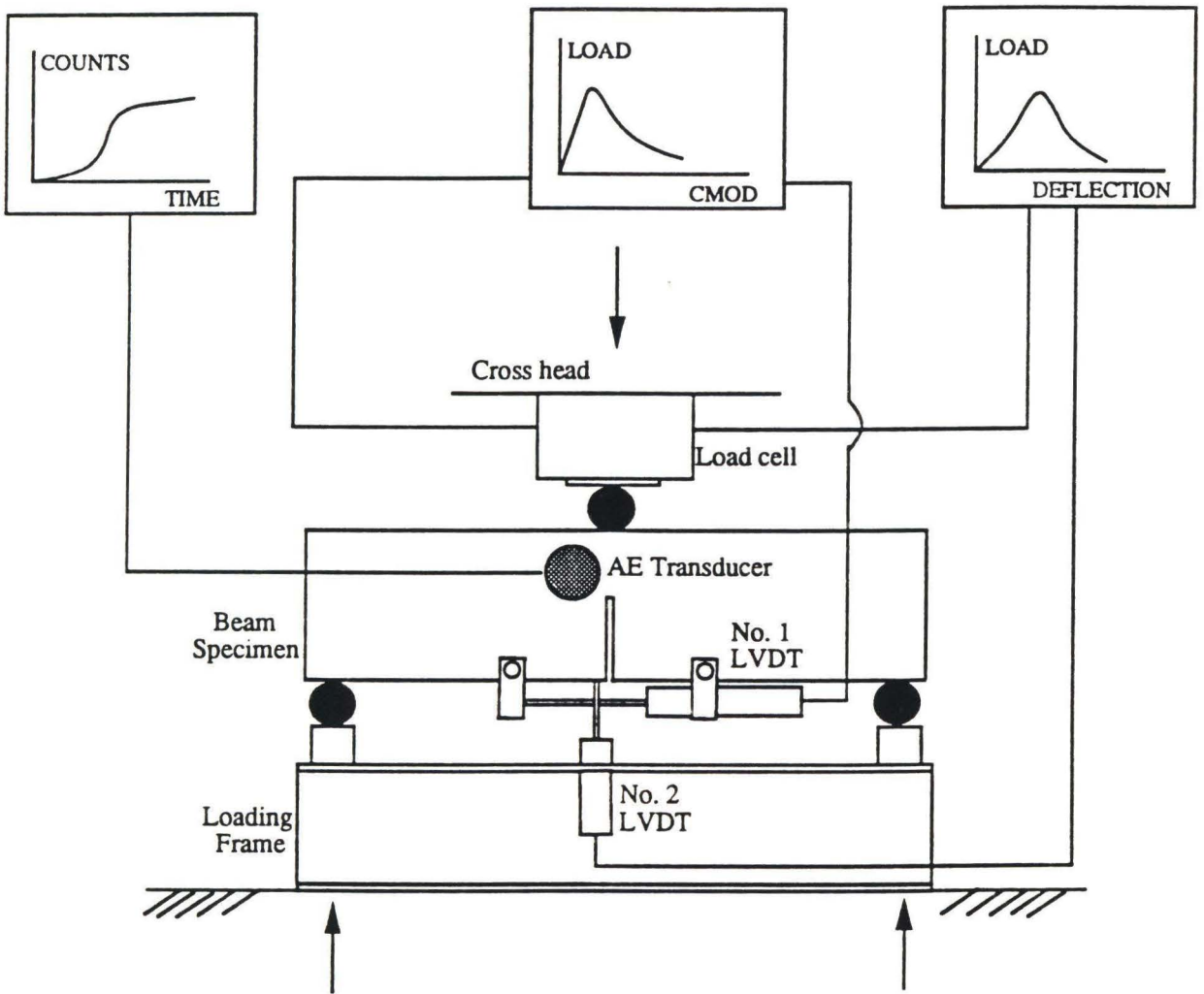
Fig 4.8   Experimental Setup for the Three-point Beam Bending Test

The specimens were connected in parallel and flyash and regular beams were placed in separate tubs of sea water to allow for their different conductivities. Fig. 4.5a shows the experimental set up for accelerated corrosion, and a close-up view of the transducers affixed to the beam specimen with silicone sealant is shown in Fig. 4.5b.

The fracture mechanics test setups are shown in Fig. 4.6 through 4.8. While Fig. 4.6 shows the statical system of the wedge splitting test, Fig. 4.7 illustrates the experimental setup for the split-cube compression test. The experimental setup for the three-point beam bending test is shown in Fig. 4.8.

Additionally, AE was also used to monitor the ultimate load test of a multi-box beam bridge model in February 1989. A cross-sectional view of the bridge with the transducer location is shown in fig. 4.9. Three transducers were placed on the underside of the bridge at the midspan with one at center line and the other two at the extremities. The photograph of the bridge model is given in Fig. 5.32.
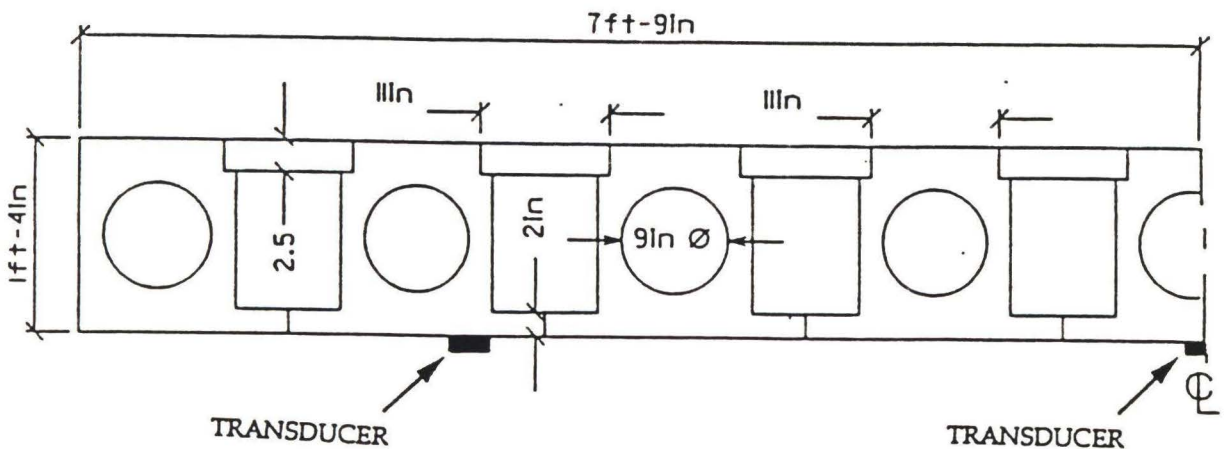
Fig. 4.9 Sectional view of the multi-box beam bridge model.

Chapter 5

RESULTS AND DISCUSSION

5.1 CORROSION CURRENT

Monitoring the current fluctuation every 24 hours, while the applied voltage was maintained steady, indicated that as expected the current level rose sharply once the passive barrier was broken. Figs. 5.1a, 5.1b, and 5.1c, show the current fluctuations for both the fly ash and regular beams for one-week, two-week, and three-week tests, respectively. From the graphs it can be seen that for application of a constant voltage of 4 volts per beam in circuit, the current levels are generally higher for the normal beams than the fly ash beams. This leads one to infer that fly ash modified beams offer greater resistance to electrochemical corrosion than normal beams. This would then translate into less damage in the rebars and hence a greater retention of strength.

Another aspect is the extent of corrosion as a function of test duration. Once the passive barrier is broken, the current level increases thereby accelerating the corrosion process further. In other words, the corrosion rate increases with time. The photograph in Fig. 5.2a clearly demonstrates this. The one-week corroded beams showed only marginal surface staining. The stains were more pronounced in the two-week beams and additionally some surface cracks were observed in most of them. The staining was extremely

a)

b)

c)
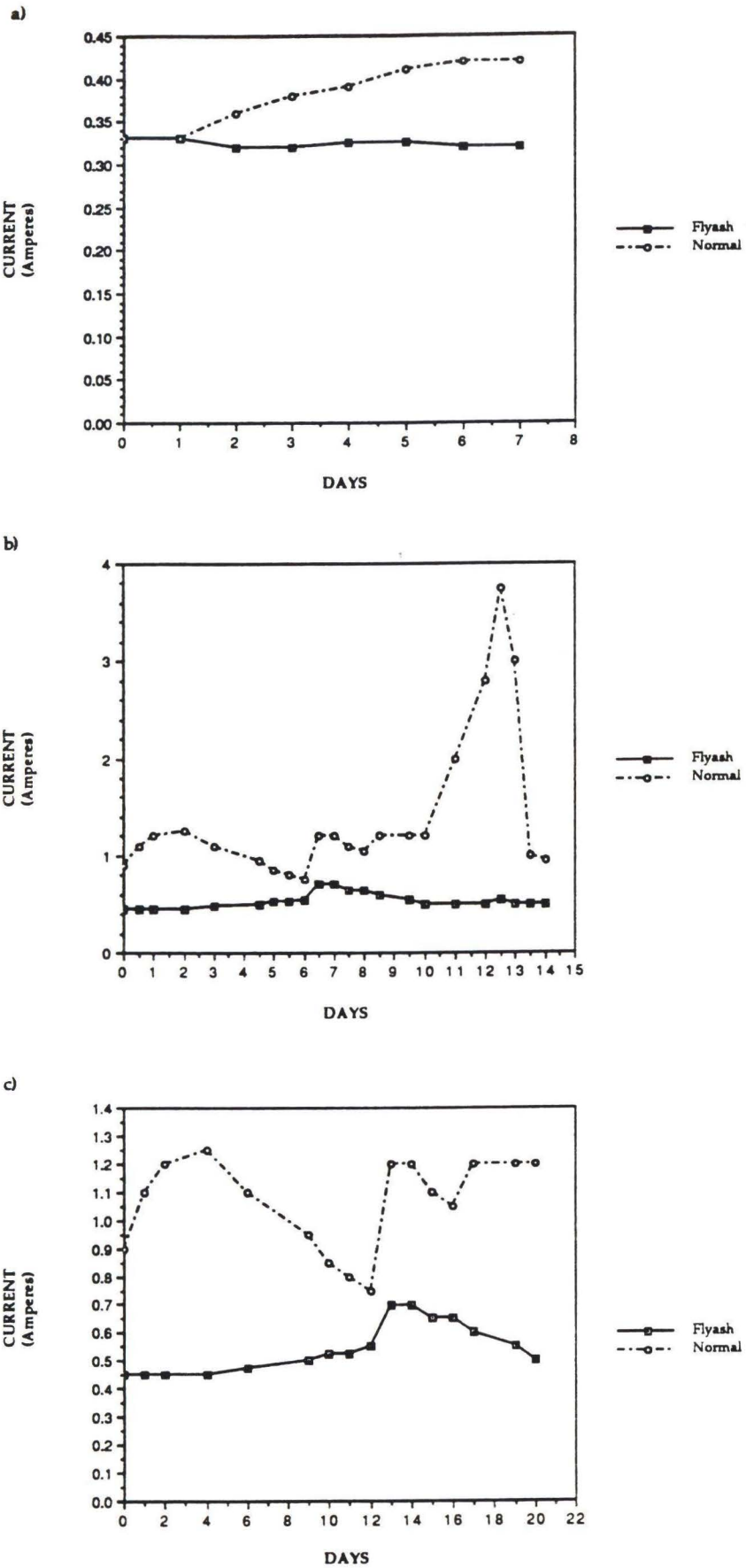
Fig. 5.1 Current fluctuation for a constant average voltage of 4V per beam

Fig. 5.2   Photographs of corroded beam specimens.

Fig. 5.3   Photographs of corrosion damage - Visible external crack and rebar corrosion.

severe in both types of three-week beams and every one of them developed cracks. The spalling was very severe in some of them and chunks of concrete fell off leaving the exposed rebars. The photograph in Fig. 5.2 b illustrates this point. Fig. 5.3a shows a visible external crack in a 2-week corroded beam, while Fig. 5.3b shows the corroded state of the rebar.

However, it must be pointed out that while earlier studies (Reddy , 1986) of field corrosion specimens at Treat Island and laboratory simulated corrosion specimens indicated correlation between three week accelerated corrosion and a twenty five year marine exposure, in the current experiment the three-week specimens appeared to have suffered a greater deterioration than those of the twenty five year field exposure specimens. Hence, more field data will have to be evaluated to enable more accurate correlations.

Table 4 gives the AE data for each beam tested in the corrosion program. Fig. 5.4 shows the average monitored AE counts as a function of test duration for both types of beams. Notice that generally AE counts were higher for normal beams than for fly ash beams. It must be pointed out that in some instances the fly ash beams showed larger counts. However, the average of the cumulative counts as well as the general data trend excluding the high points, indicate increased numbers of counts in the normal beams. This implies that normal beams deteriorated more than fly ash beams which agrees with earlier conclusions based on corrosion current data. Figs. 5.5 through 5.19 show the cumulative and as-read AE data for the various beams. However, it was also noticed that the largest single event generally occurred

Table 4 - AE count data

BEAM #	Corrosion Period (Weeks)	COUNTS	
		Cumulative	Biggest Event
F25	1	31	14
F26	1	17	9
F27	2	1362500	805000
F28	2	3136	113
F32	2	1200	89
F29	3	85830	11280
F30	3	14700000	528000
F31	3	1074720	855
B1	1	196	40
B2	1	356	176
B3	2	10340	72
B4	2	14850	100
B16	2	6300	86
B13	3	1666	78
B14	3	89100000	16660
B15	3	7267	154

Prefix 'F' denotes flyash modified reinforced concrete beam.

Prefix 'B' denotes normal reinforced concrete beam.
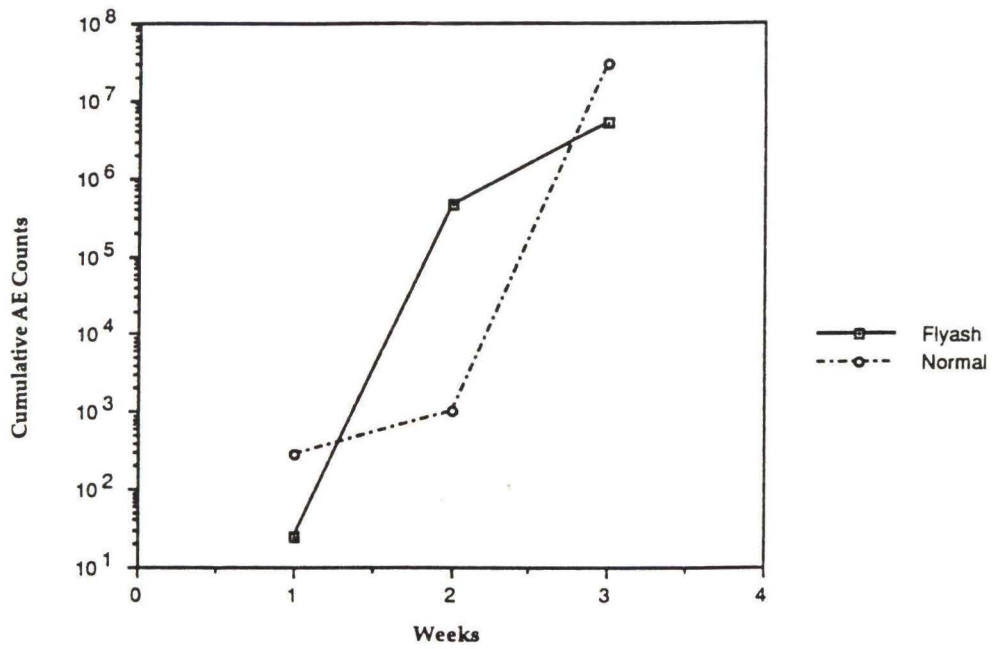
Fig. 5.4a Plot of cumulative AE counts versus period of corrosion
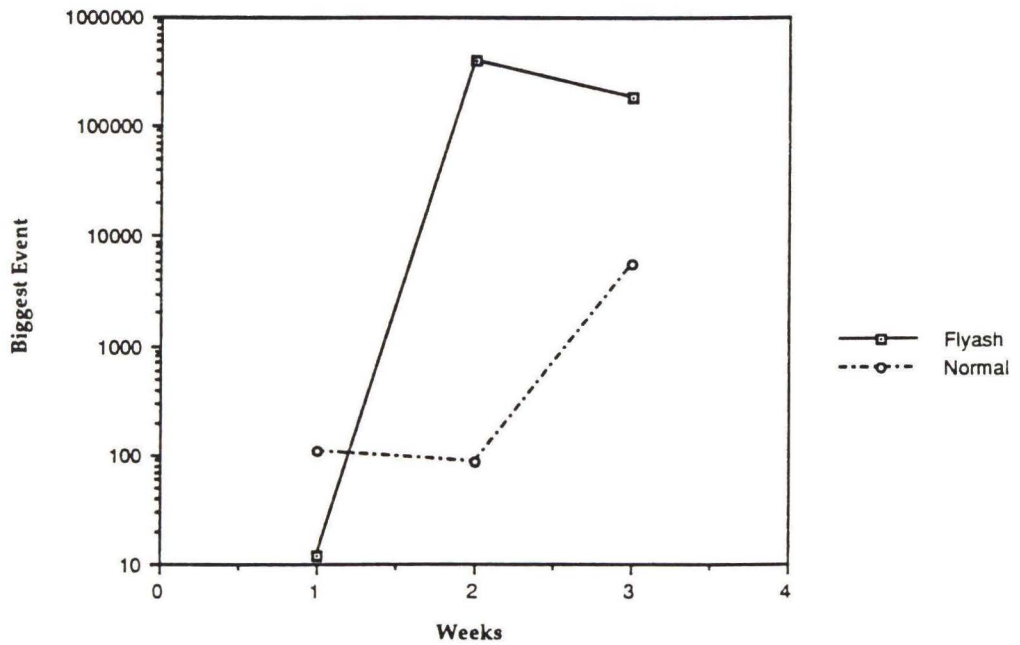
Fig. 5.4b Plot of biggest single event versus corrosion period
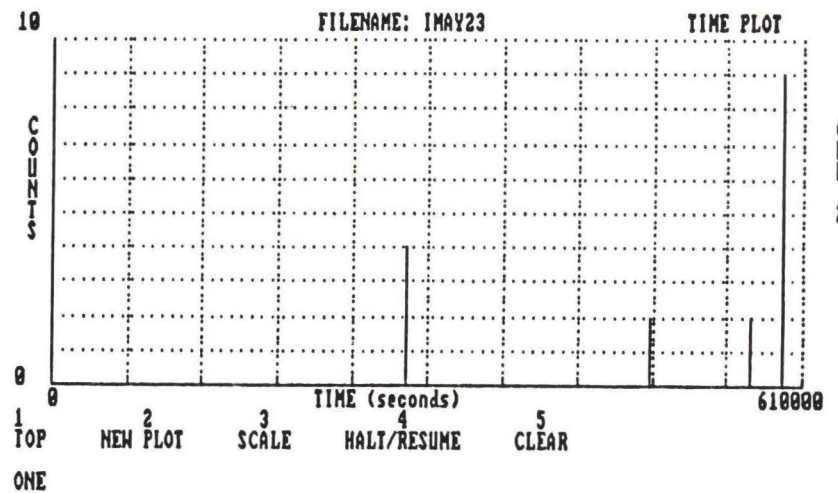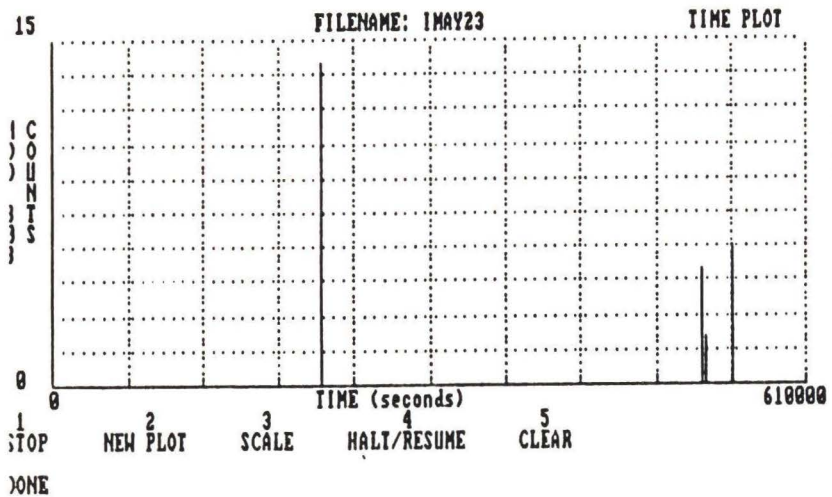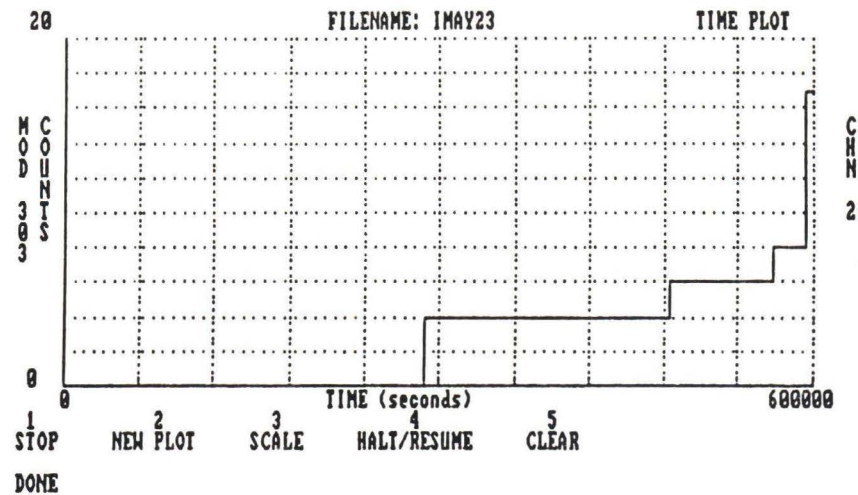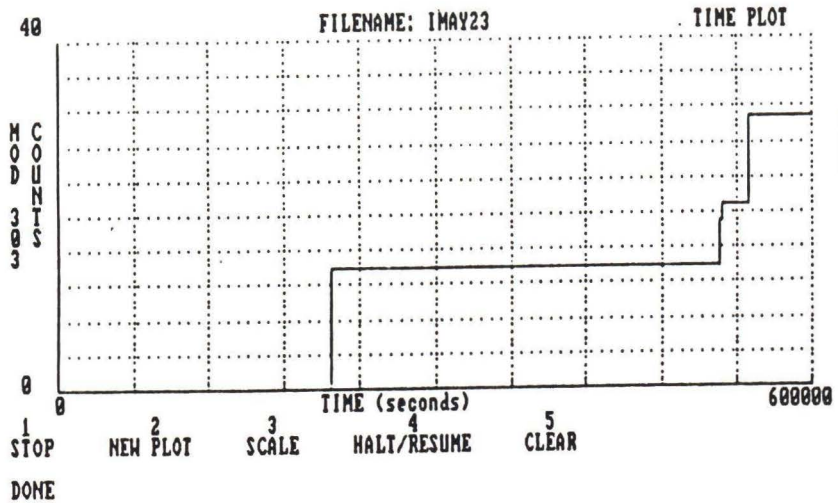
Fig. 5.5   Cumulative and as-read AE data for 1-week corrosion test. Flyash beams F25 & F26 on channels 1 & 2.
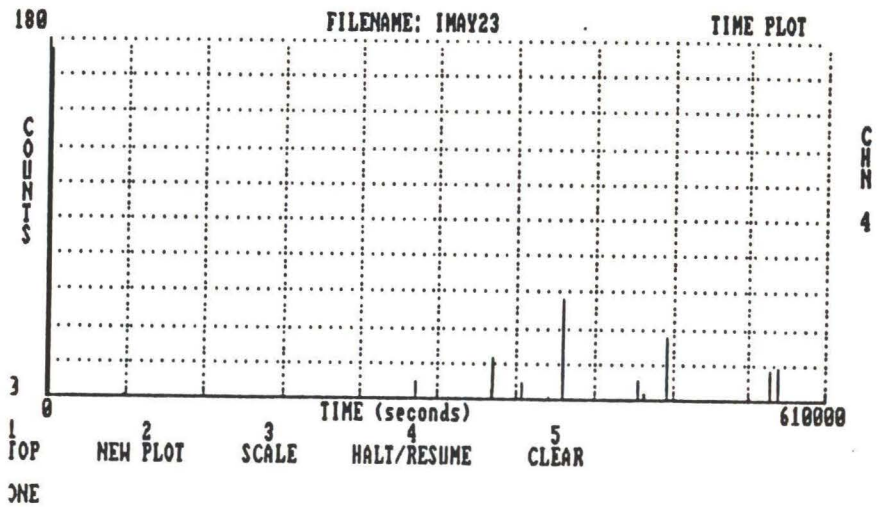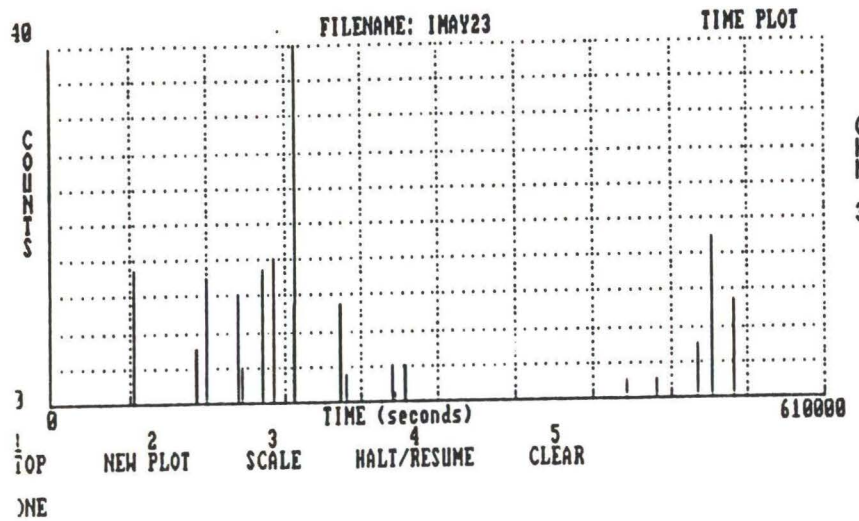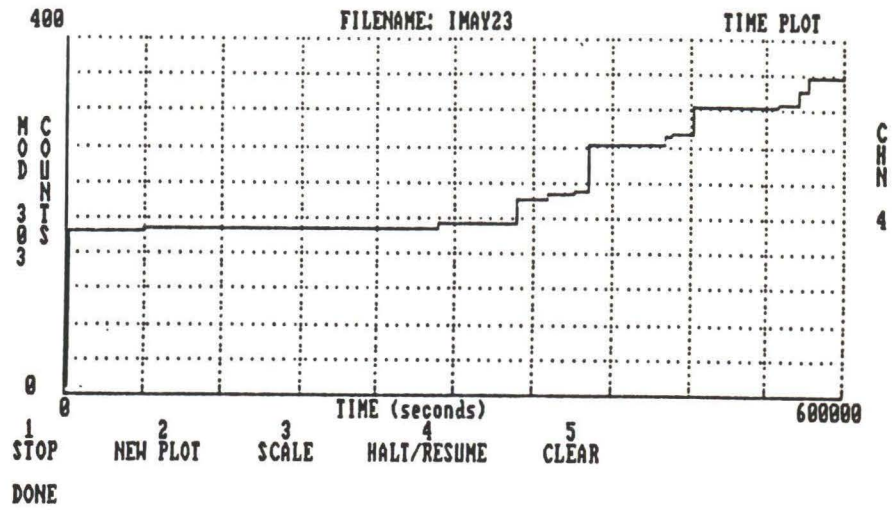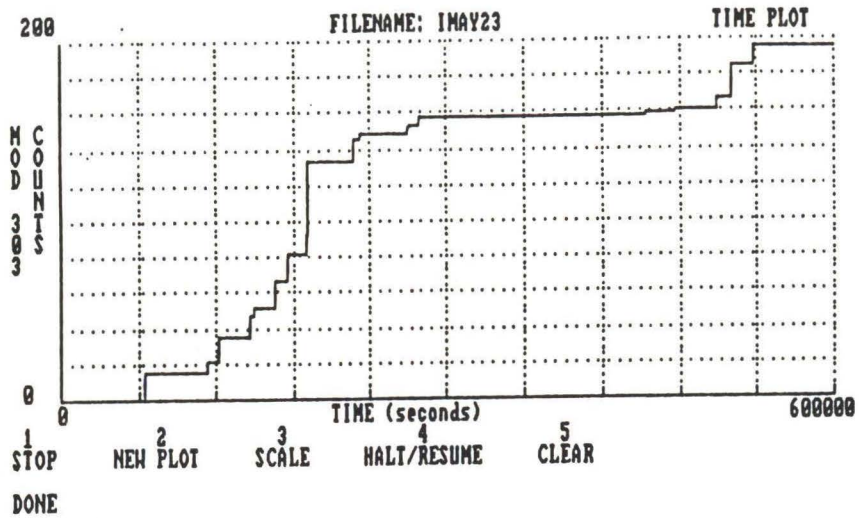
Fig. 5.6   Cumulative and as-read AE data for 1-week corrosion test. Normal
beams B1 & B2 on channels 3 & 4.
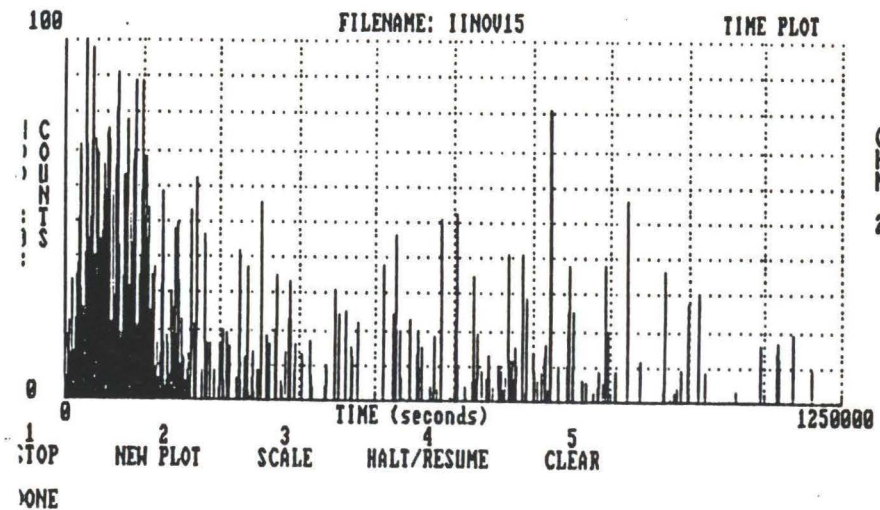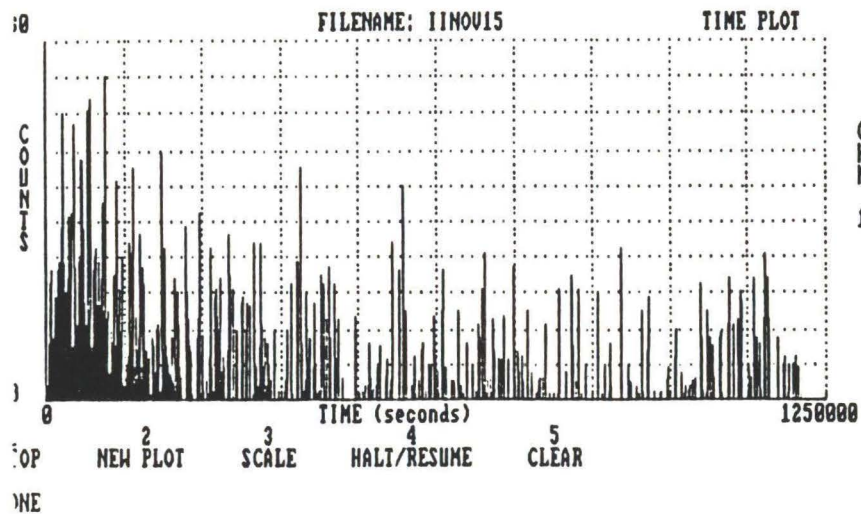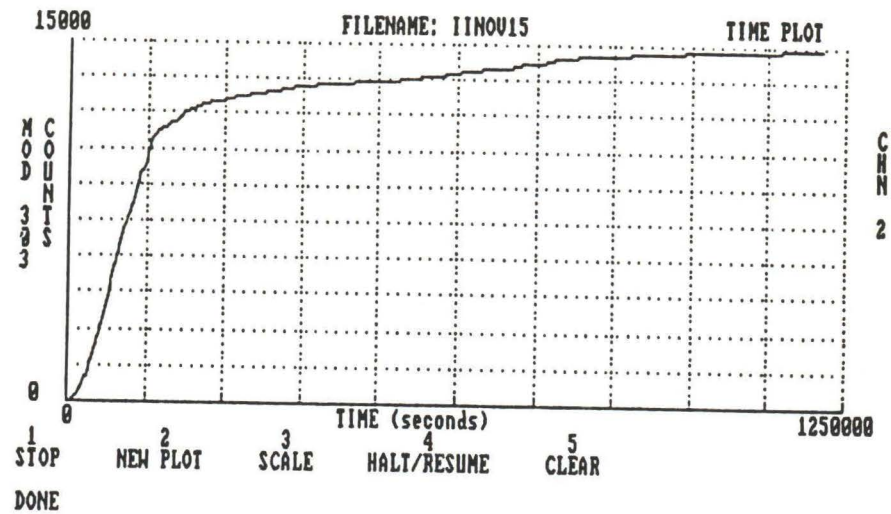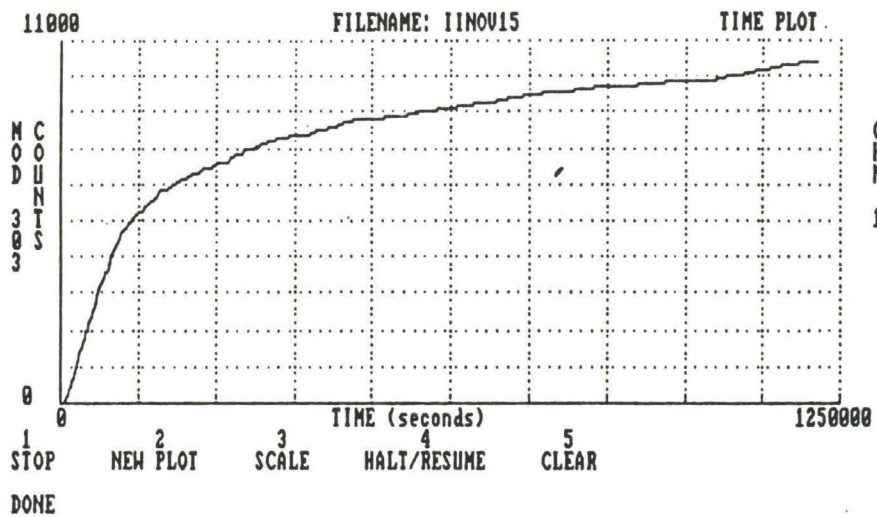
Fig. 5.7 Cumulative and as-read AE data for 2-week corrosion test. Normal
beams B3 & B4 on channels 1 & 2.
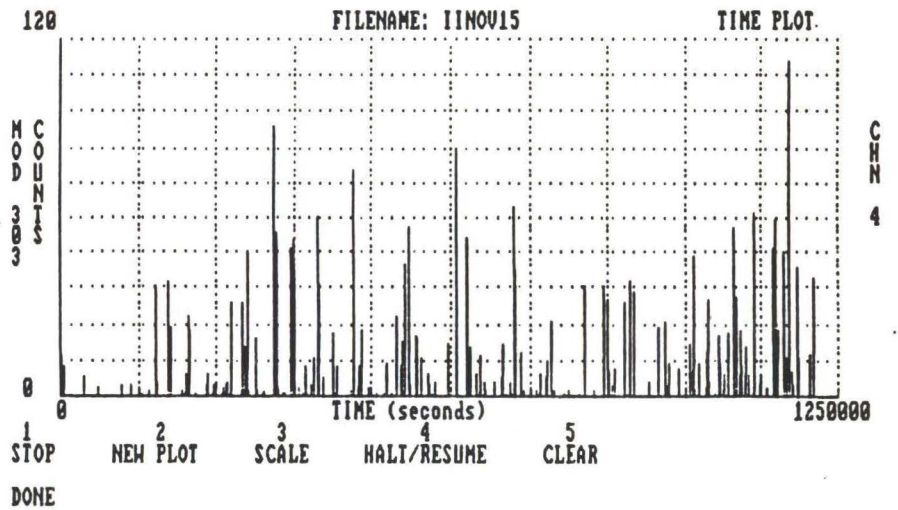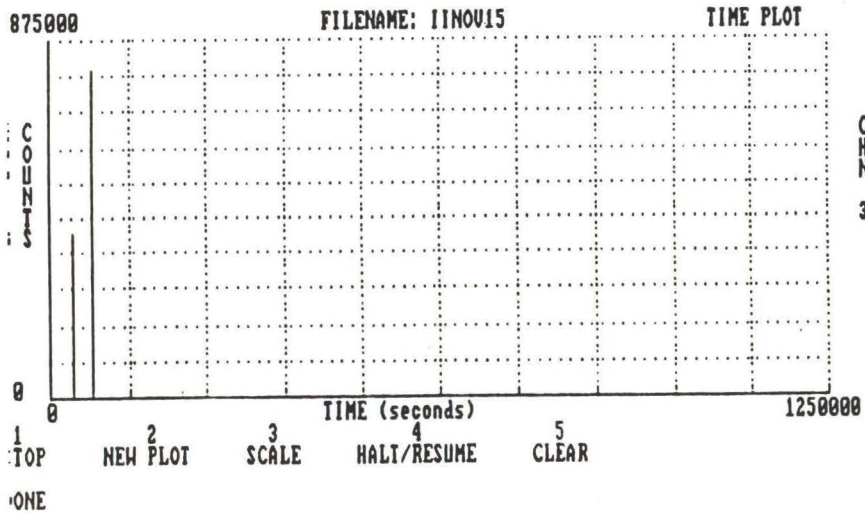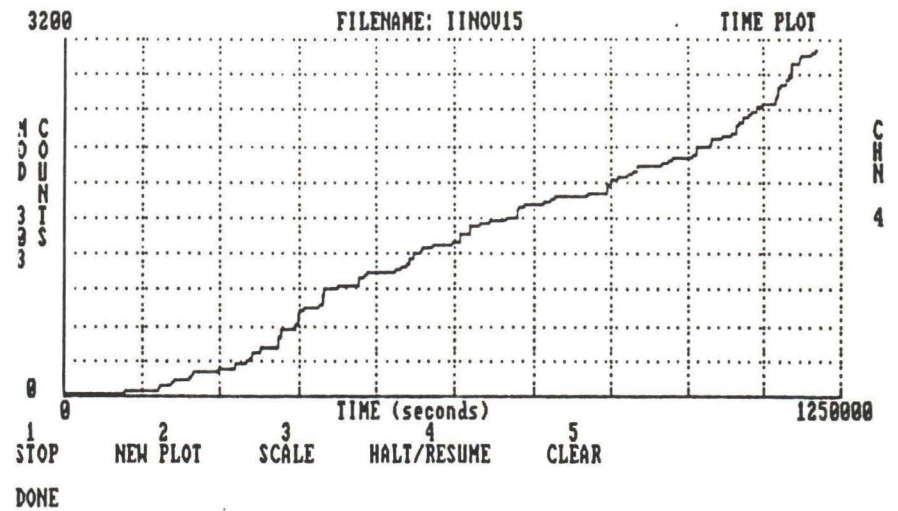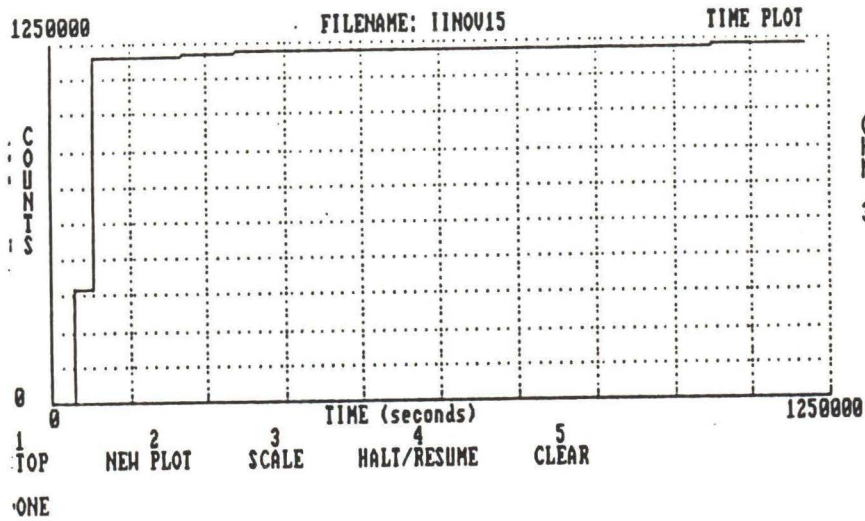
Fig. 5.8   Cumulative and as-read AE data for 2-week corrosion test. Flyash
beams F27 & F28 on channels 3 & 4.
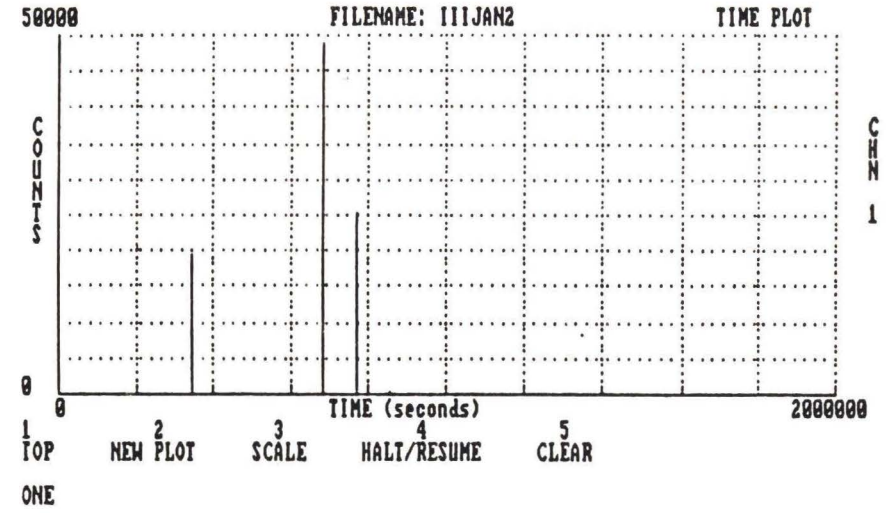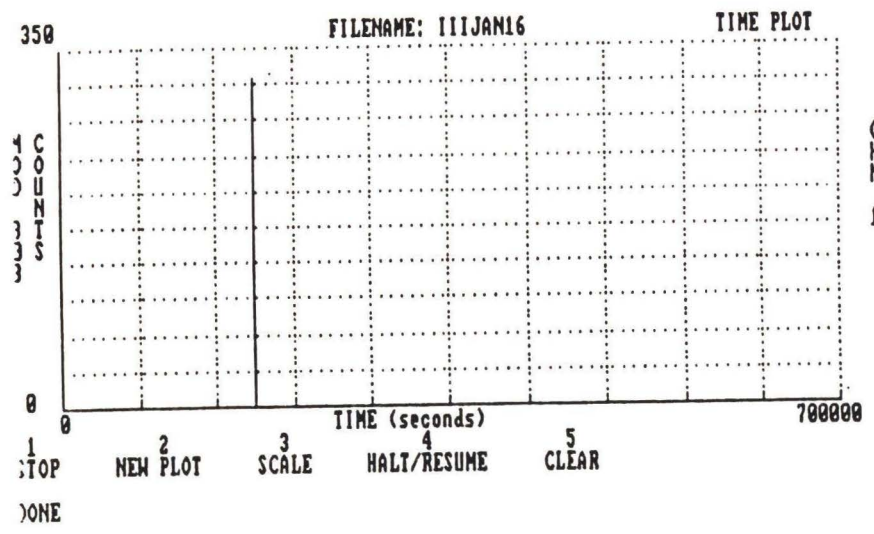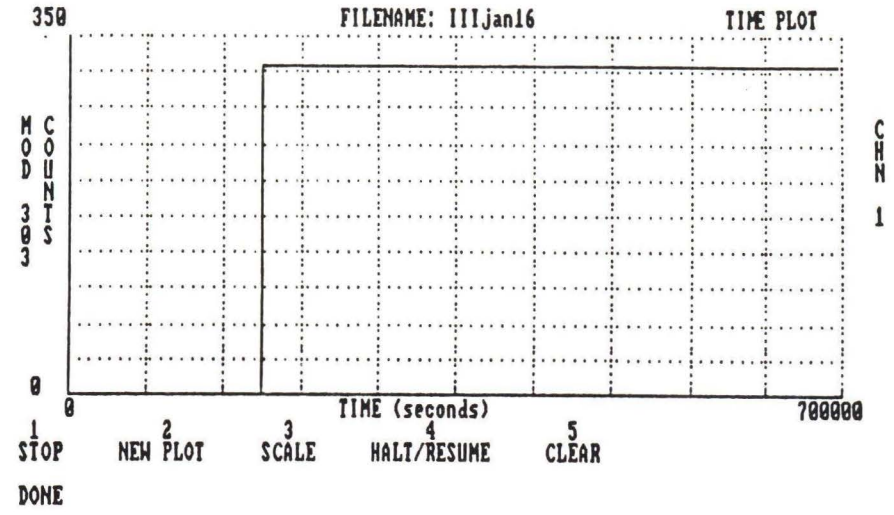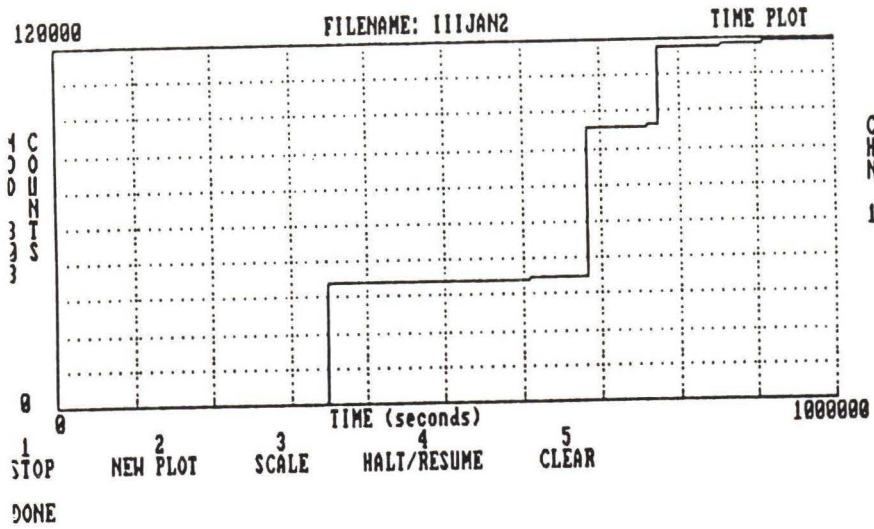
Fig. 5.9   Cumulative and as-read AE data for 3-week corrosion test. Flyash
beam F29 on channel 1.

Top-left plot:
1.5E+07
FILENAME: IIIJAN2
TIME PLOT
M O D 3 0 3 | C O U N T S
C H N 2
0
TIME (seconds)
0 1000000
1 STOP   2 NEW PLOT   3 SCALE   4 HALT/RESUME   5 CLEAR
HALT

Top-right plot:
5E+07
FILENAME: IIIjan16
TIME PLOT
M O D 3 0 3 | C O U N T S
C H N 2
0
TIME (seconds)
0 700000
1 STOP   2 NEW PLOT   3 SCALE   4 HALT/RESUME   5 CLEAR
DONE

Bottom-left plot:
550000
FILENAME: IIIJAN2
TIME PLOT
M O D 3 0 3 | C O U N T S
C H N 2
0
TIME (seconds)
0 1000000
1 STOP   2 NEW PLOT   3 SCALE   4 HALT/RESUME   5 CLEAR
DONE

Bottom-right plot:
700000
FILENAME: IIIJAN16
TIME PLOT
M O D 3 0 3 | C O U N T S
C H N 2
0
TIME (seconds)
350000 425000
1 STOP   2 NEW PLOT   3 SCALE   4 HALT/RESUME   5 CLEAR
DONE

Fig. 5.10 Cumulative and as-read AE data for 3-week corrosion test. Flyash beam F30 on channel 2.
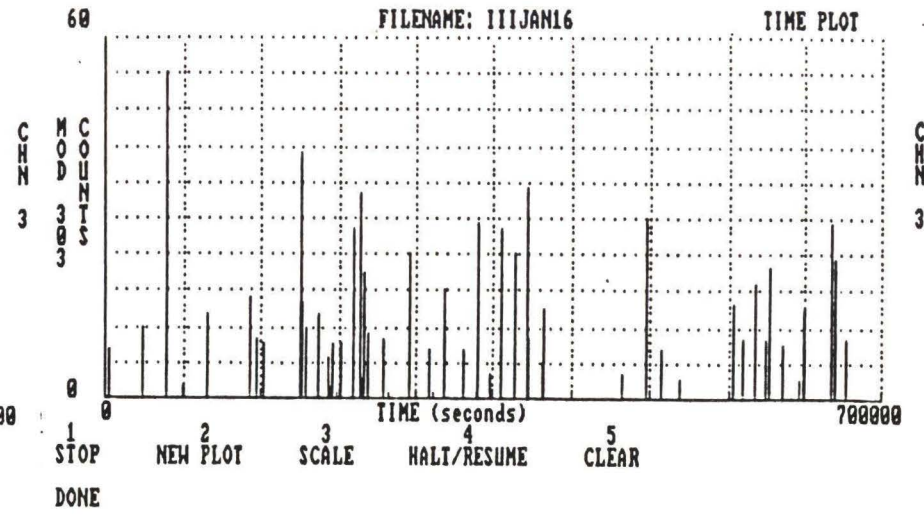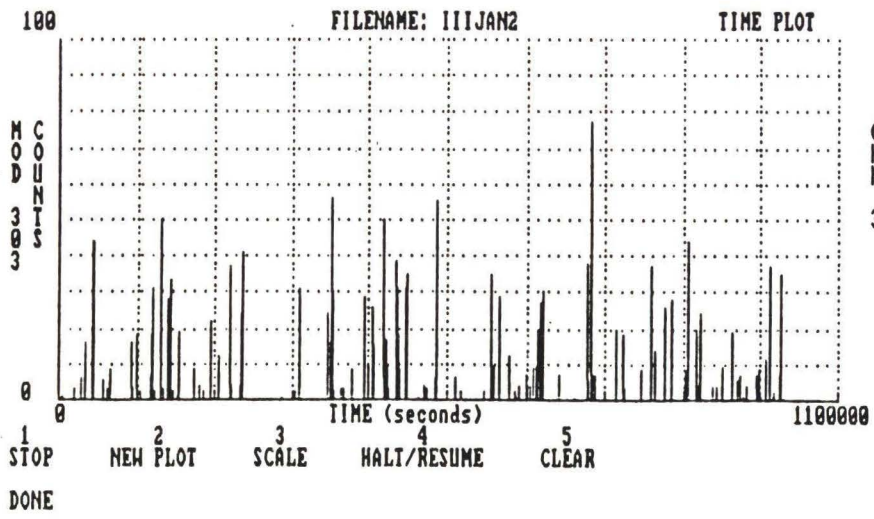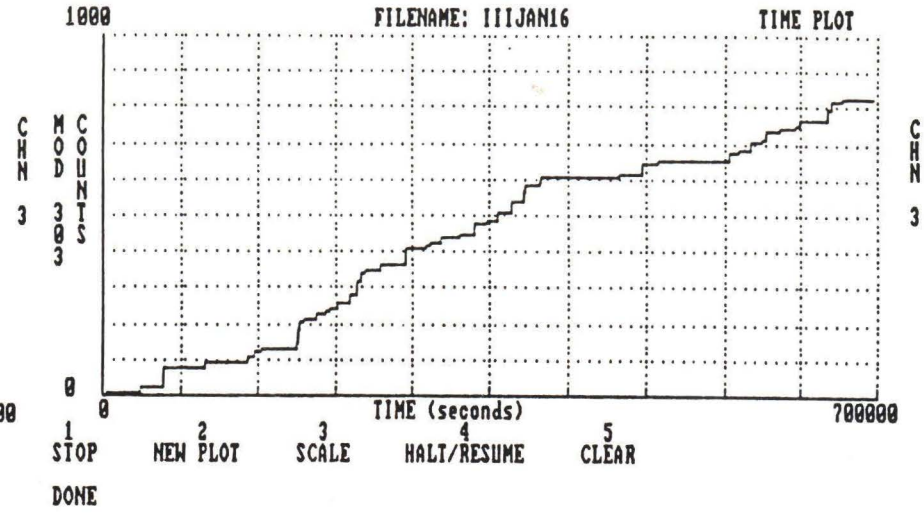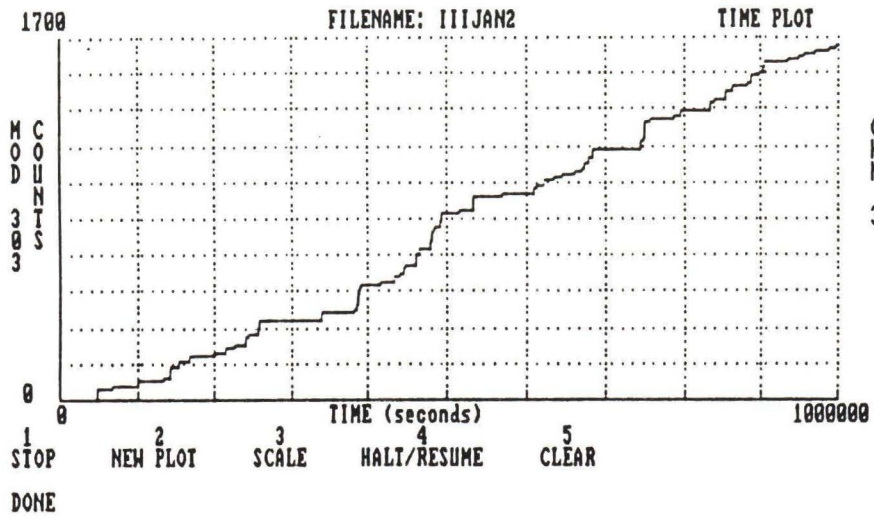
Fig. 5.11 Cumulative and as-read AE data for 3-week corrosion test. Normal beam B13 on channel 3.
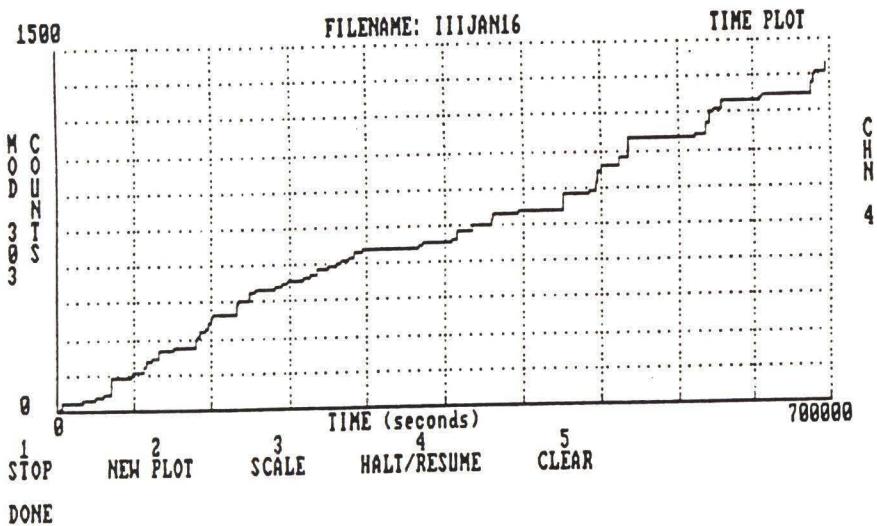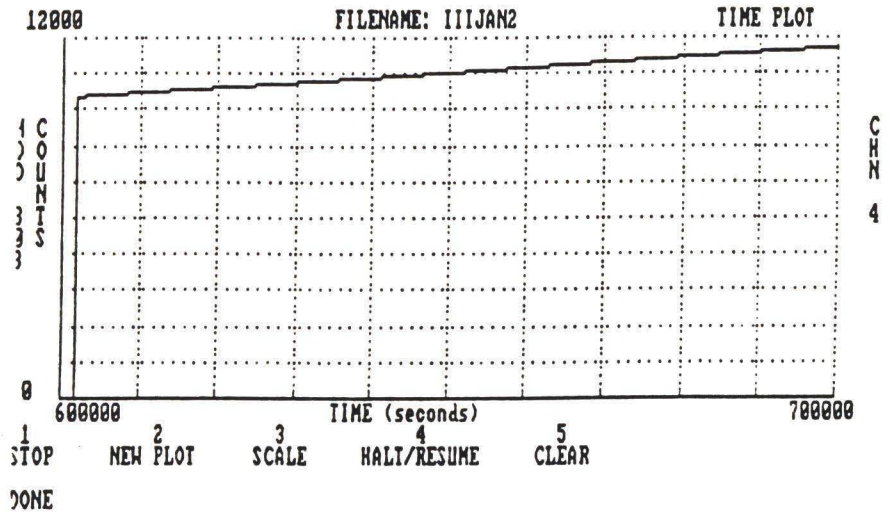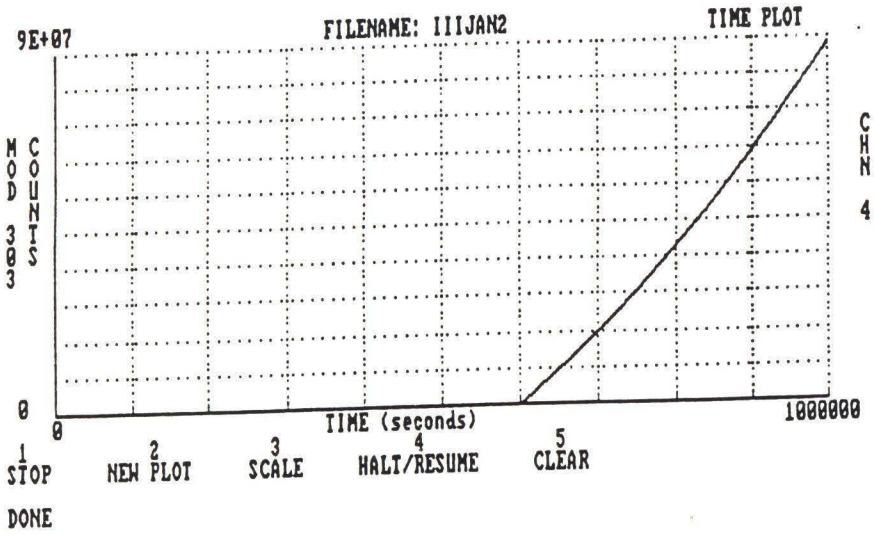
Fig. 5.12 Cumulative AE data for 3-week corrosion test. Normal beam B14 on channel 4.
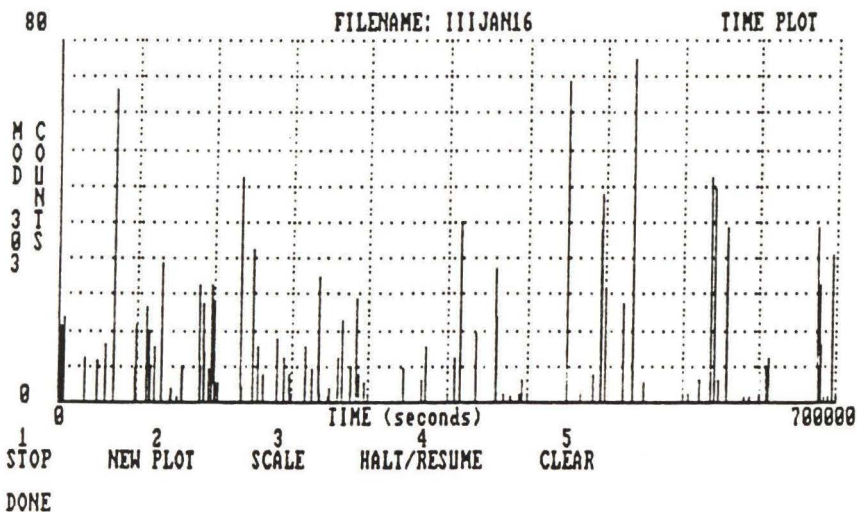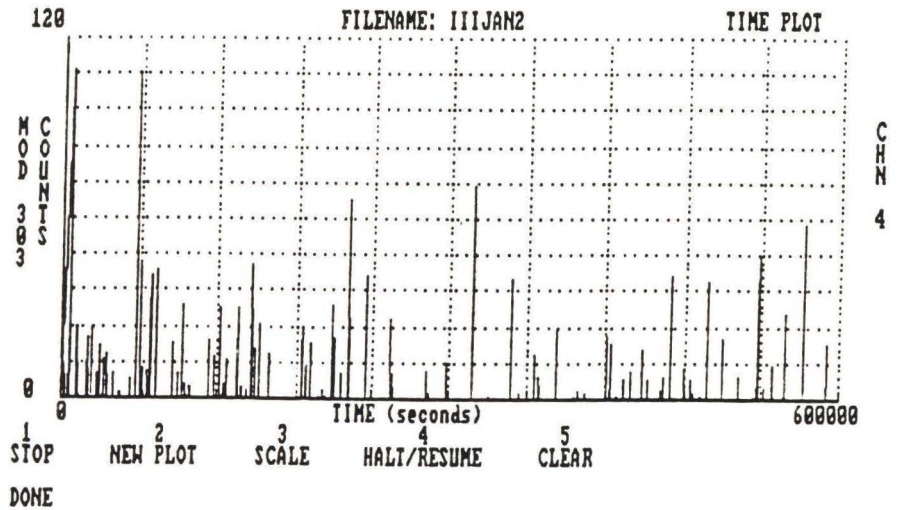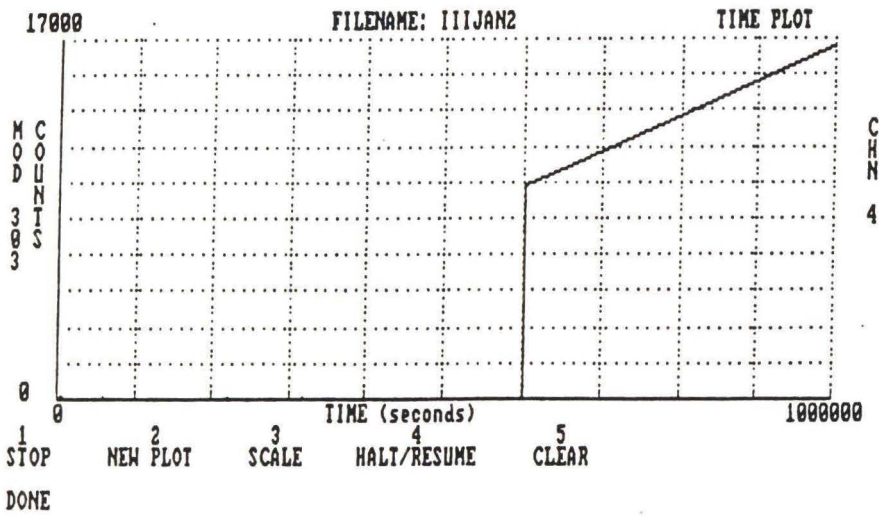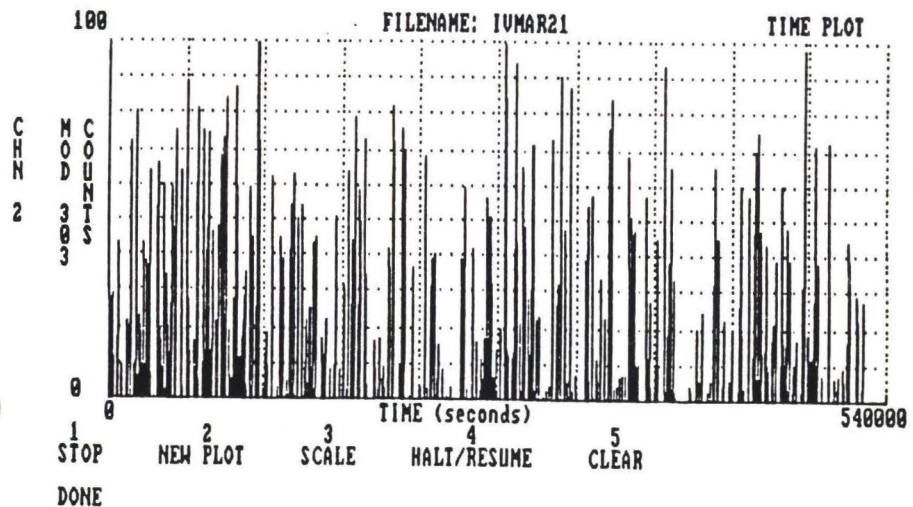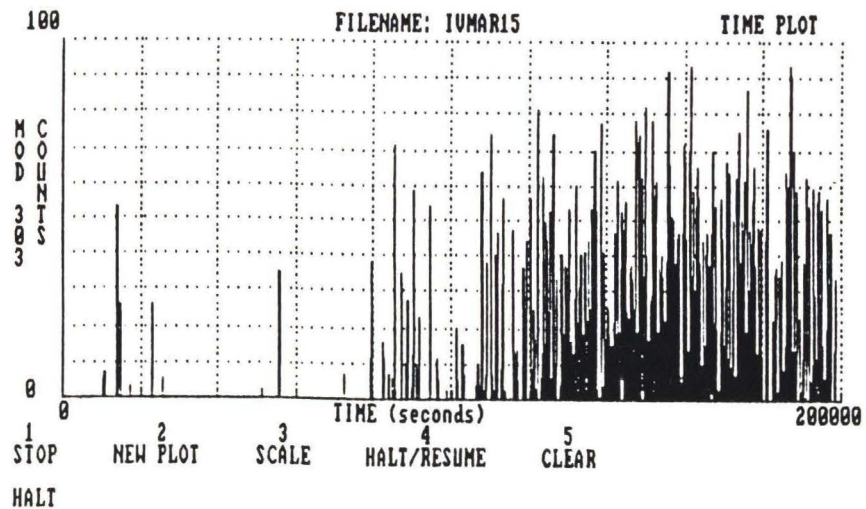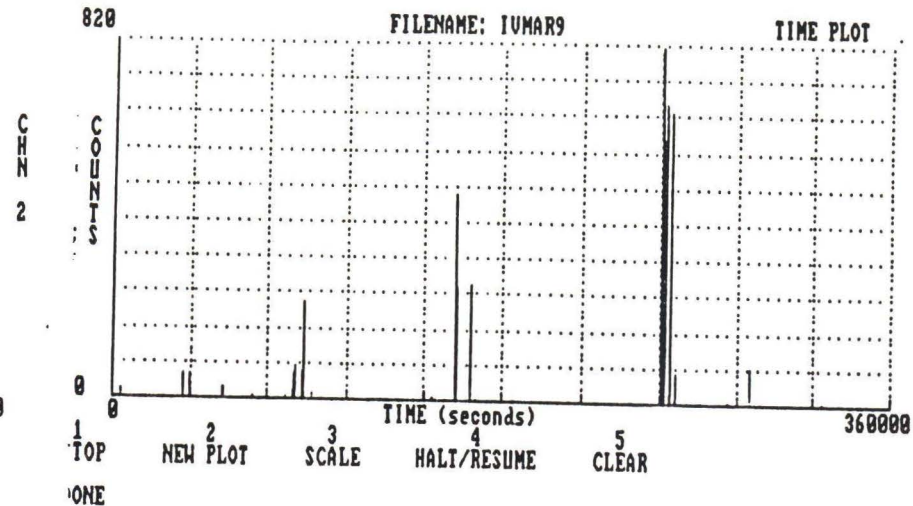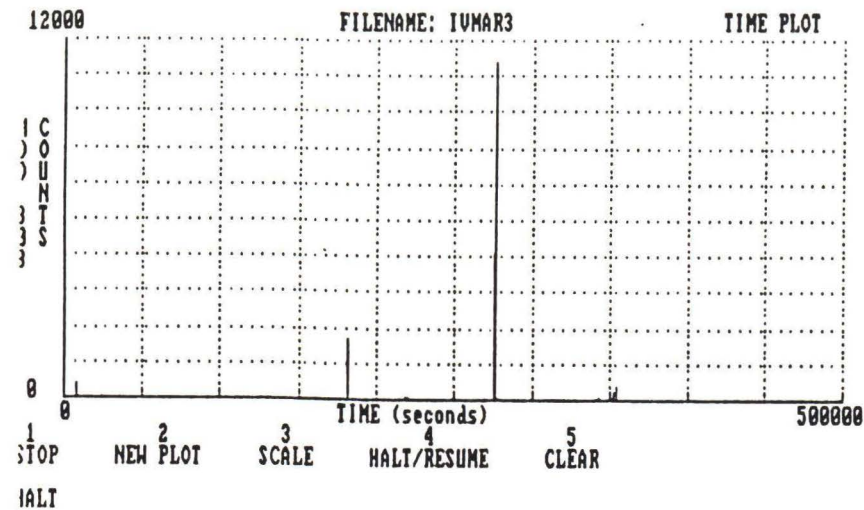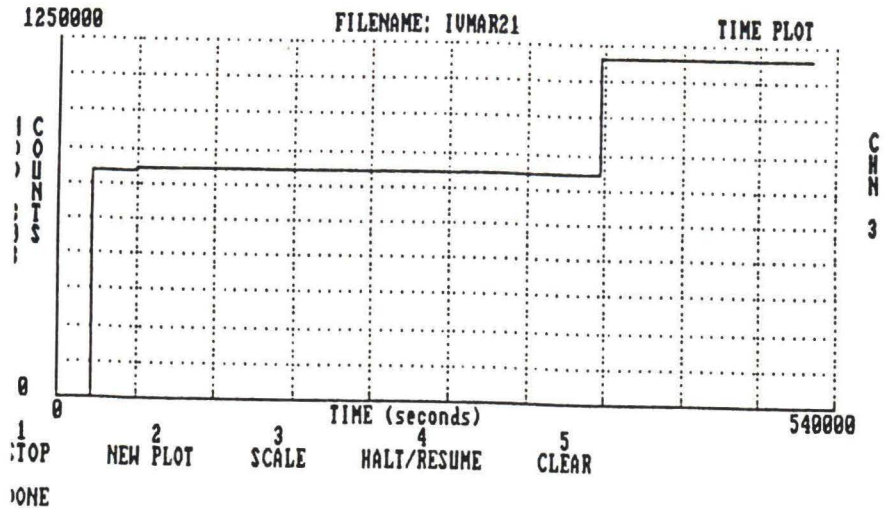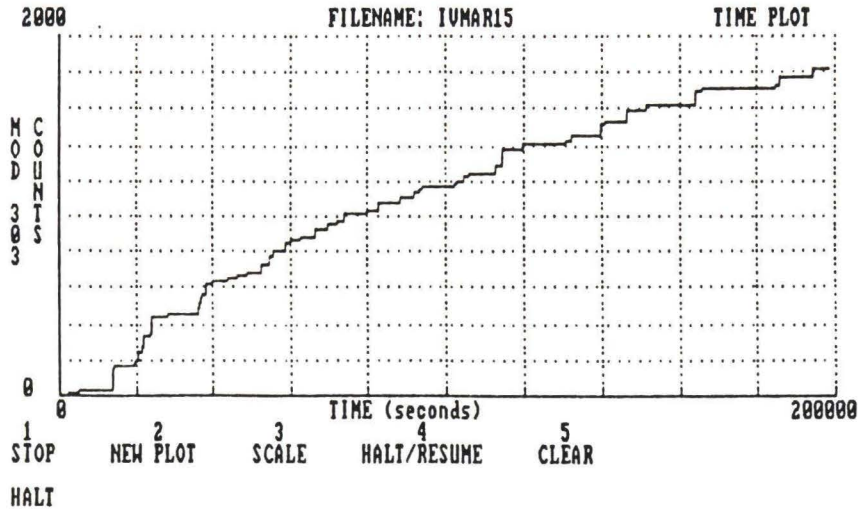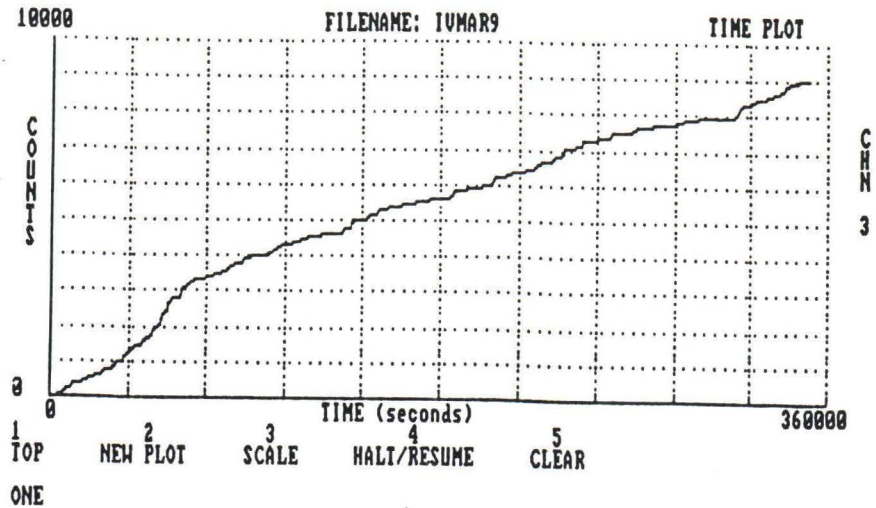
Fig. 5.13 As-read AE data for 3-week corrosion test. Normal beam B14 on channel 4.
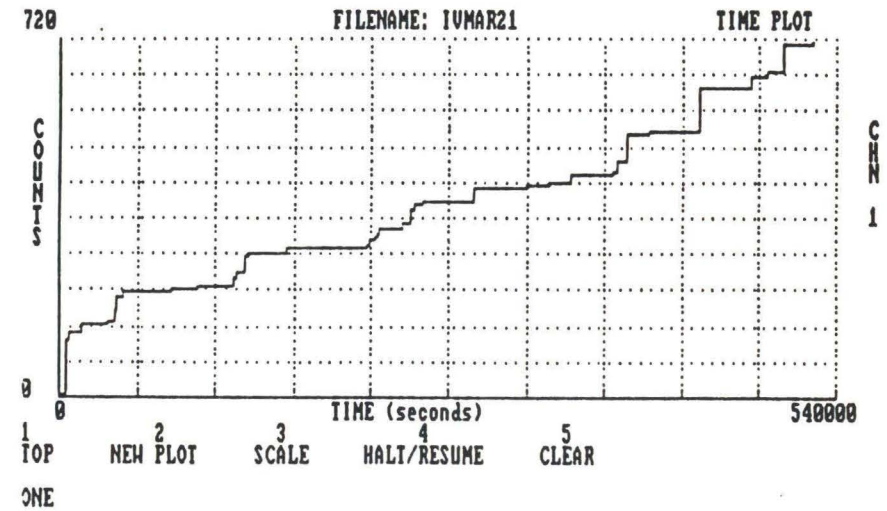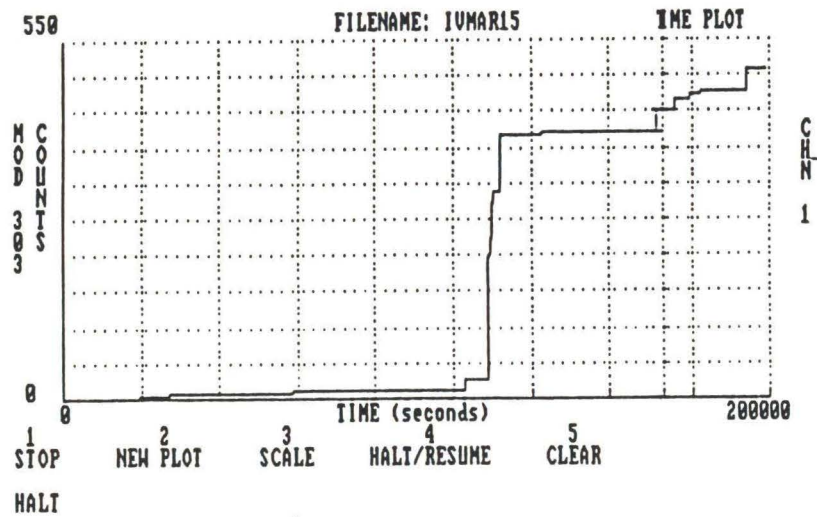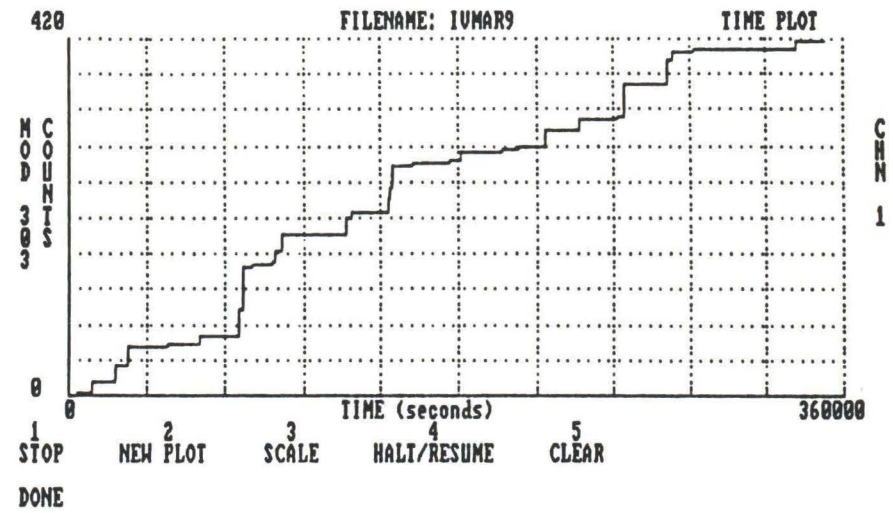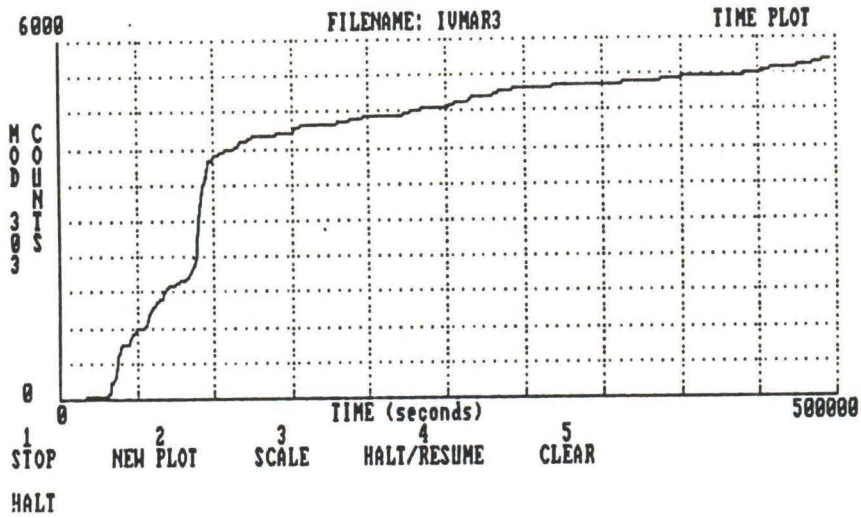
Fig. 5.14 Cumulative AE data for 3-week corrosion test. Normal beam B15 on channel 1.
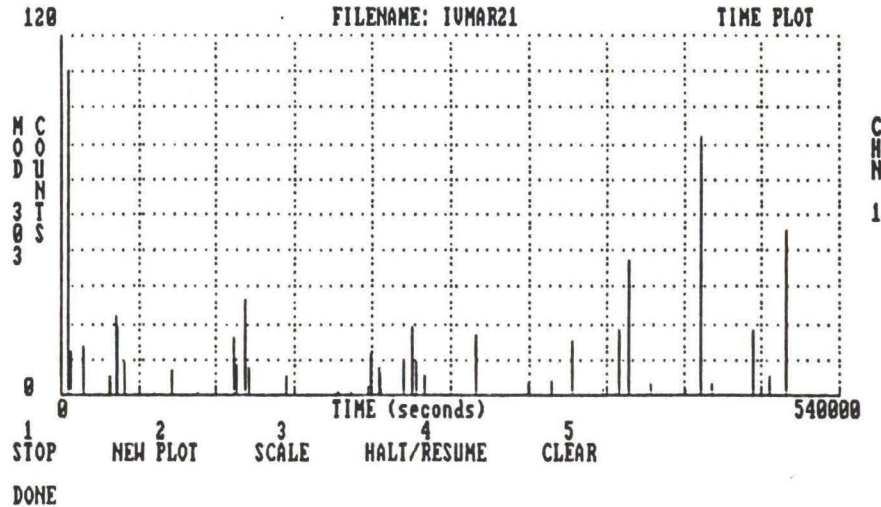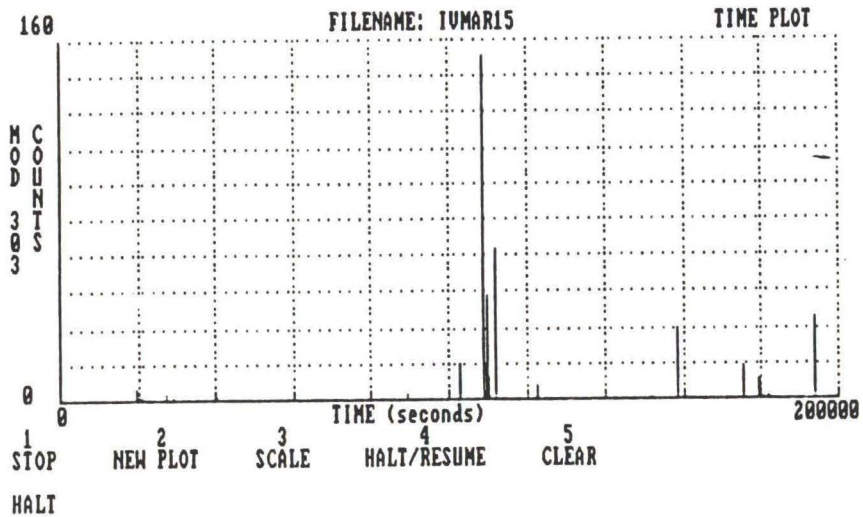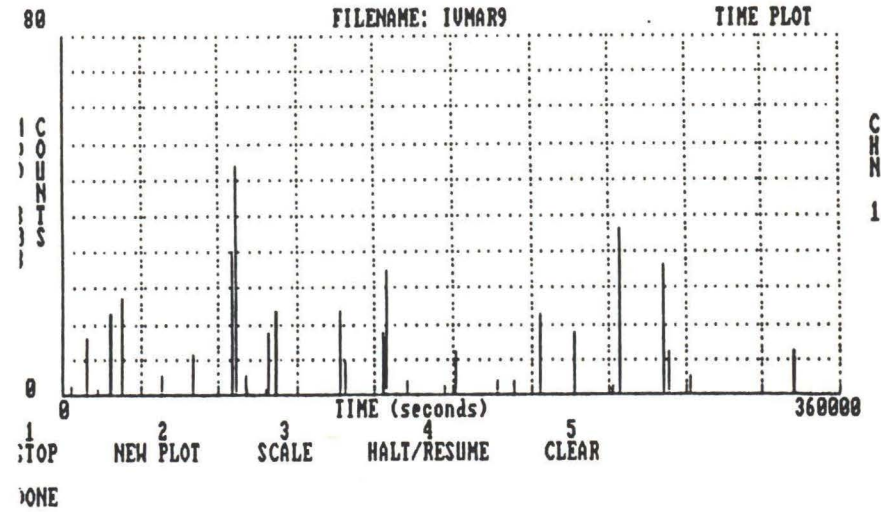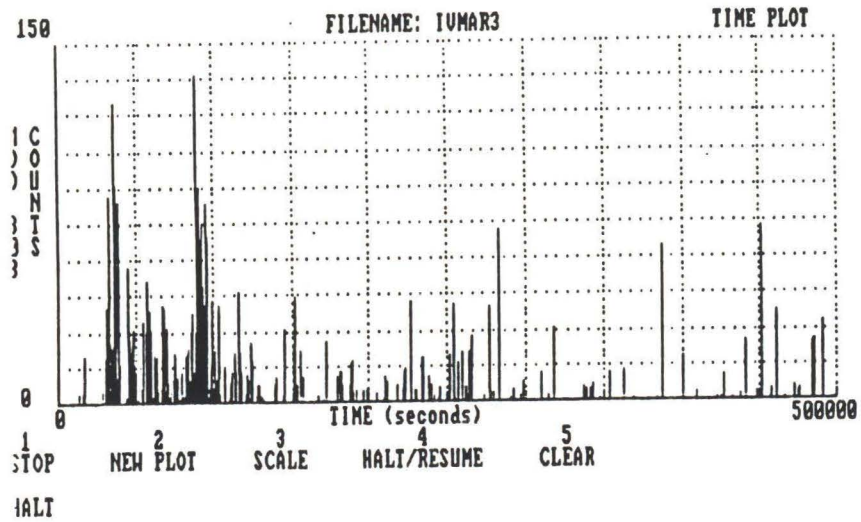
Fig. 5.15 As-read AE data for 3-week corrosion test. Normal beam B15 on channel 1.

62
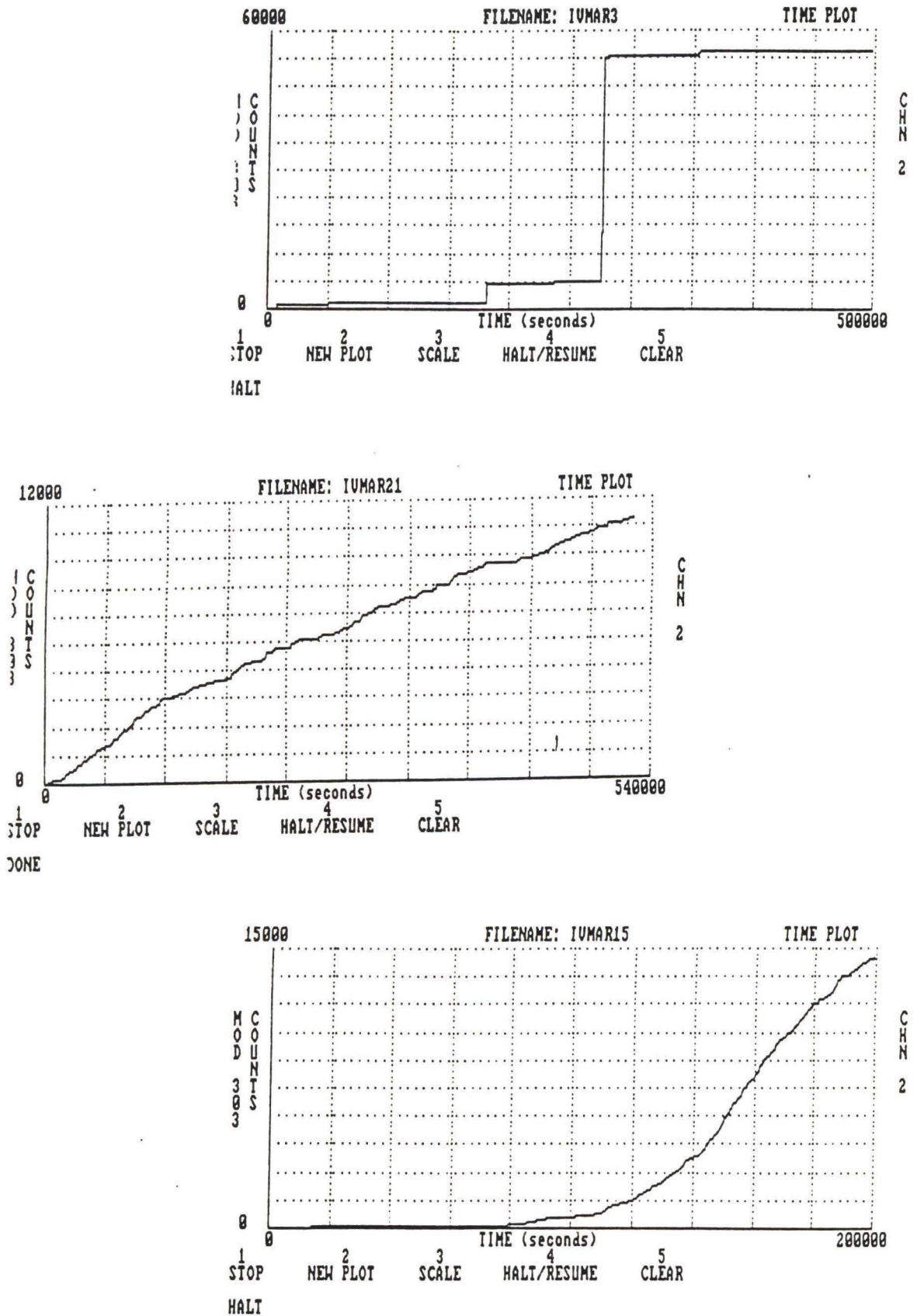
Fig. 5.16 Cumulative AE data for 3-week corrosion test. Flyash beam F29 on channel 2.

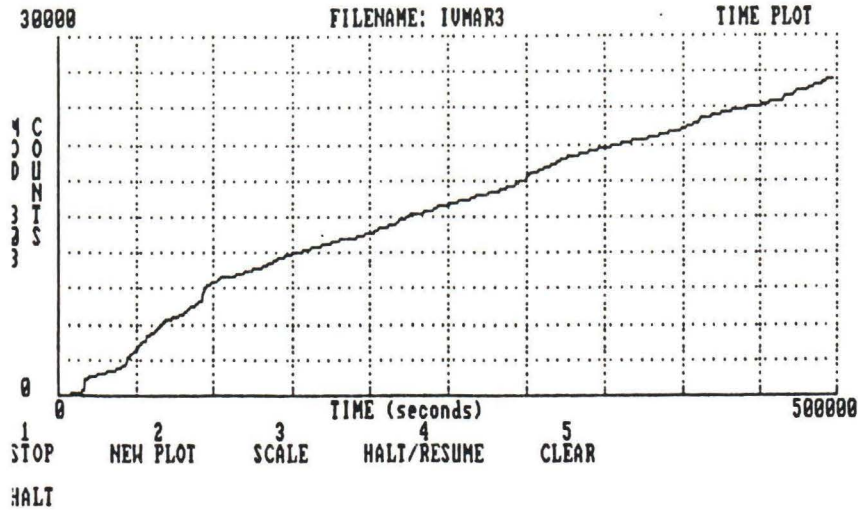Fig. 5.17   As-read AE data for 3-week corrosion test. Flyash beam F29 on channel 2.

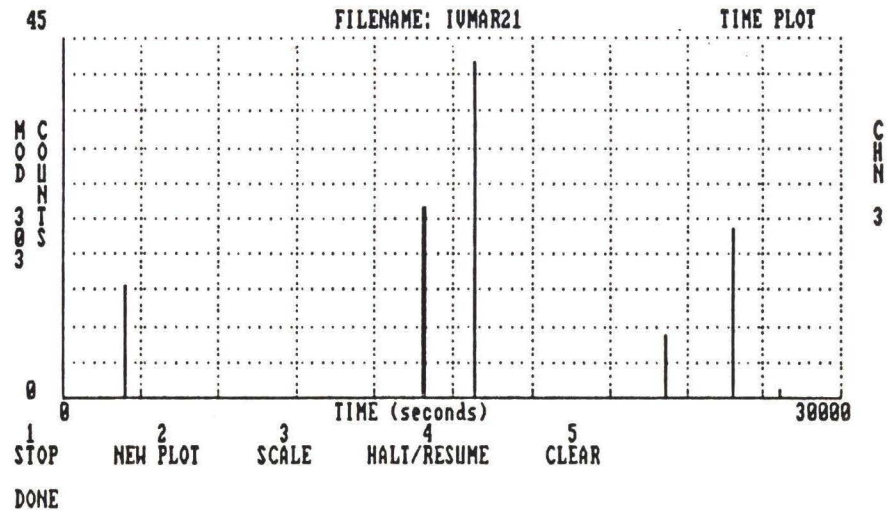Fig. 5.18 Cumulative AE data for 3-week corrosion test. Flyash beam F31 on channel 3.
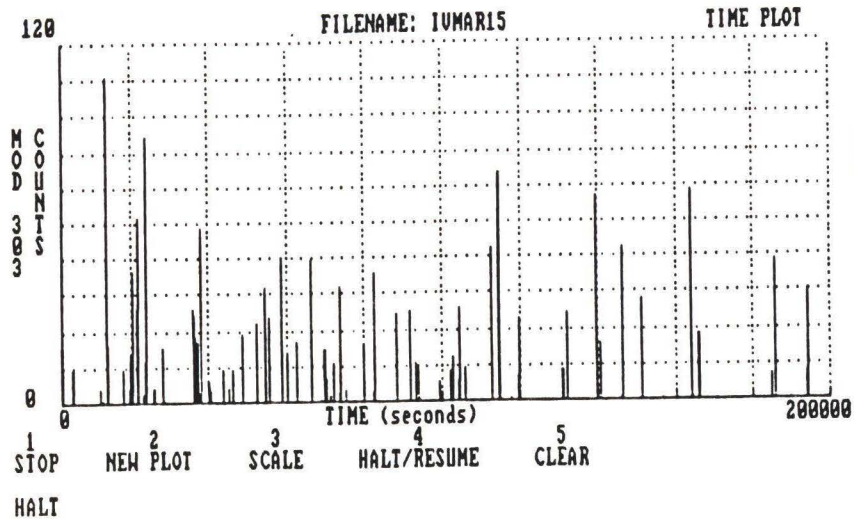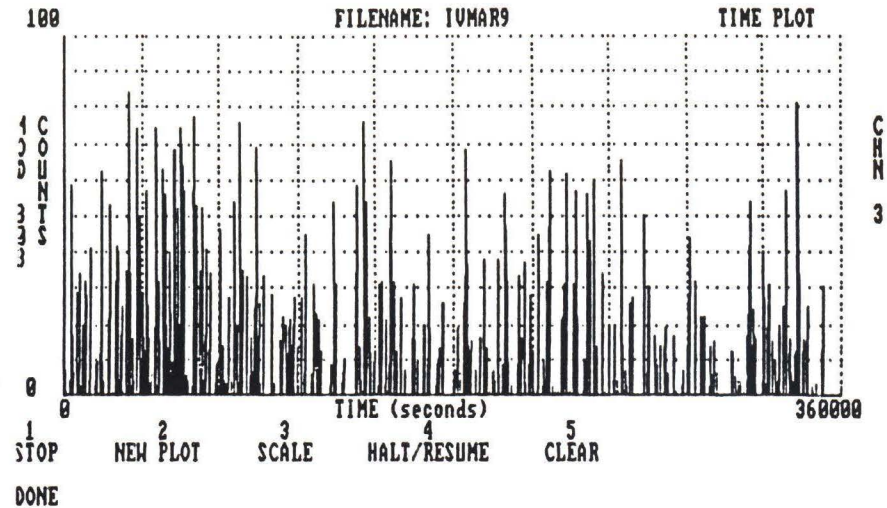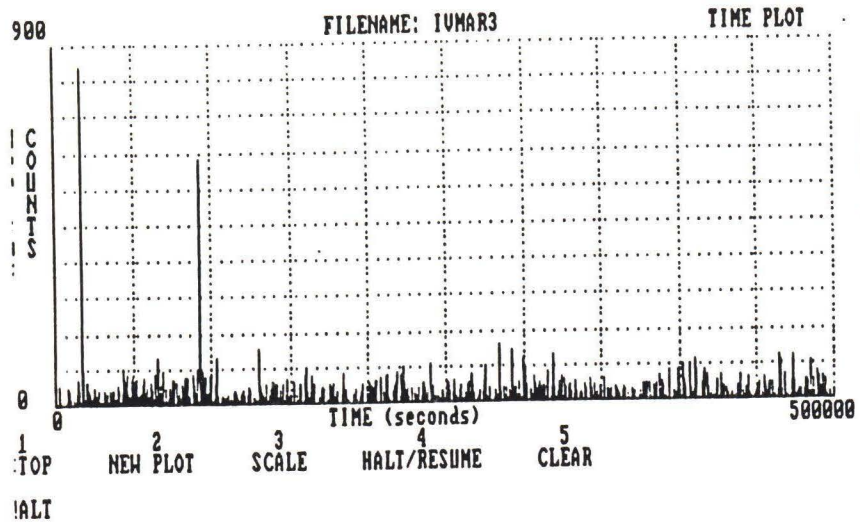
Fig. 5.19 As-read AE data for 3-week corrosion test. Flyash beam F31 on channel 3.

in the fly ash beams rather than the normal beams. In other words, the fly ash beams crack with the louder pop. This leads to the inference that fly ash beams are perhaps more brittle. Also, the event occurrence appears to be at random and a particular pattern cannot be perceived. Though the actual number of counts in a particular beam does not necessarily increase with test duration, for a set of beams as a whole this does seem to be the case. Moreover, corrosion induces continuous rather than discrete emissions, as can be seen from the as-read graphs.

5.2 FLEXURE TESTS

Eight beams were subjected to flexure tests and the test set up is shown in the photographs in Fig. 5.20. Since all the beams have the same type and configuration of reinforcement, it would be fair to compare their performance based on their rupture moduli calculated as

$$R = Pl/bd^2 \tag{12}$$

where

R = rupture modulus (psi)

P = failure load (lb.),

l = span (in.),

b = beam width (in.), and
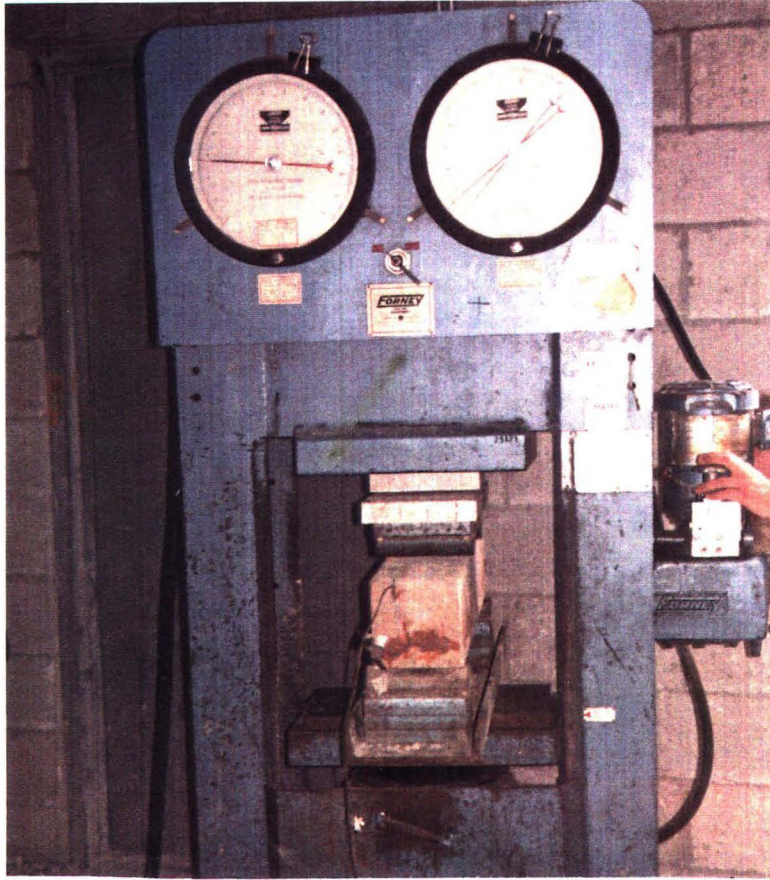
d = beam depth (in.).

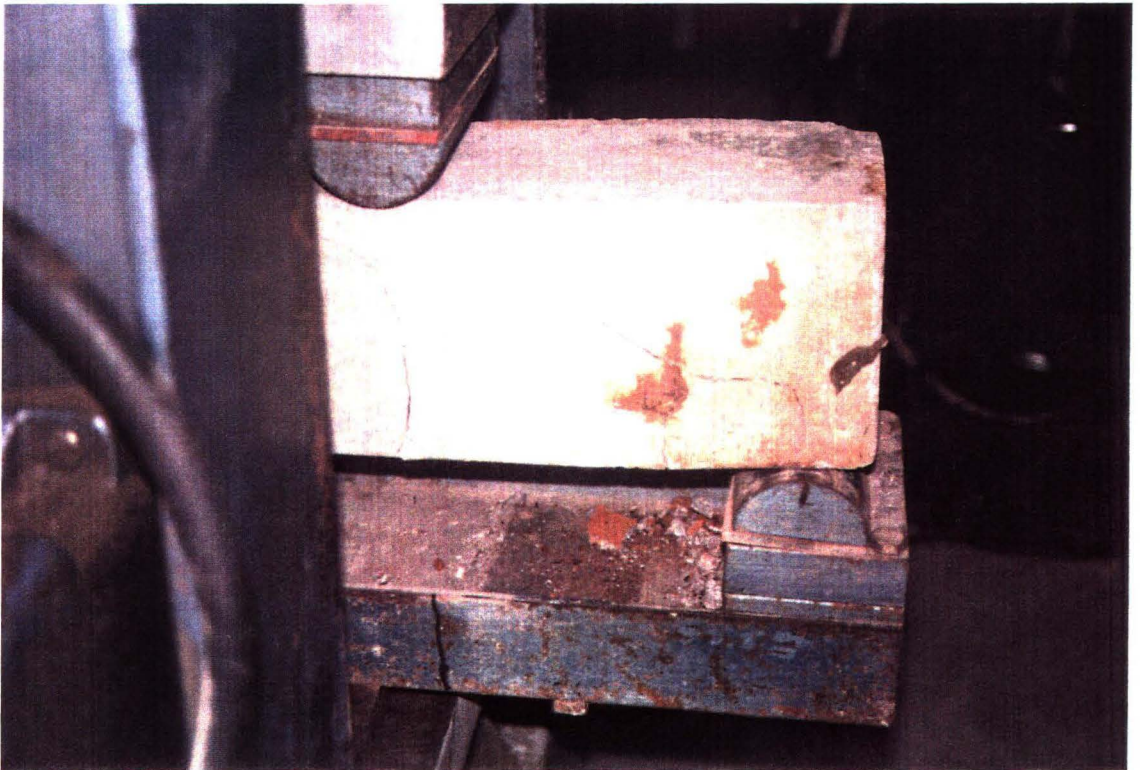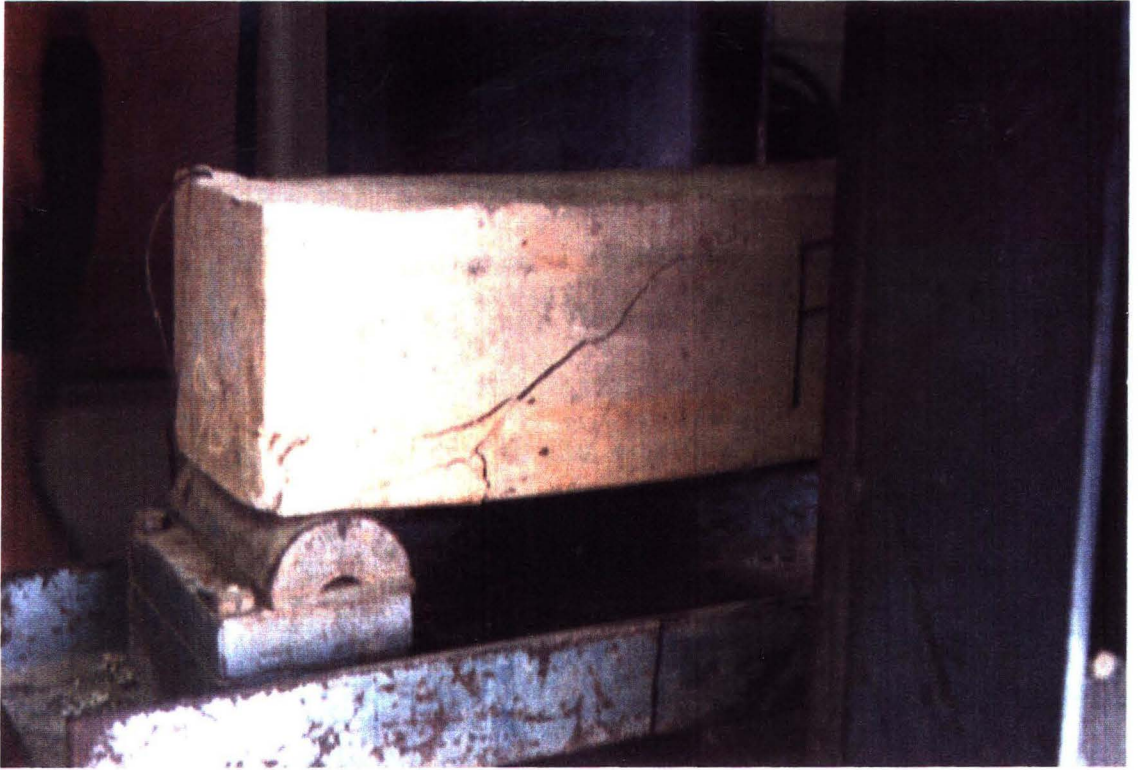Fig. 5.20 Photographs of flexure test setup.

Fig. 5.21   Photographs of flexural cracks.

The flexural cracks can be seen in the photographs in fig. 5.21.

Table 5 gives the flexure test results. The normal concrete beams performed better in flexure than the fly ash beams especially as the test duration increased. In the two and three-week tests, the rebars are more corroded and their influence on the flexural performance is greatly diminished. The test performances depend more on the intrinsic tensile strengths of the two types of concrete. This leads us to infer once again that fly ash modified concrete has less tensile strength and is more brittle. Fig. 5.22a shows the graph of ultimate load against corrosion period, while the graph in Fig.5.22b is a plot of the load at first crack versus the corrosion period. This illustrates the fact that normal concrete is capable of withstanding tensile loads better than fly ash concrete.

5.3 IMPACT TESTS

The impact test was performed on eight beams with the test setup shown in Fig. 5.23. This test setup is the same as that was used by Desnoyers (1987). However the test parameters were modified to suit the changed specimen configuration.

The specimens were placed on hinge supports with a 28 in. clear span. The drop height was set at 5 ft. to ensure plastic failure. The impact velocity was 546 cm./sec. A 0.25 in. thick rubber pad was introduced in the tup-

Table 5 - Flexure Test Results

BEAM #	Corrosion Period (Weeks)	Load at First Crack (lb)	Ultimate Load (lb)	Modulus of Rupture (psi)
F26	1	6200	19200	2400
F28	2	4000	10500	1310
F32	2	4700	11100	1390
F30	3	4100	5300	660
B2	1	8400	17500	2190
B4	2	6200	11400	1420
B16	2	6000	12200	1520
B15	3	4900	10000	1250

Table 6 - Impact Test Results

BEAM #	Corrosion Period (Weeks)	Peak Load (kip)	Energy (ft-lb)
F25	1	2.7	120.0
F27	2	2.3	110.0
F29	3	2.2	104.0
F31	3	1.8	66.0
B1	1	2.5	112.0
B3	2	2.6	108.0
B13	3	1.8	68.0
B14	3	1.9	80.0

Prefix 'F' denotes flyash modified reinforced concrete beam.
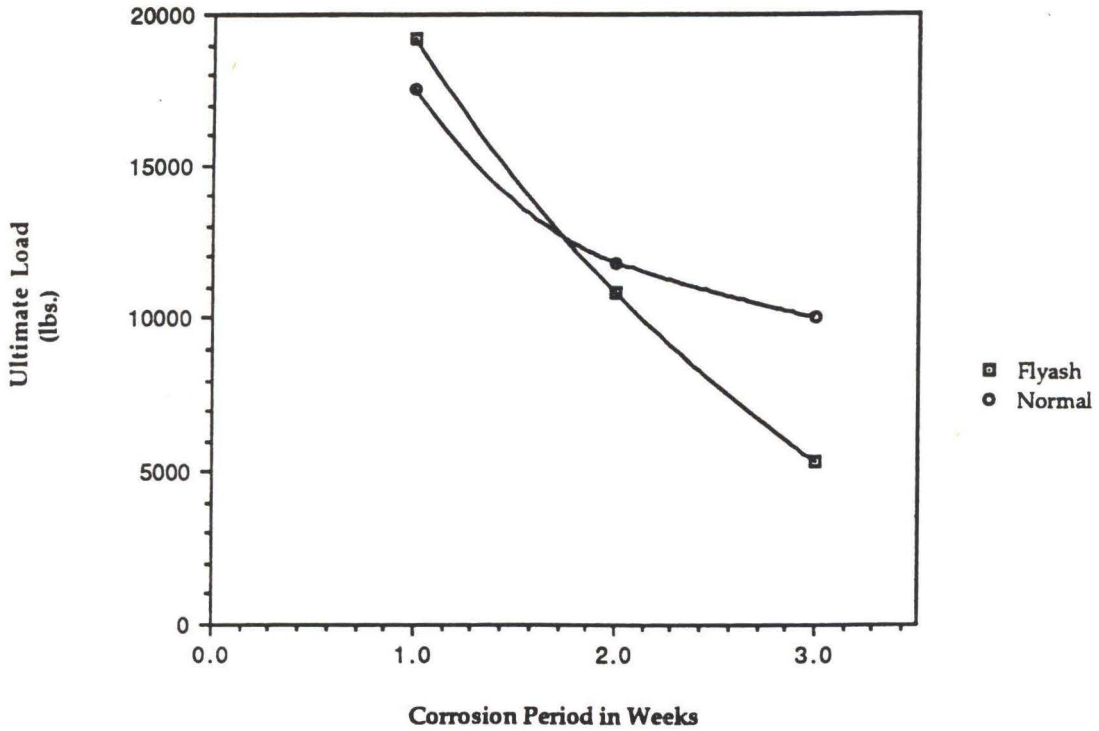Prefix 'B' denotes normal reinforced concrete beam.

Fig 5.22a Ultimate flexural strength of flyash and normal concrete beams
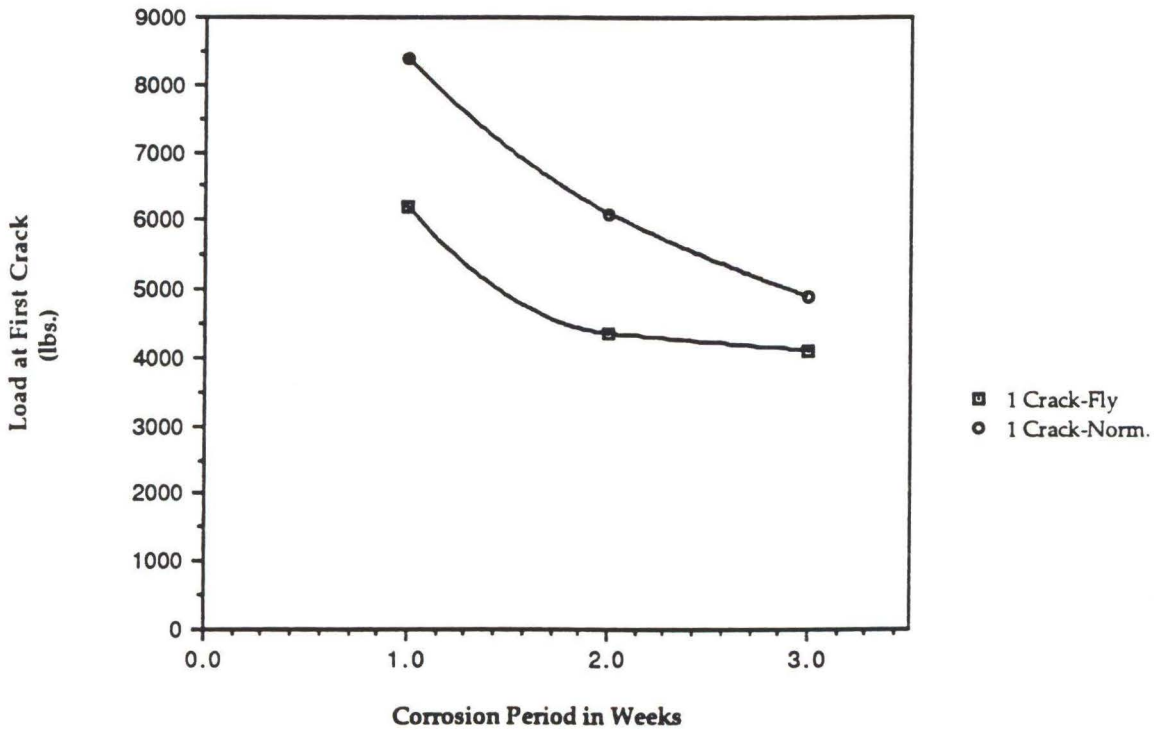

Fig. 5.22b Load at first crack for flyash and normal concrete beams in flexure

specimen contact zone to minimize the inertial effects. The dual sweep magnitudes were set at 2 µs., while the load and energy traces were calibrated to 1 kip/division and 20 ft-lb./division respectively. Table 6 shows the impact test results. Fig. 5.24a shows the oscilloscope, while Fig. 5.24b shows the yielded steel. The fly ash beams performed better than the normal concrete beams as can be seen from Table 6.

The photographs in Fig. 5.25a show the oscilloscope traces for a fly ash and a normal concrete beam respectively. Here again one can see the rebound as a clearly defined hump in both the load and energy traces of the normal beam; the fly ash beam does not display this characteristic. This again alludes to the fact that the fly ash beams are more brittle.

Fig. 5.25b(i) is a plot of impact energy versus corrosion period. The loss in the bond strength between the rebars and the concrete, due to corrosion, leads to the reduction in strength as can be seen from the decreasing strength with increasing duration of accelerated corrosion. Fig. 5.25b(ii) shows the graph of peak load versus corrosion period.

5.4 FRACTURE MECHANICS TESTS

The AE monitoring of the fracture mechanics tests showed some interesting facts. Each test method has its own AE plot pattern. The stable slow crack growth can be identified by a gradual increase in AE counts with
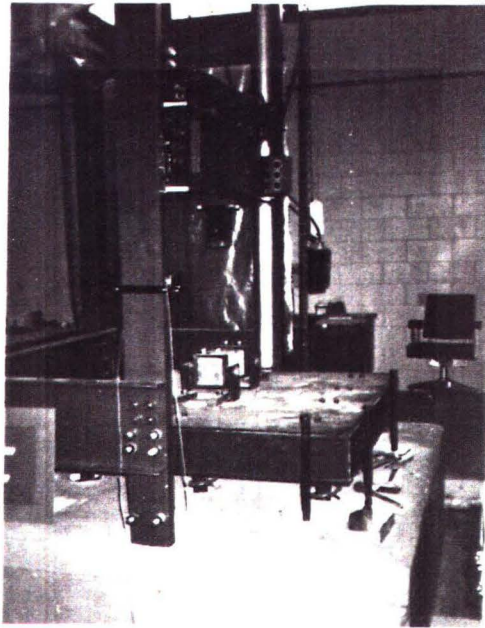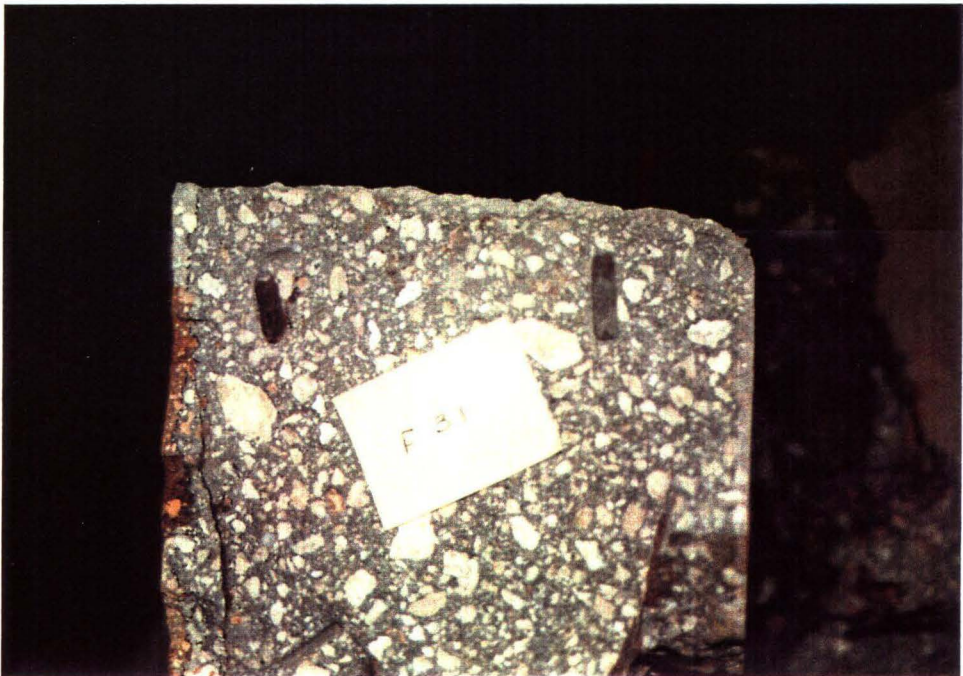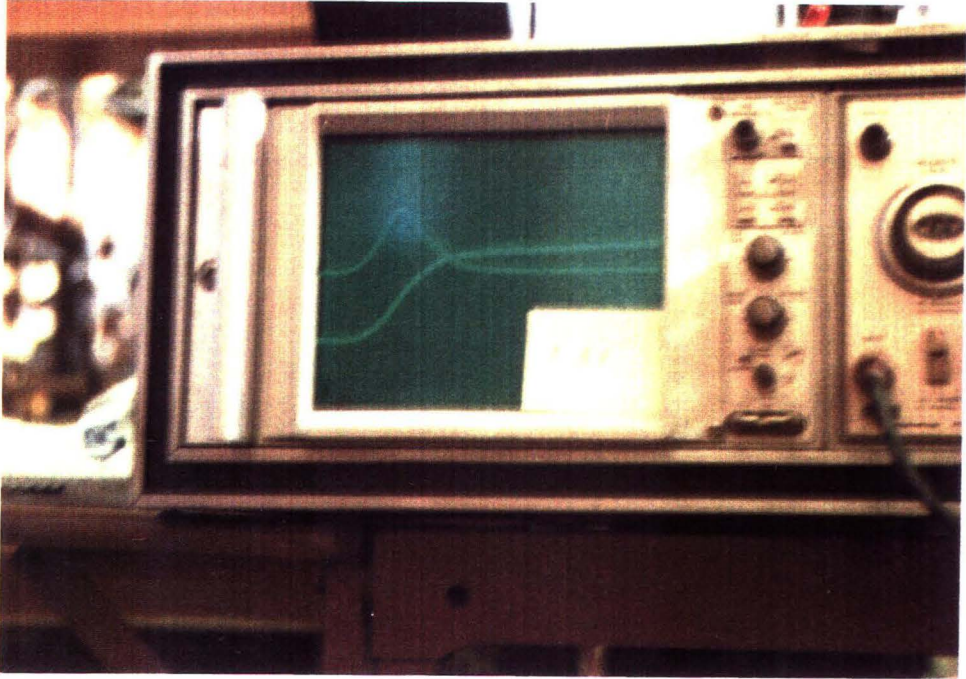
Fig. 5.23 Photographs of the impact test setup.

Fig. 5.24   Photographs of the oscilloscope and yielded steel.
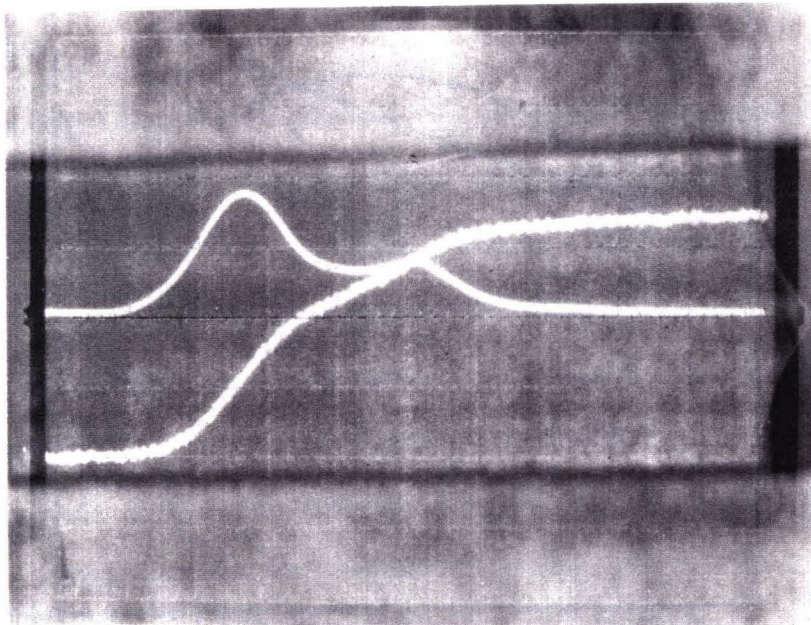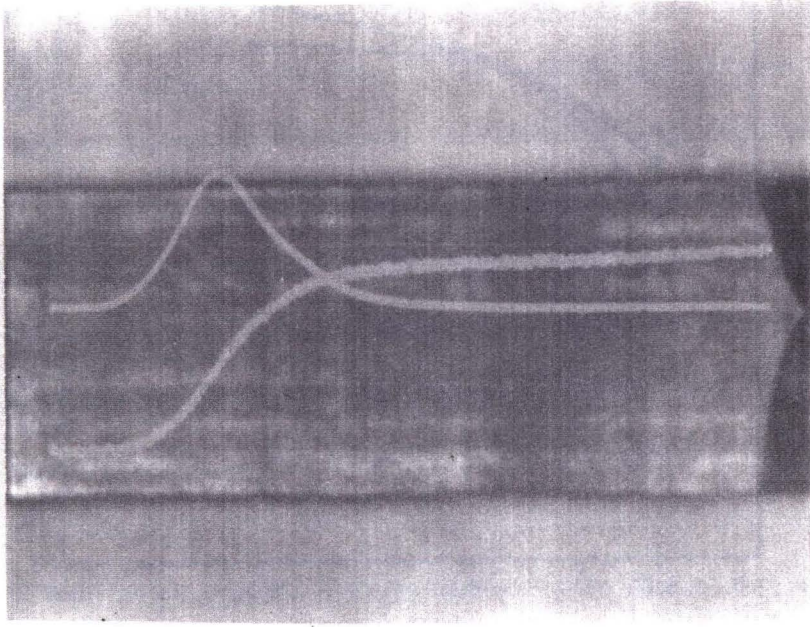
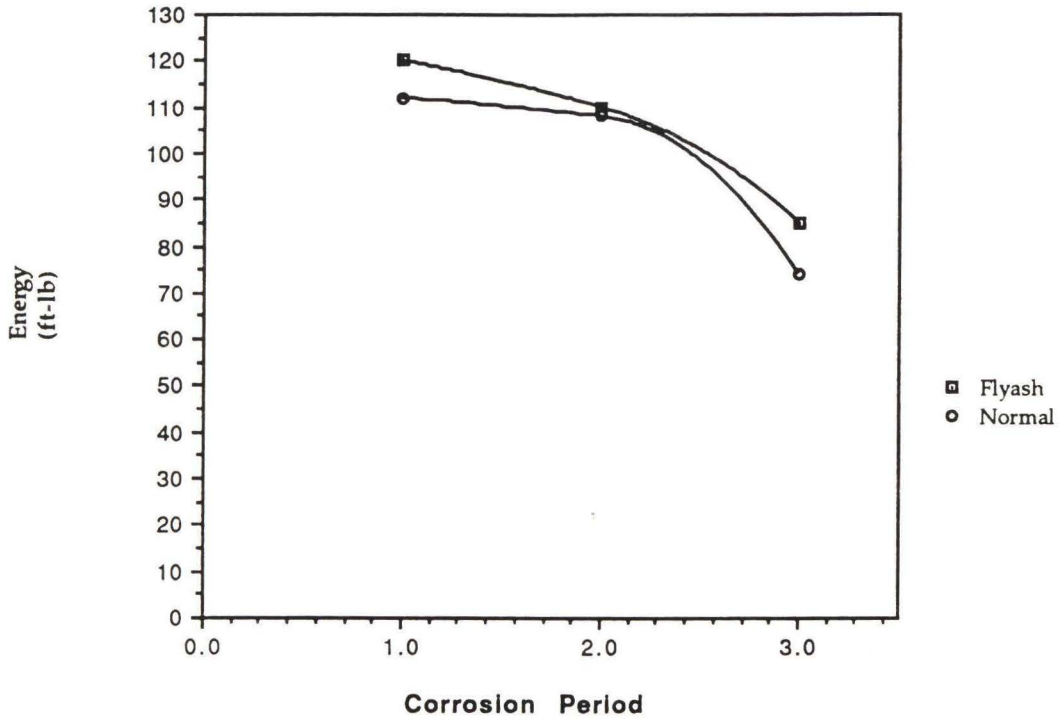Fig. 5.25a   Oscilloscope traces for flyash and normal beams.

Fig. 5.25b(i) Impact energies to failure of flyash and normal concrete beams
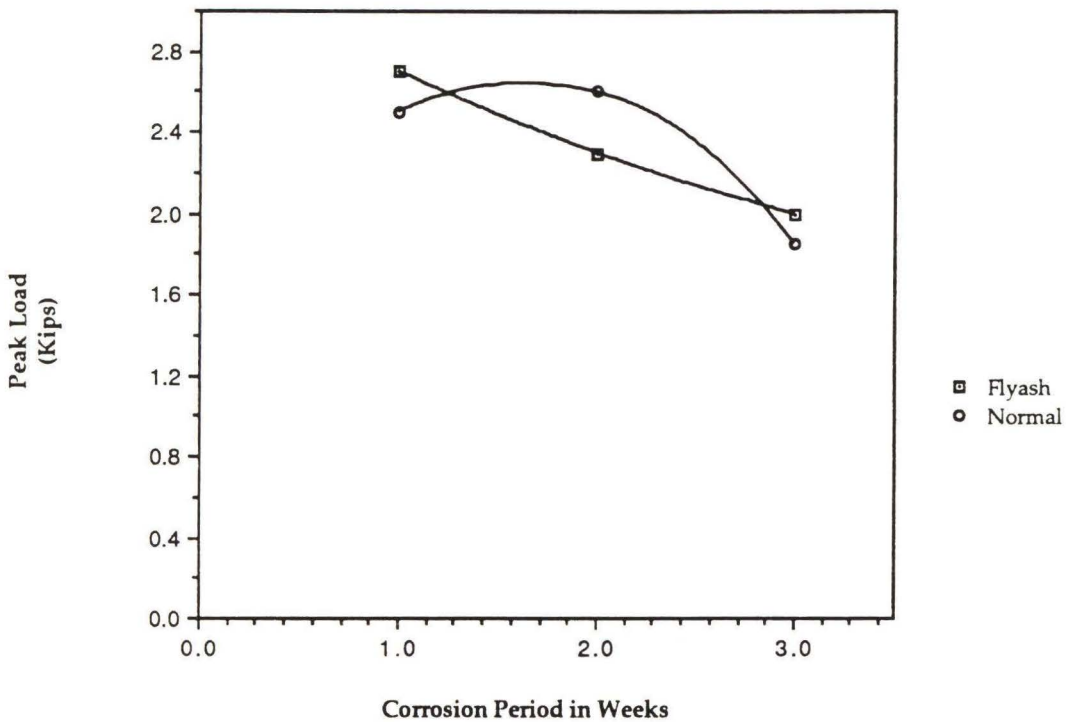

Fig. 5.25b(ii) Peak load in impact for flyash and normal concrete beams

time, upto a certain instant in time when AE plot jumps up sharply. The wedge splitting test (WST) indicated the most stable slow crack growth, while the split cube compression test (SCCT) showed an abrupt and steep growth tendency. The common phenomenon observed in both tests was a sudden jump of AE counts at a certain time. The region from initiation to sudden jump of AE counts corresponds to the region from zero to a point just below the maximum applied load. In order to investigate this region closely, another plot was made with several selected WST data. The load P as a function of peak load P_{max} was computed and the ratio P / P_{max} divided into three regions. This was done because in all the fracture mechanics tests, the AE plots showed three distinct regions - a slow rate of increase in AE counts, a sudden jump in the AE counts corresponding to instant failure and third a post-failure slow AE count growth till it reaches a plateau was reached and no further counts were recorded.

The load histories explained below, were obtained from a study performed by Lee (1990). The first region corresponds to $0 < P / P_{max} < 0.14 \sim 0.4$, the second to $0.14 \sim 0.4 < P / P_{max} < 0.93 \sim 0.97$, and the third to $0.93 \sim 0.97 < P / P_{max} < 1.0$. Region I can be explained as the initial compaction of voids and elastoplastic deformations of cement paste with initial formation of microcracks. Region II is the formation and coalescing of microcracks in an intense manner into a macrocrack. Region III corresponds to unstable macrocrack propagation. This is illustrated in Fig. 5.29 a. The end of region II corresponds to the K_{1c} value of the tested specimens. From the comparative AE plots, it is seen that this area of interface between regions II and III corresponds to between 93 and 97 % of the ultimate load. On an average basis,
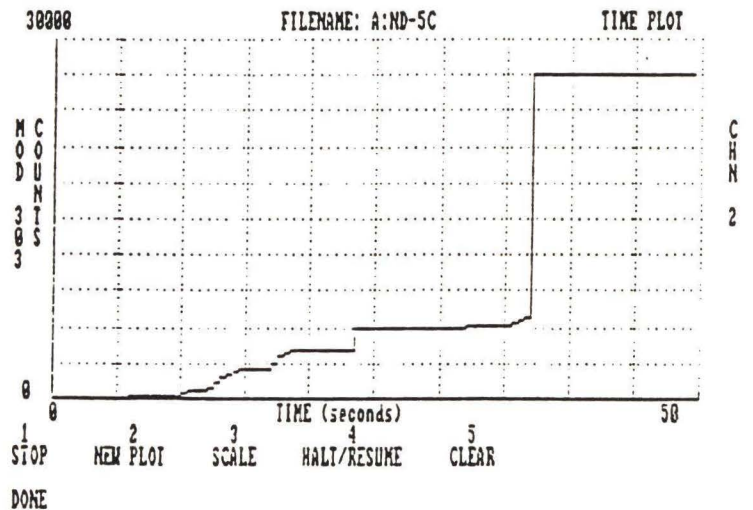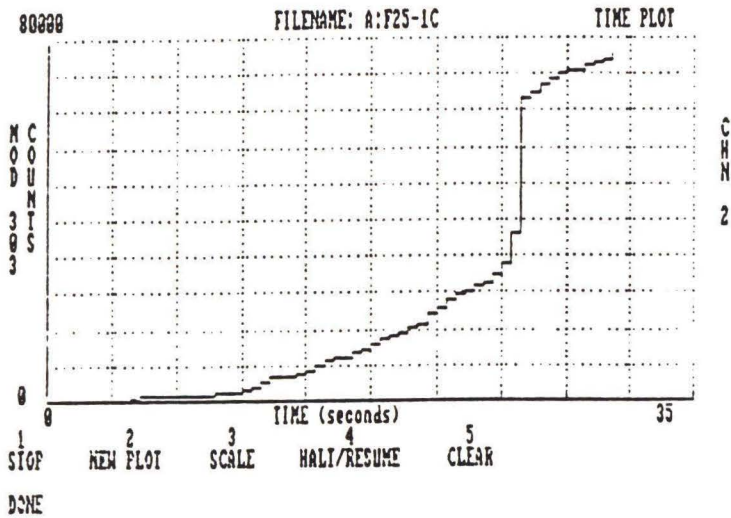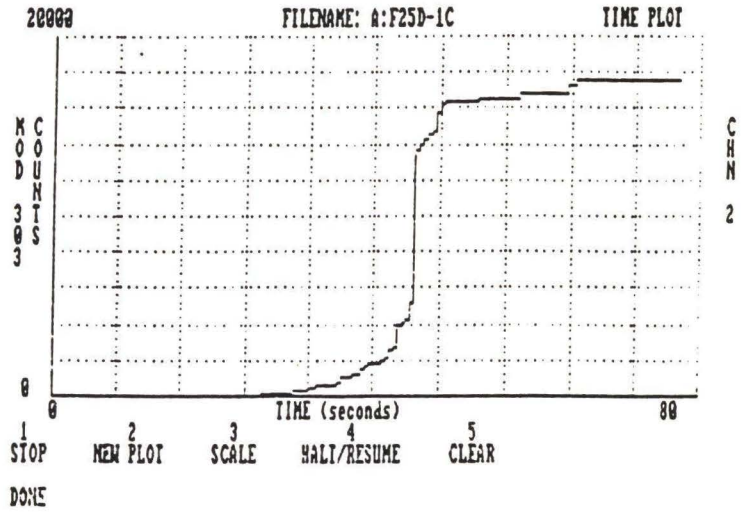
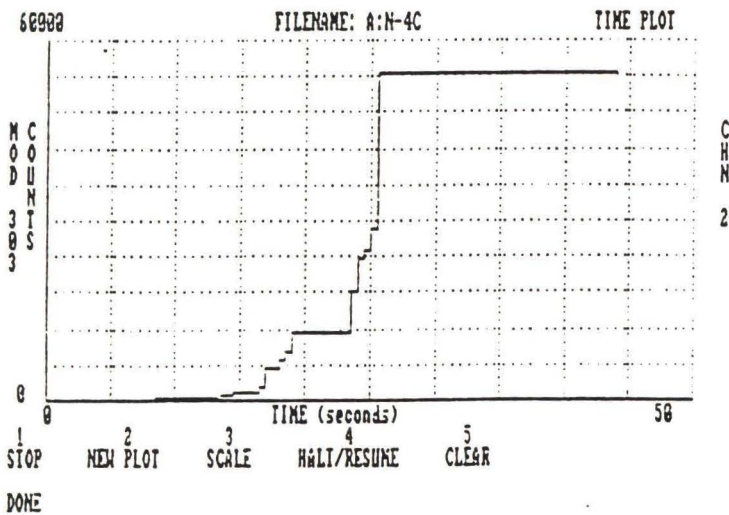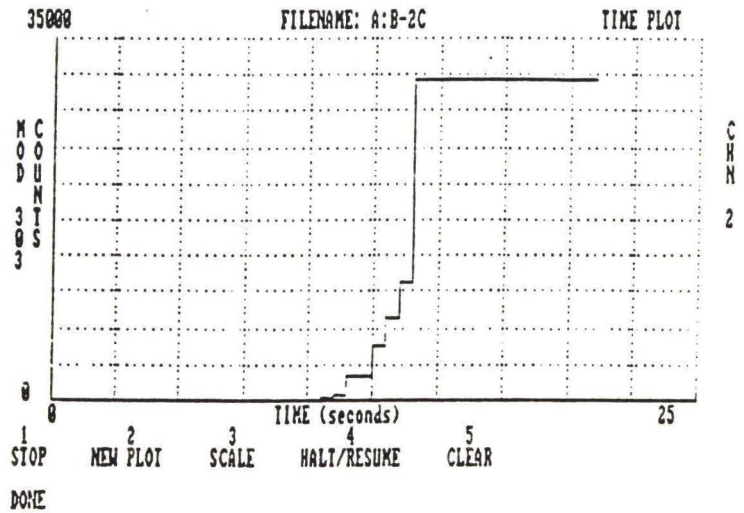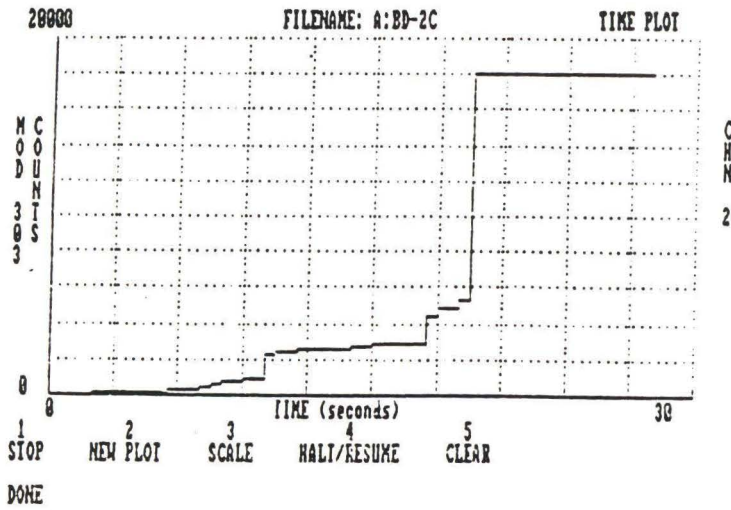Fig. 5.26a AE plots of the split-cube compression test.
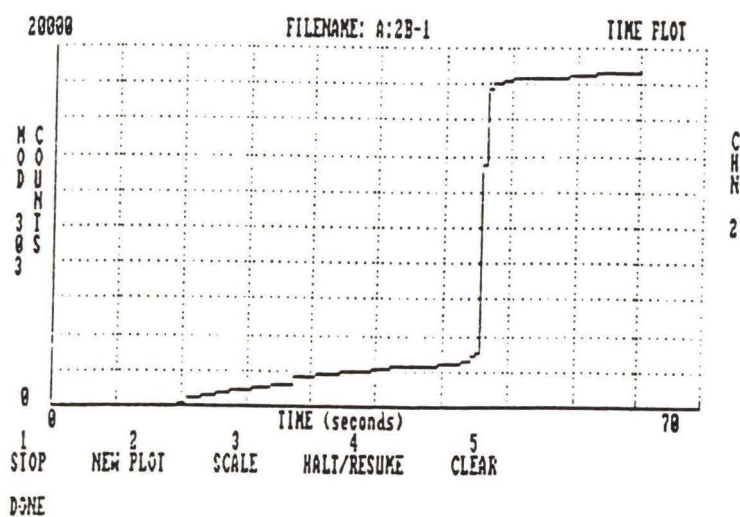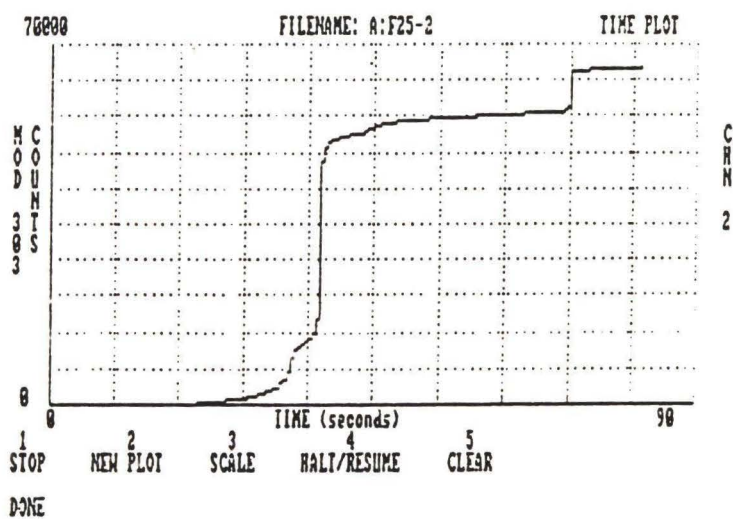
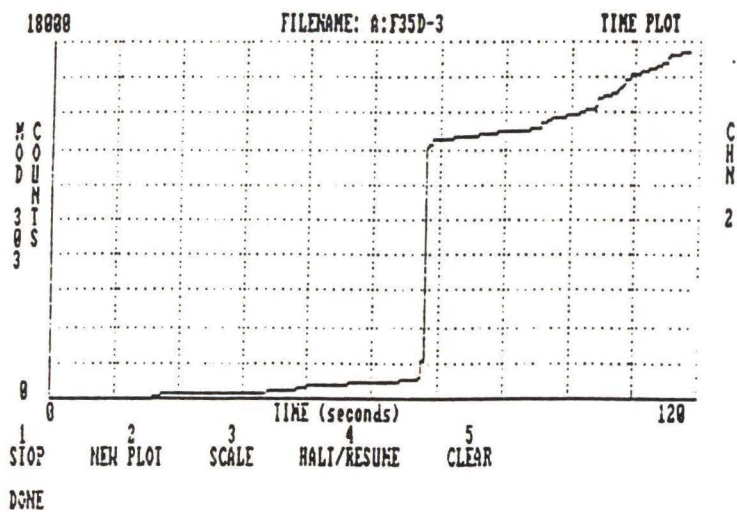Fig. 5.26b AE plots of the split-cube compression test.
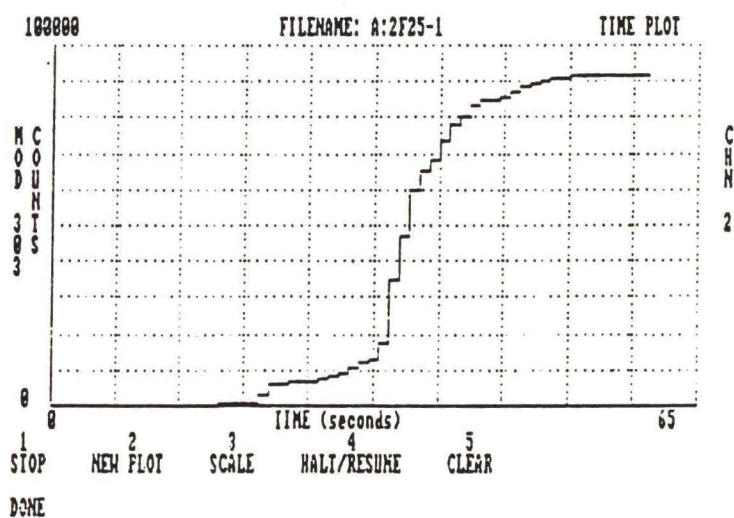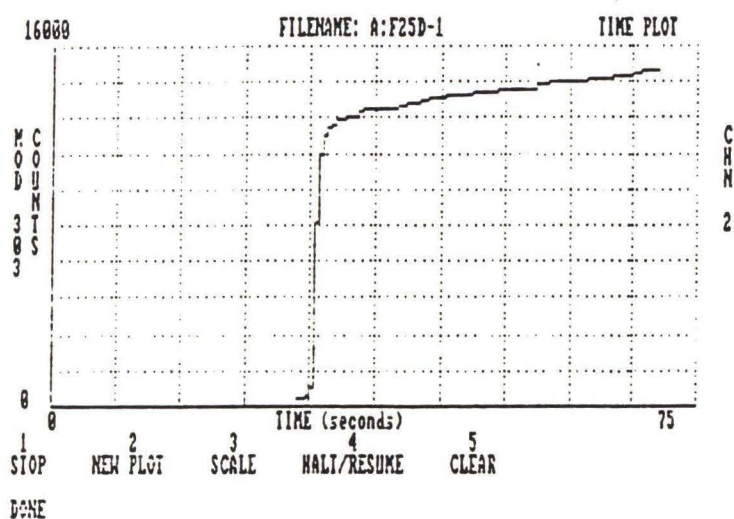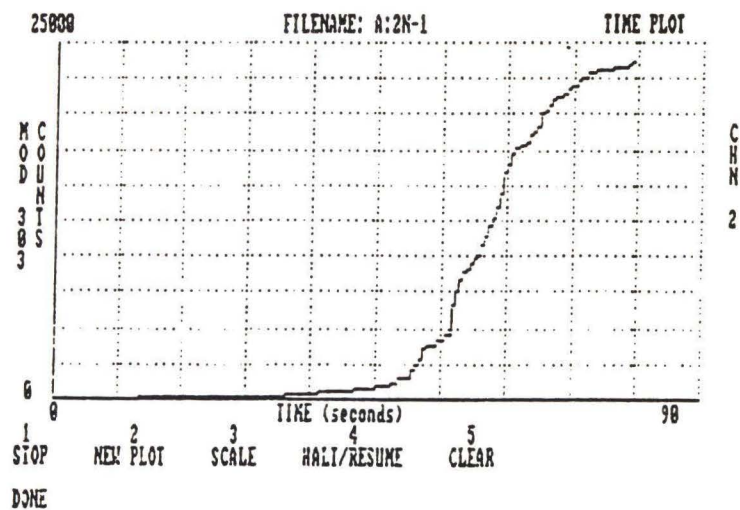
80

Fig. 5.27a AE plots of the wedge splitting test.
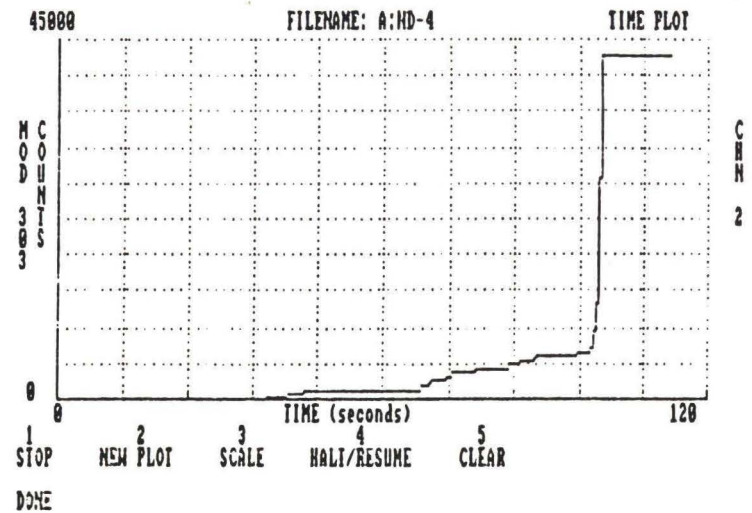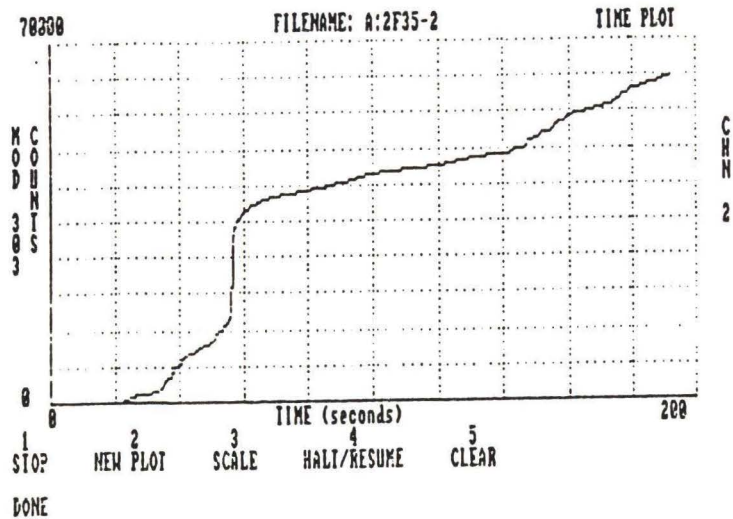
Fig. 5.27b AE plots of the wedge splitting test.
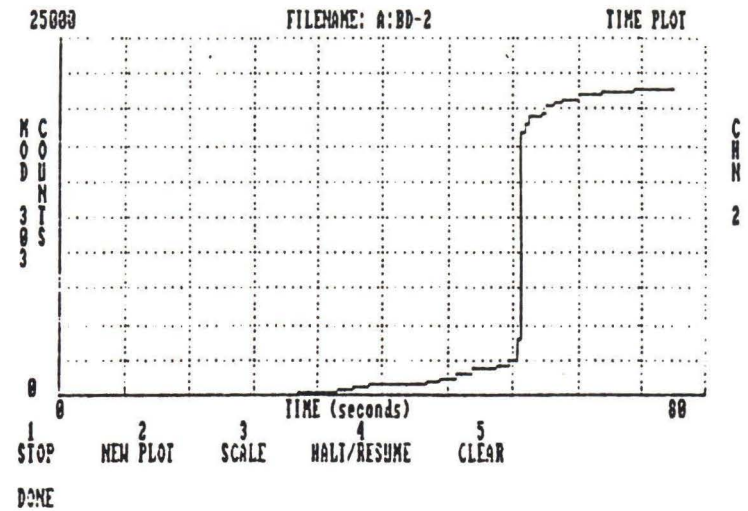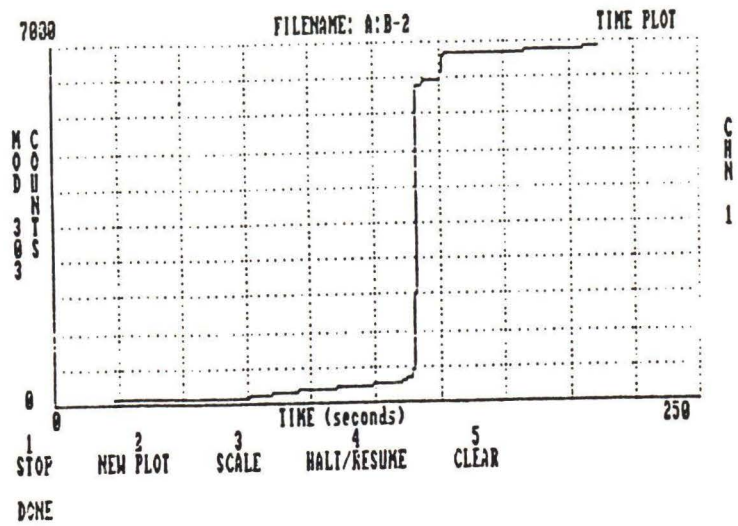
Fig. 5.27c AE plots of the wedge splitting test.
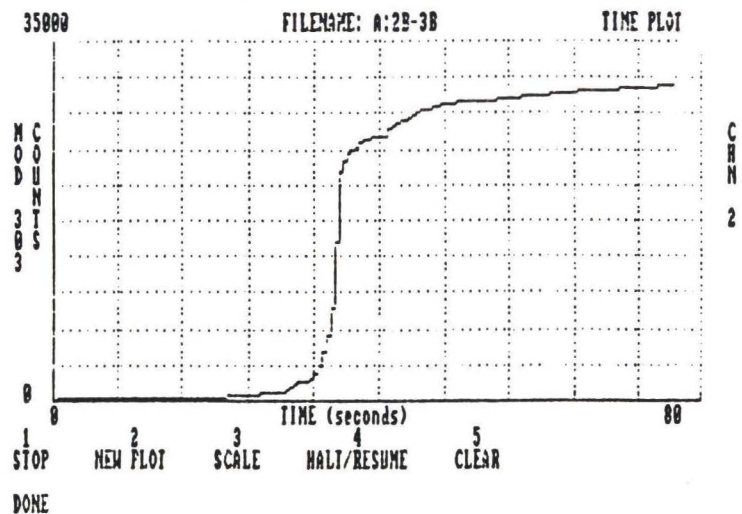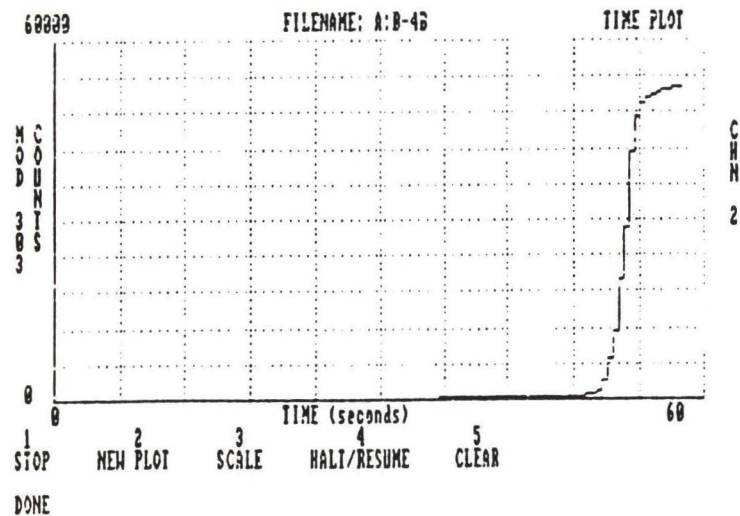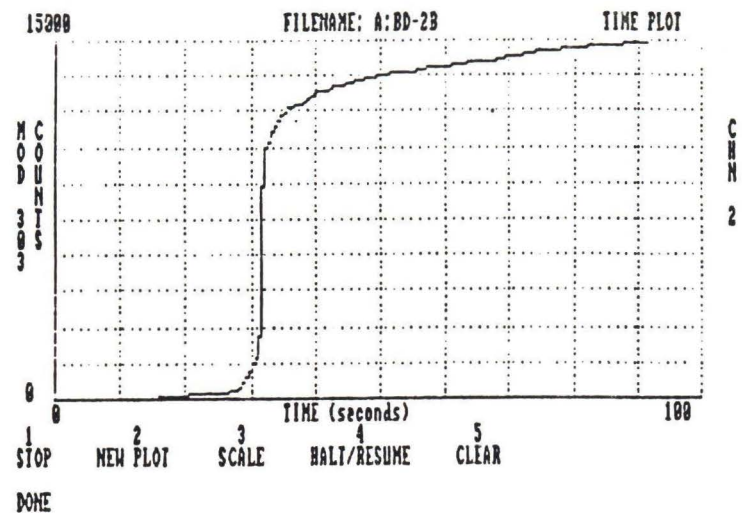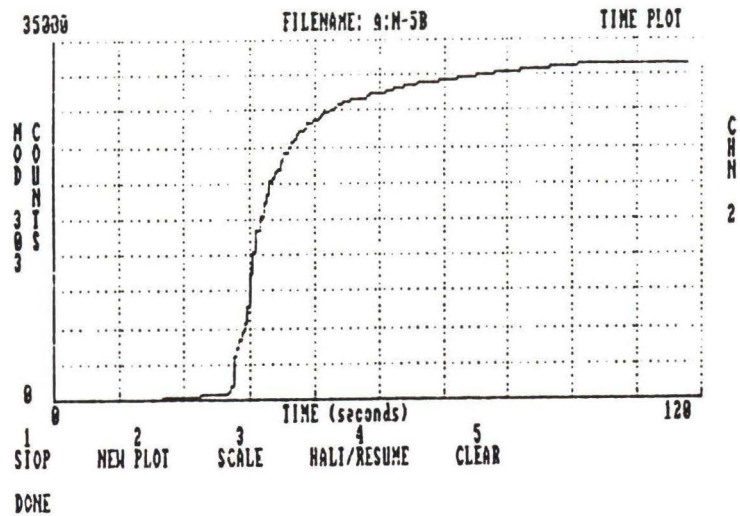
Fig. 5.28a AE plots of the 3-point beam bending test.
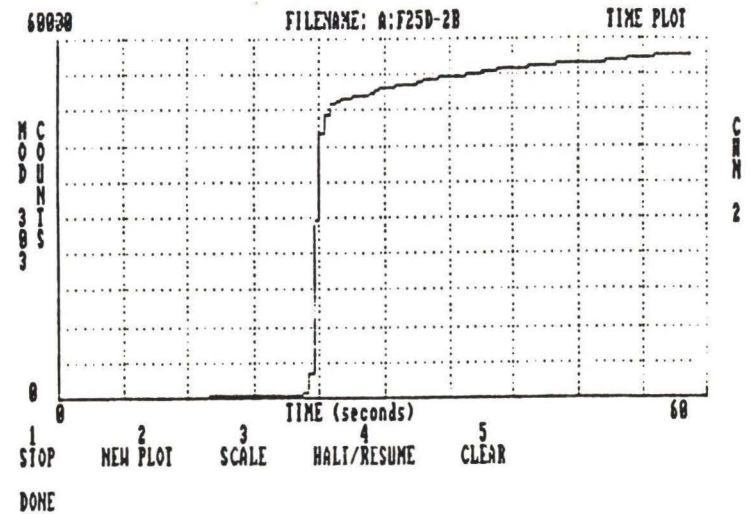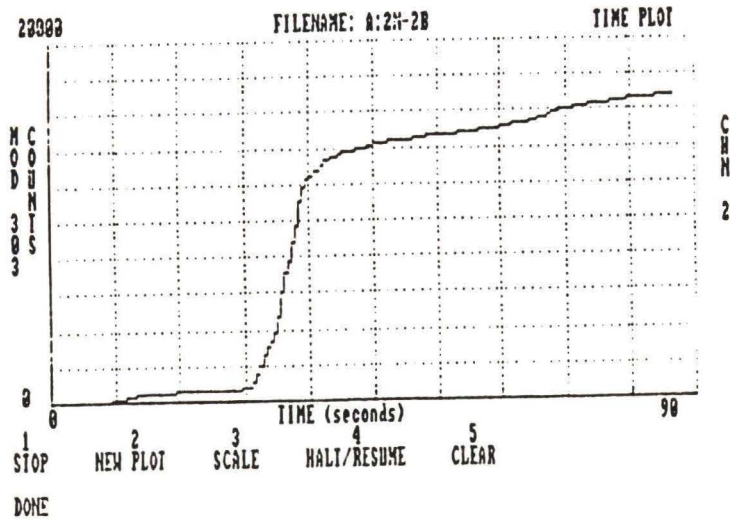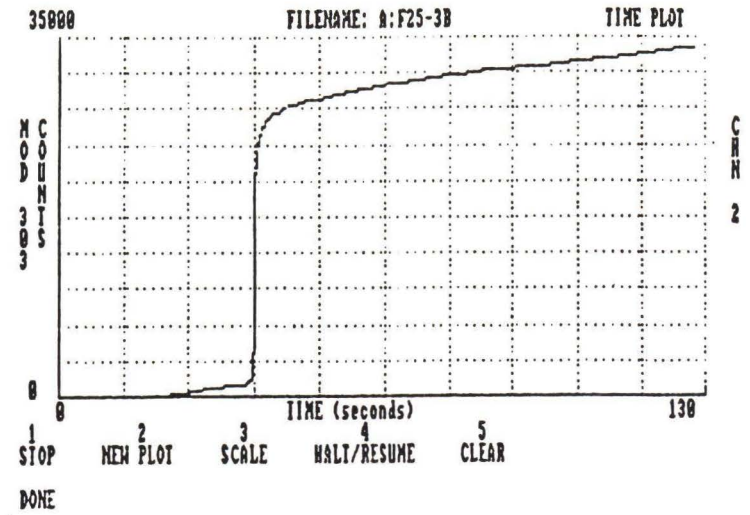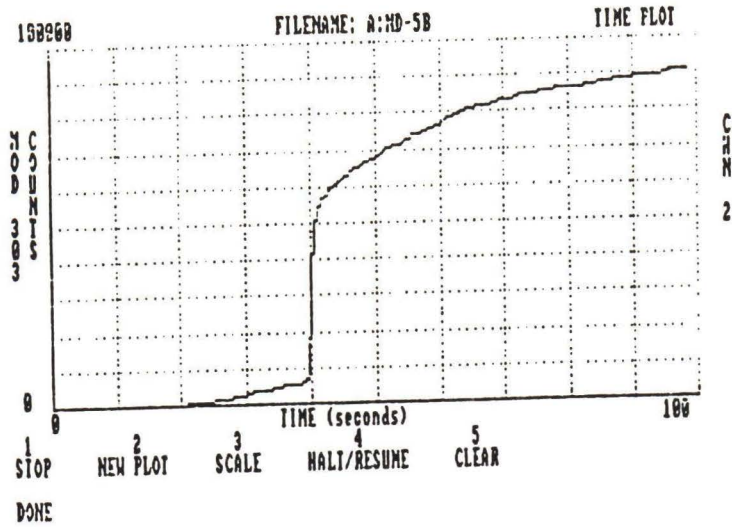
Fig. 5.28b AE plots of the 3-point beam bending test.
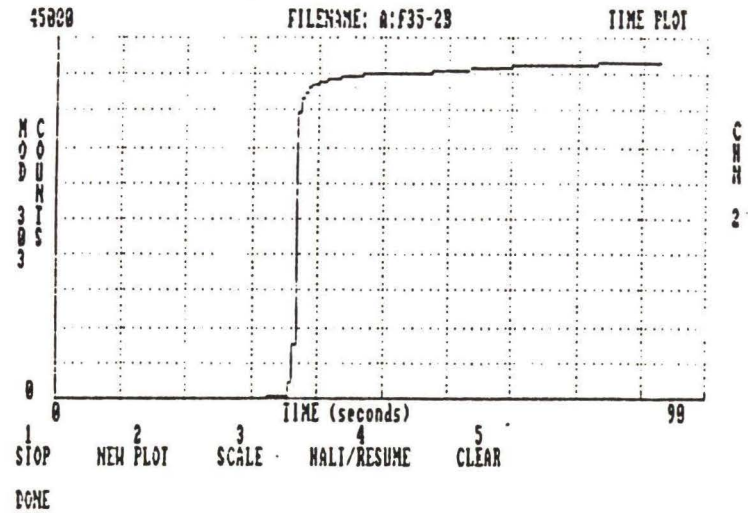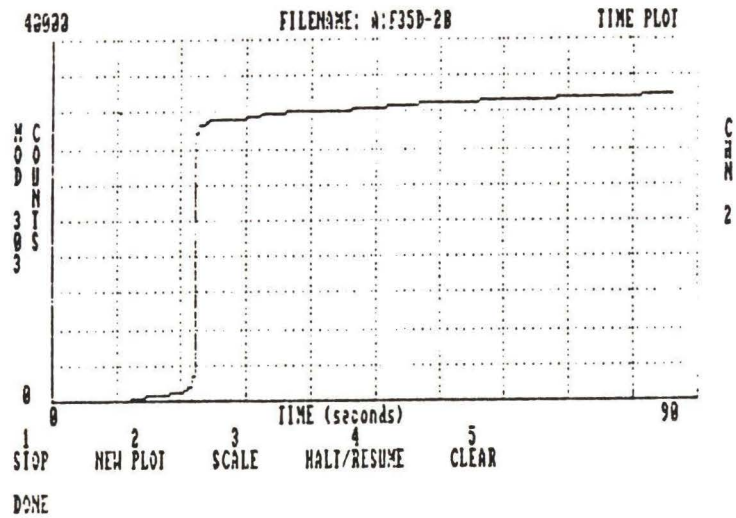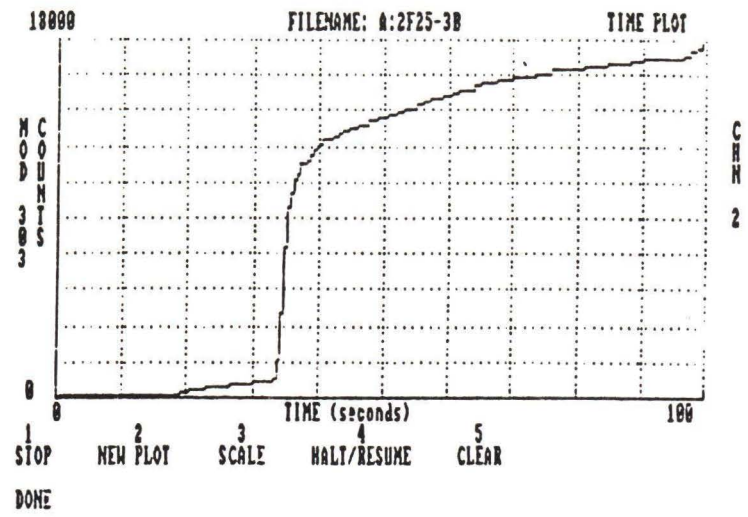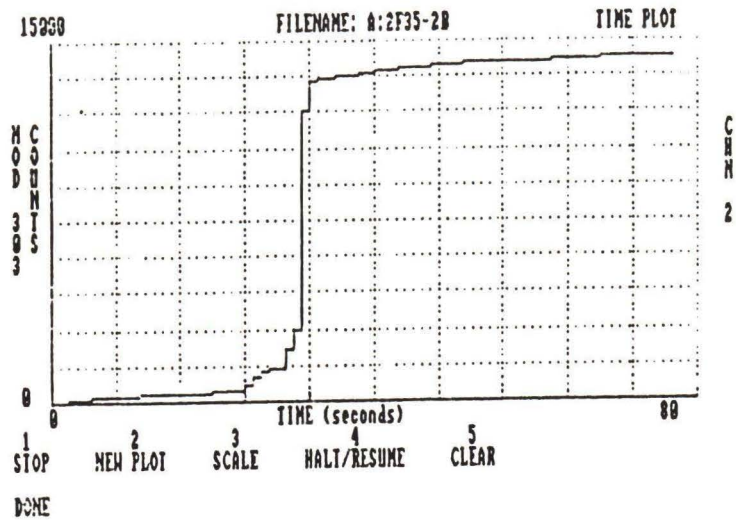
Fig. 5.28c AE plots of the 3-point beam bending test.

it would be safe to state that this point coincides with 95% of ultimate load. In other words, unstable crack propagation was found to start at 95% of the maximum load.

In Figs. 5.26 through 5.28, some of the monitored AE plots are shown. The specimen nomenclature is defined as follows:

The specimen ID (filename) has two alpha-numeric parts - one before the hyphen and one after. The pre-hyphen notation is

N   - Regular concrete

F 25   - 25% fly ash replacement

F 35   - 35% fly ash replacement

B   - Blended (15.5% fly ash)

D   - Durability tested.

The post hyphen notation is

- Wedge specimen no.

#B   - Beam specimen no.

#C   - Cube specimen no.

Notice that the three different test types have distinctive AE plot patterns. This is illustrated in Fig 5.30. However in the beam bending tests one can discern that the slow crack growth period is about 5 percent larger for the
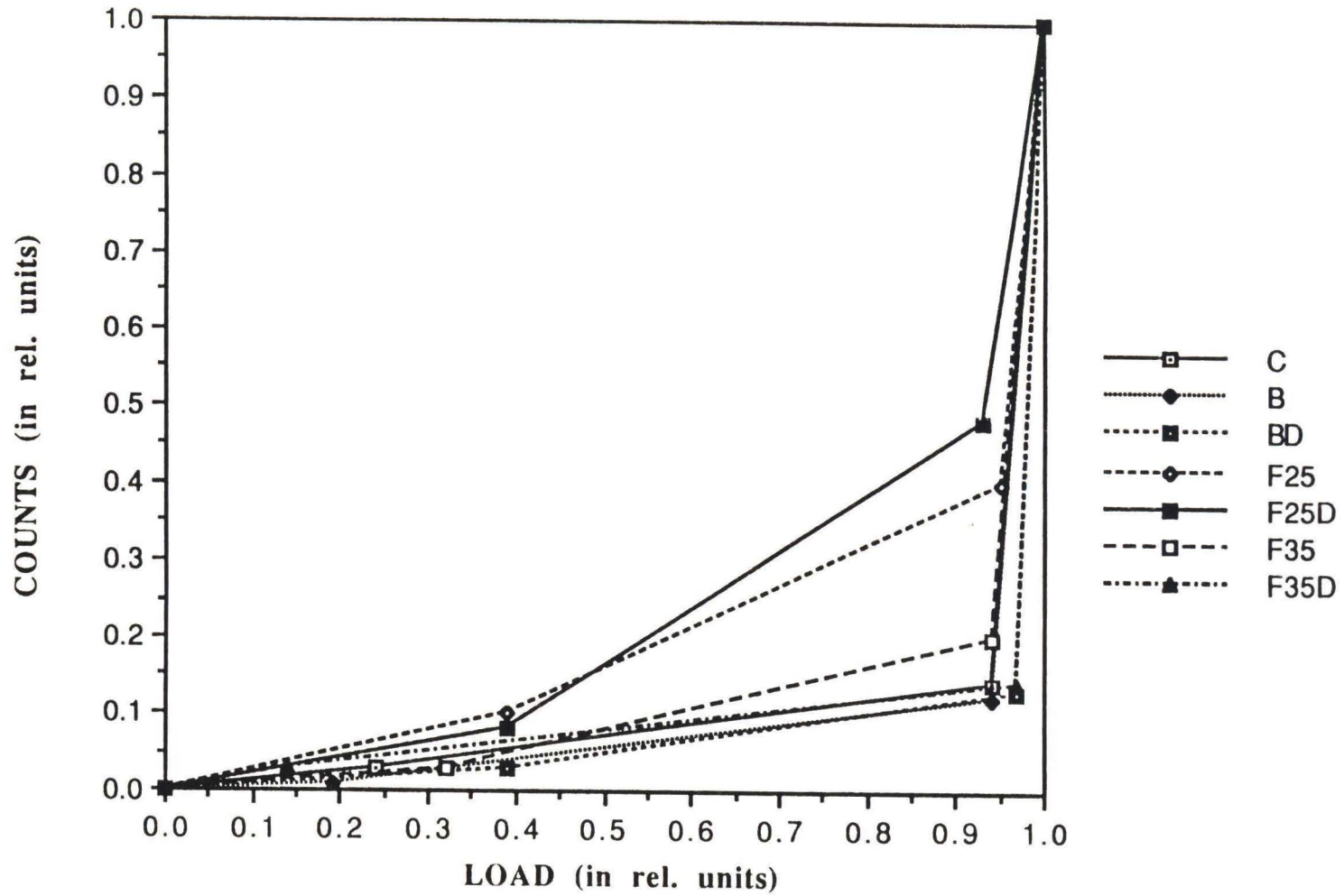
Fig. 5.29a Plot of Counts versus Load in Relative Units (Lee, 1990).
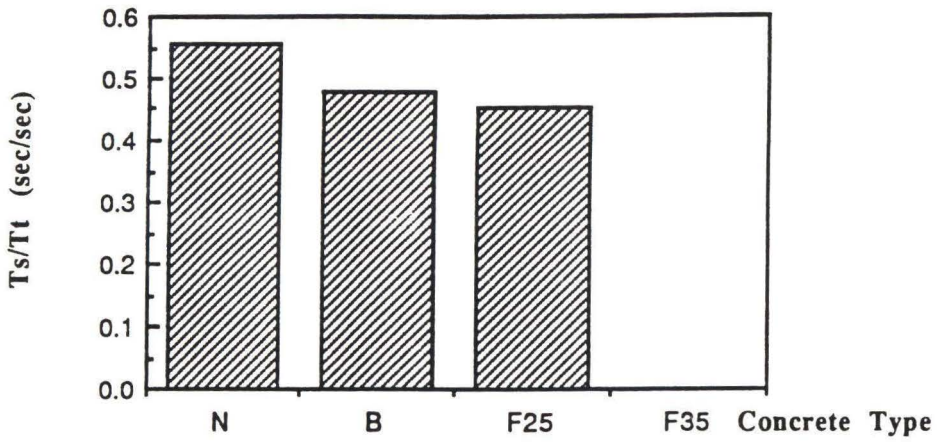
i) Split Cube Compression Test
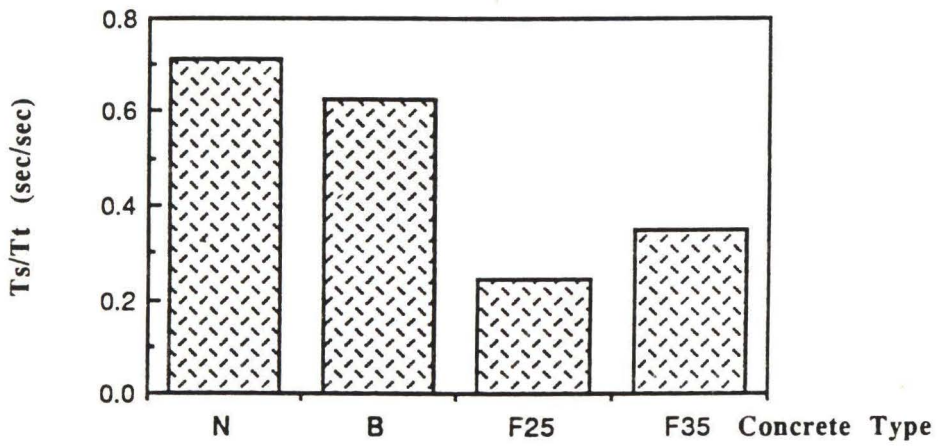
ii) Wedge Splitting Test
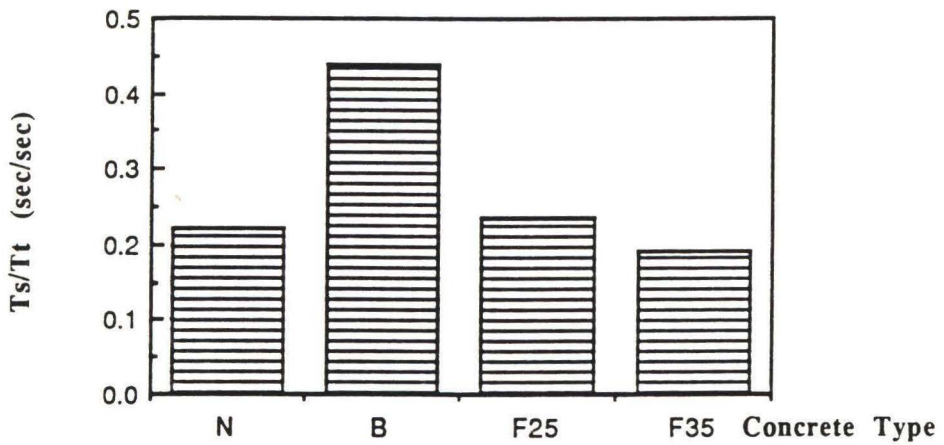
iii) Three-point Bending Test

Fig. 5.29b Slow crack growth time expressed as a ratio of total test duration

WEDGE (*SPLIT*) TEST

BEAM (3 *POINT BENDING*) TEST

CUBE (*COMPRESSION*) TEST
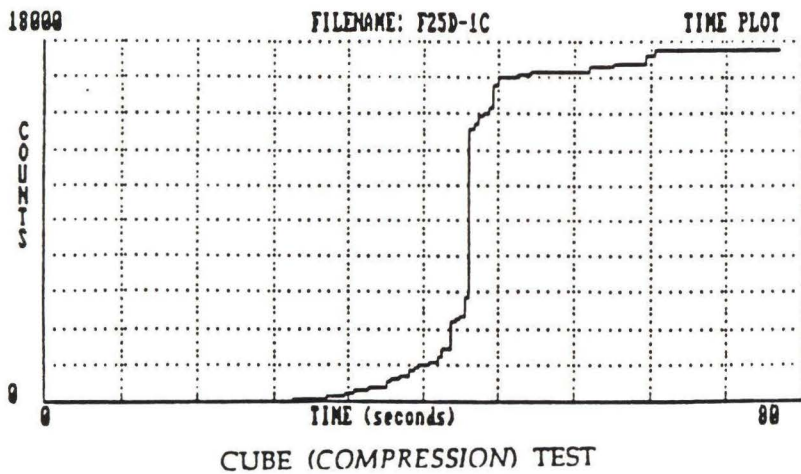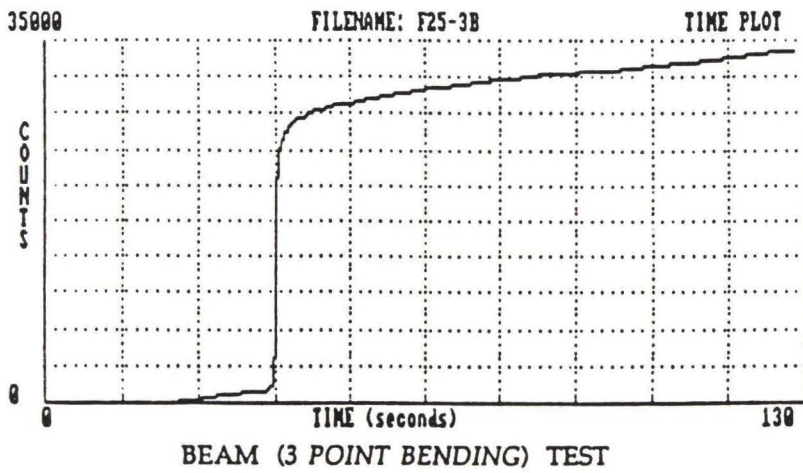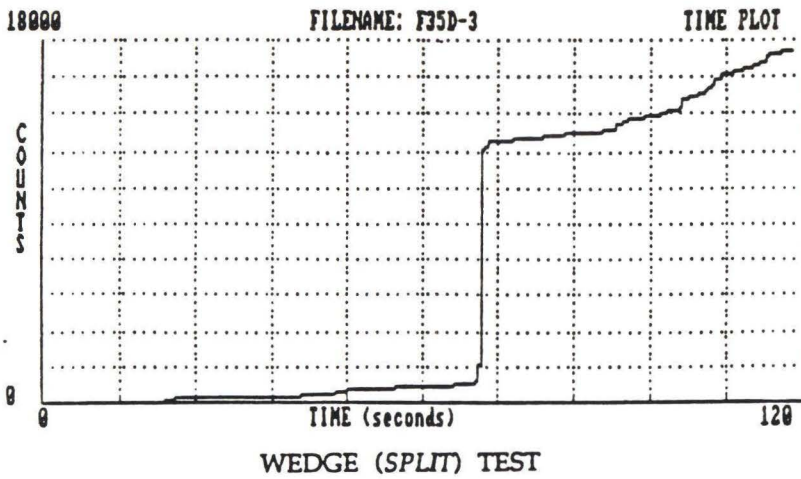
Fig. 5.30 Typical AE plots for the three fracture mechanics tests.

normal and blended concrete than for the fly ash concrete. This agrees very well with the results of the flexure tests done on the corroded specimens, where the loads at first crack were higher for the normal concrete than those for the fly ash concrete.

Considering all the fracture mechanics specimens in all the test modes, the average slow crack growth time for normal concrete was about 24 percent greater than that for fly ash concrete mixes. This is illustrated in Fig. 5.29b, where the slow crack growth time is expressed as a ratio of the total test duration. In the split cube compression test the graph for 35% fly ash concrete is not plotted owing to insufficient data. Fig. 5.29b again indicates that, irrespective of the test mode, fly ash concrete is more brittle.

The photographs in Fig. 5.31a, b & c show the three fracture mechanics tests. The affixed AE transducers can be clearly seen in these photographs. The transducer locations were chosen to maximize the picking up of the acoustic emissions without hindering the fracture mechanics test process.

5.5 BRIDGE ULTIMATE LOAD TEST

During the ultimate load test of the multi-box beam bridge model, shown in Fig. 5.32, the AE were monitored by affixing three transducers at the mid-span. The AE plots from the central transducer and one of the side transducer are given in Figs. 5.33 and 5.34.
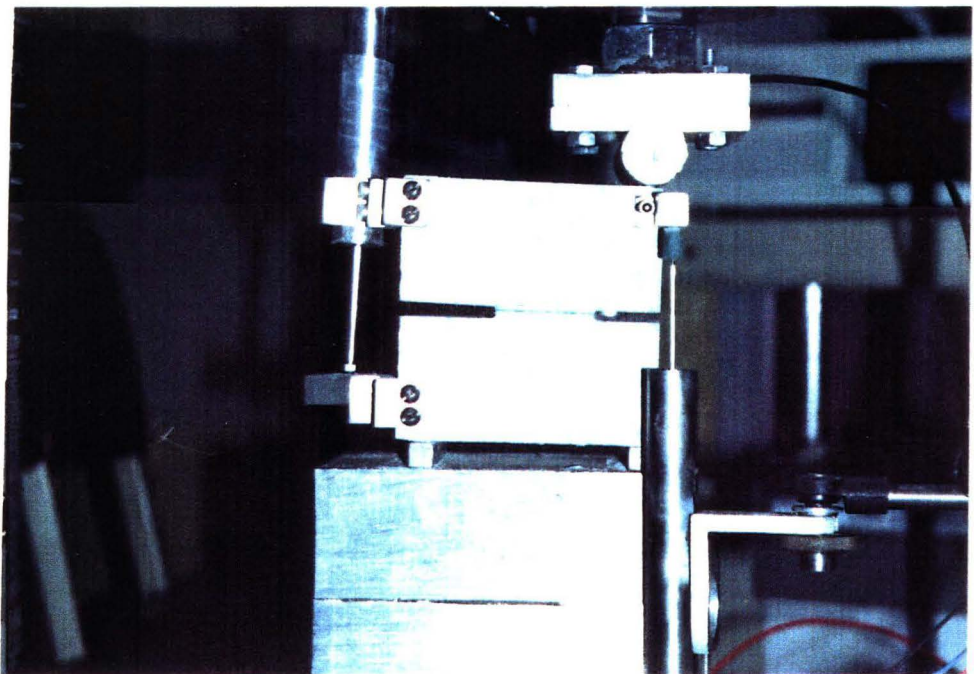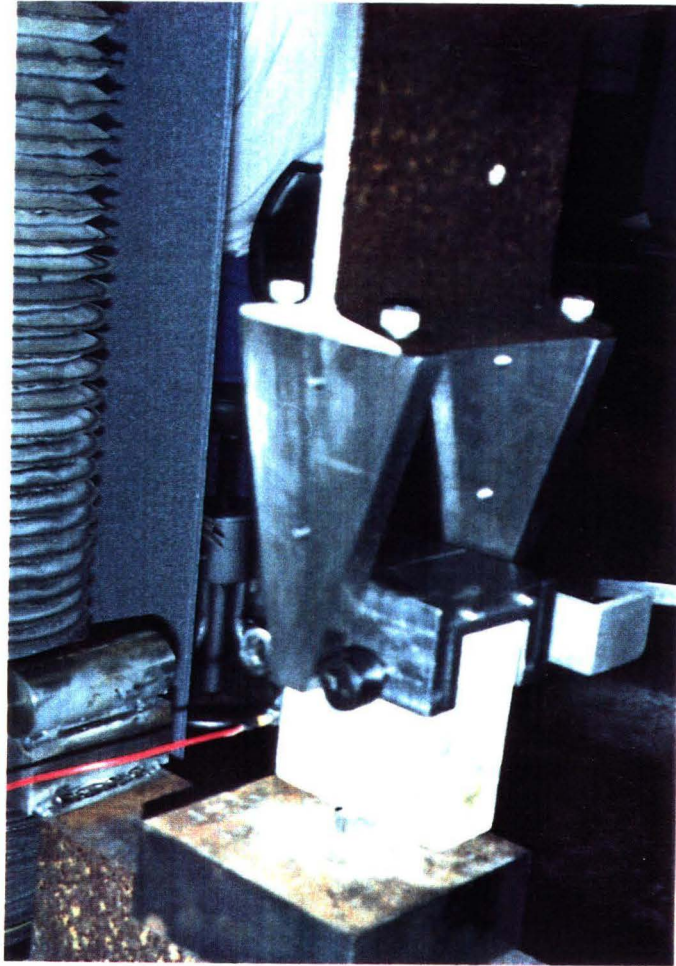
Fig. 5.31a & b Photographs of wedge split test and split-cube compression test.
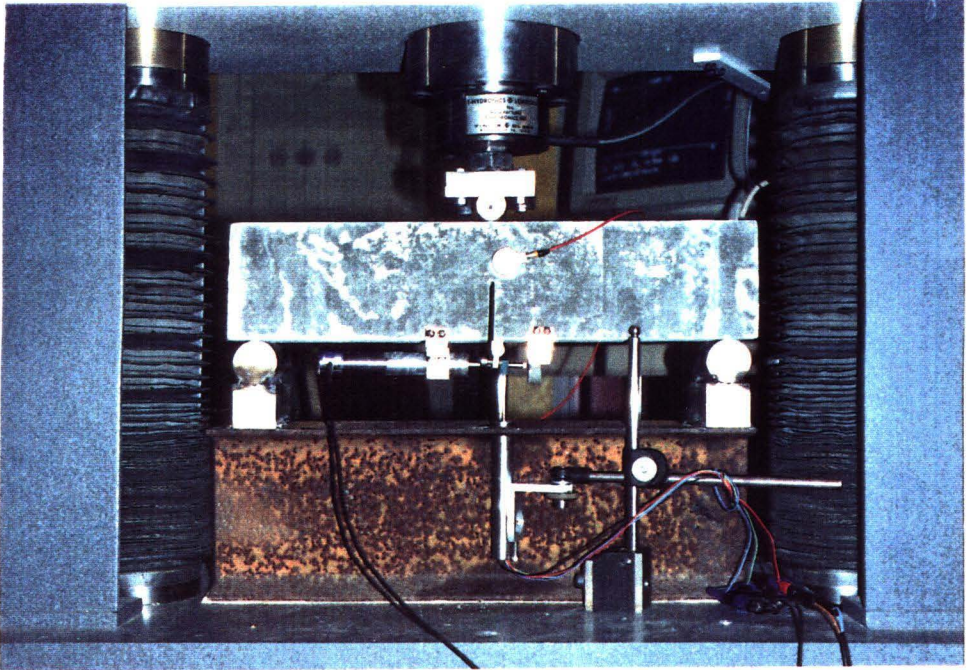
Fig.5.31c Photograph of 3-point beam bending test.
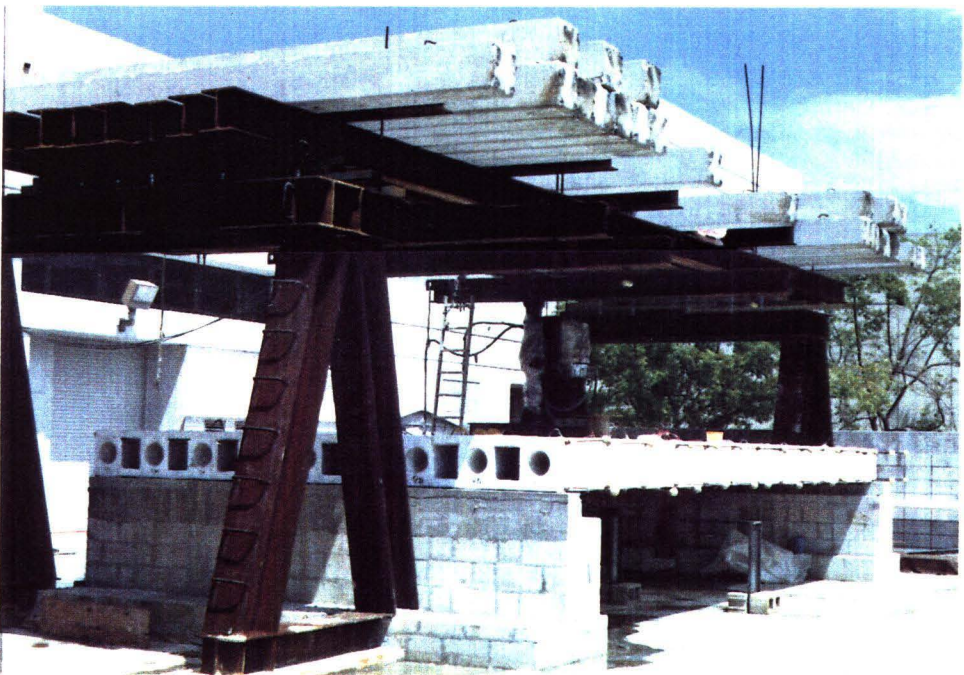
Fig. 5.32   Photograph of the bridge model.
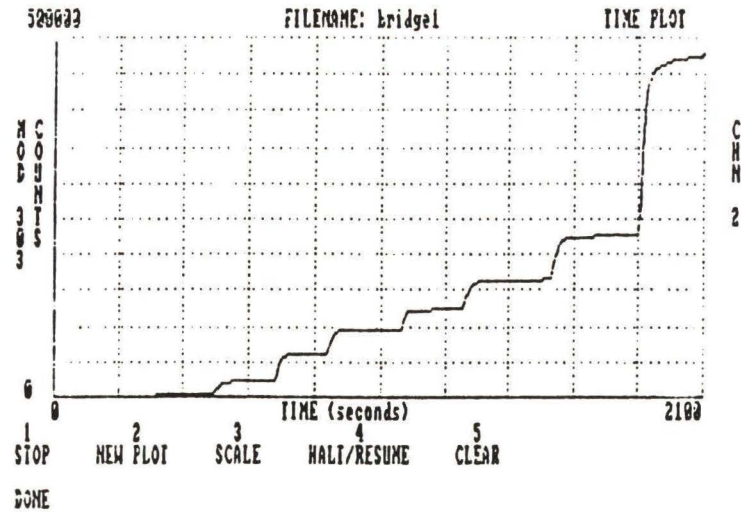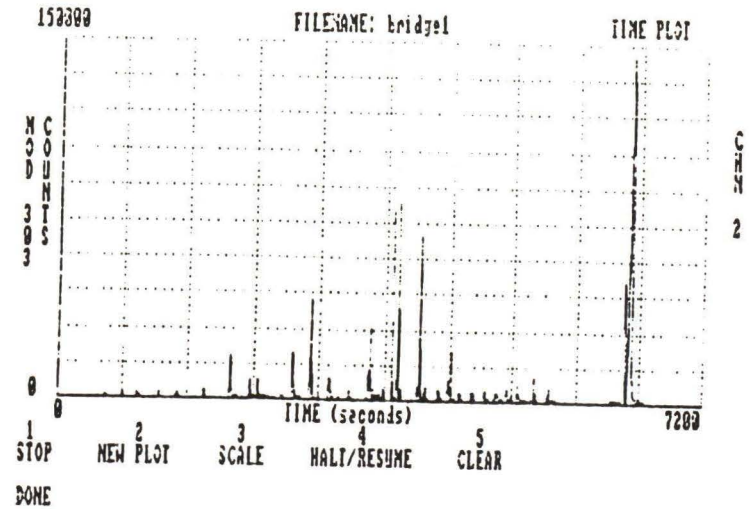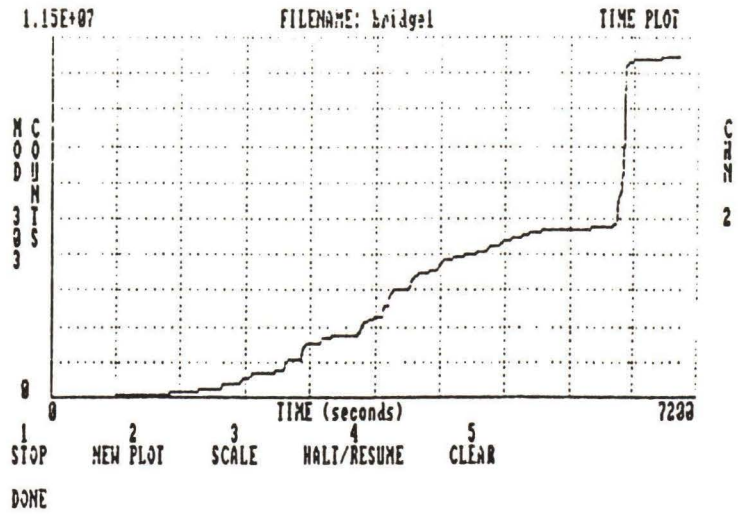
Fig. 5.33   AE recorded by the central transducer.
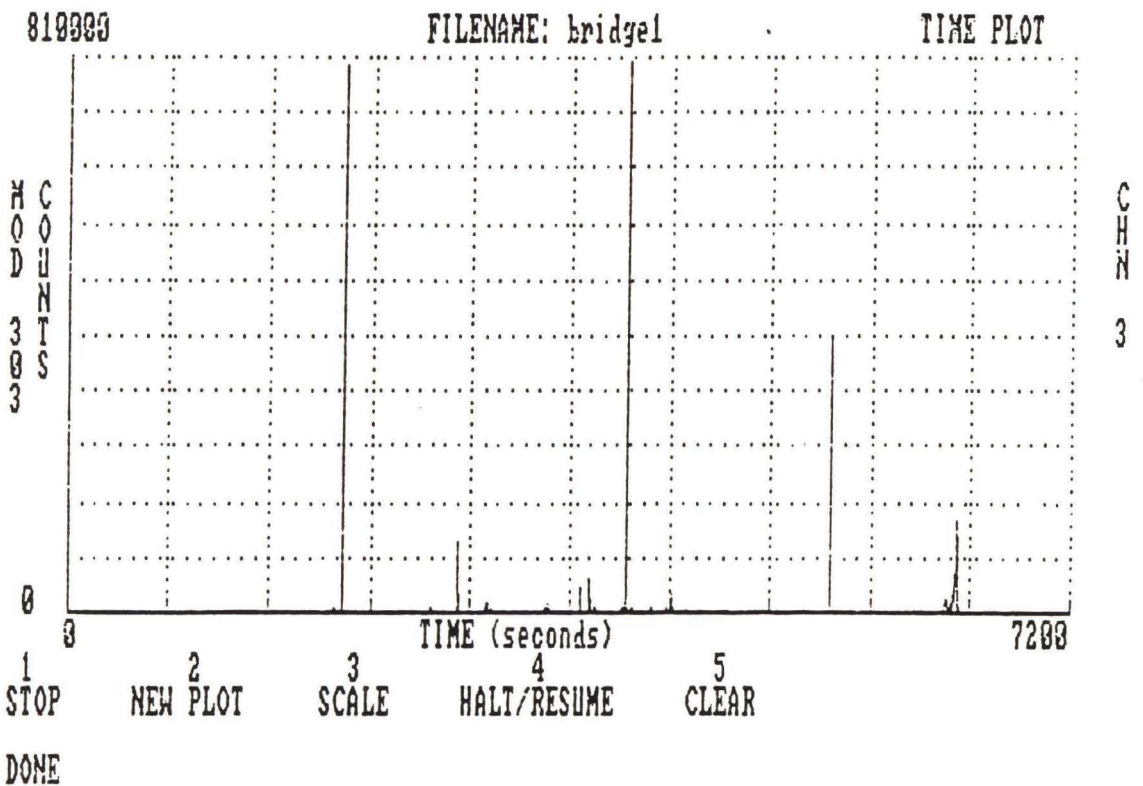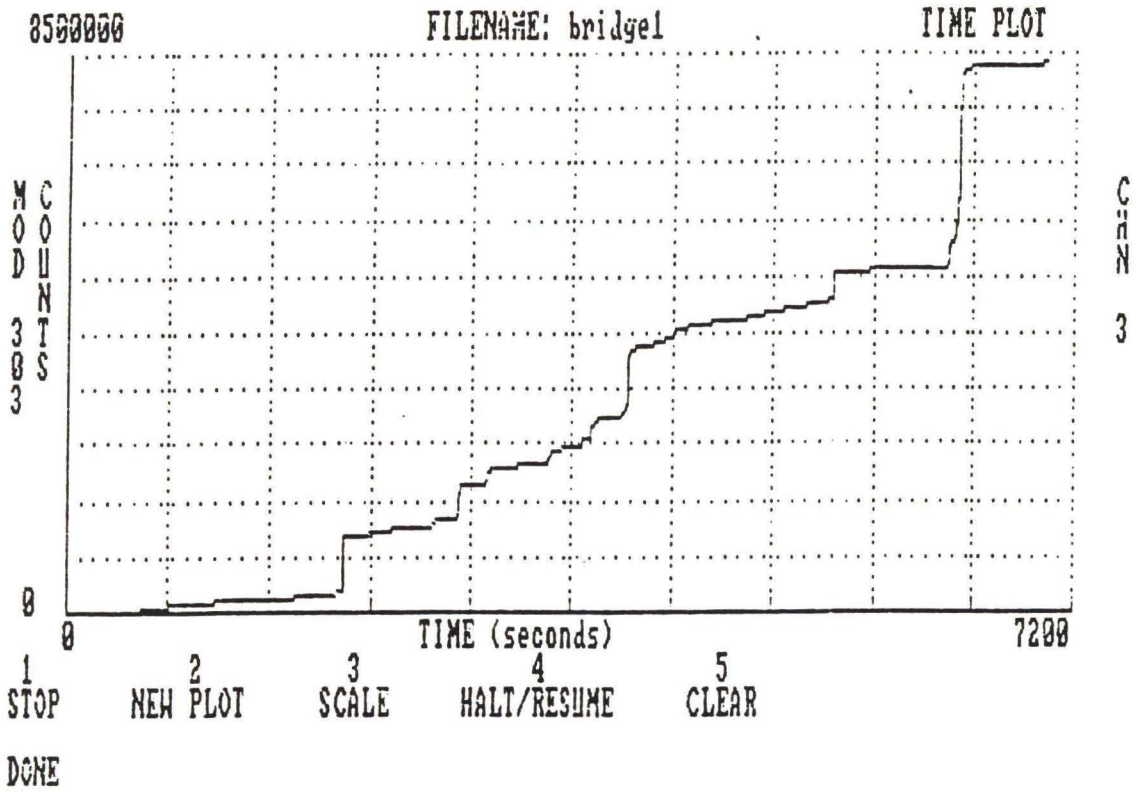
Fig. 5.34   AE recorded by the side transducer.

The loading periods are clearly delineated. Hence each incremental loading period can be discerned by the bounding plateaus in the graphs. The as read graphs also show this as discrete AE bursts. One can also notice two regions where the slopes are steeper. The first region corresponds to the load when the bridge begins to yield. The second corresponds to the load just prior to the failure. The load - deflection curve, which amply illustrates this, is shown in Fig. 5.35. Also, there is a similarity between the bridge AE plots and the beam fracture mechanics test plots. The three regions are clearly defined. However, in the bridge plots, the slow crack growth region is more extensive. This can be attributed to the presence of rebars in the bridge. Consequently, Regions II and III corresponding to the intensive microcracking and coalescence into a macrocrack and unstable macrocrack propagation are shorter.

During the load test, although a time base was not maintained for the loading sequence, one could observe on the computer screen, that the magnitude of the AE plot jumps clearly predicted the impending incremental deflection magnitudes.

5.6 DISCUSSION

While at least two specimens were used for each test method for each case, it is felt that larger specimen sets would generate more relevant data for a typical specimen group, for analysis and as a confirmation of evolving results. Moreover the varying periods of accelerated corrosion greatly reduced
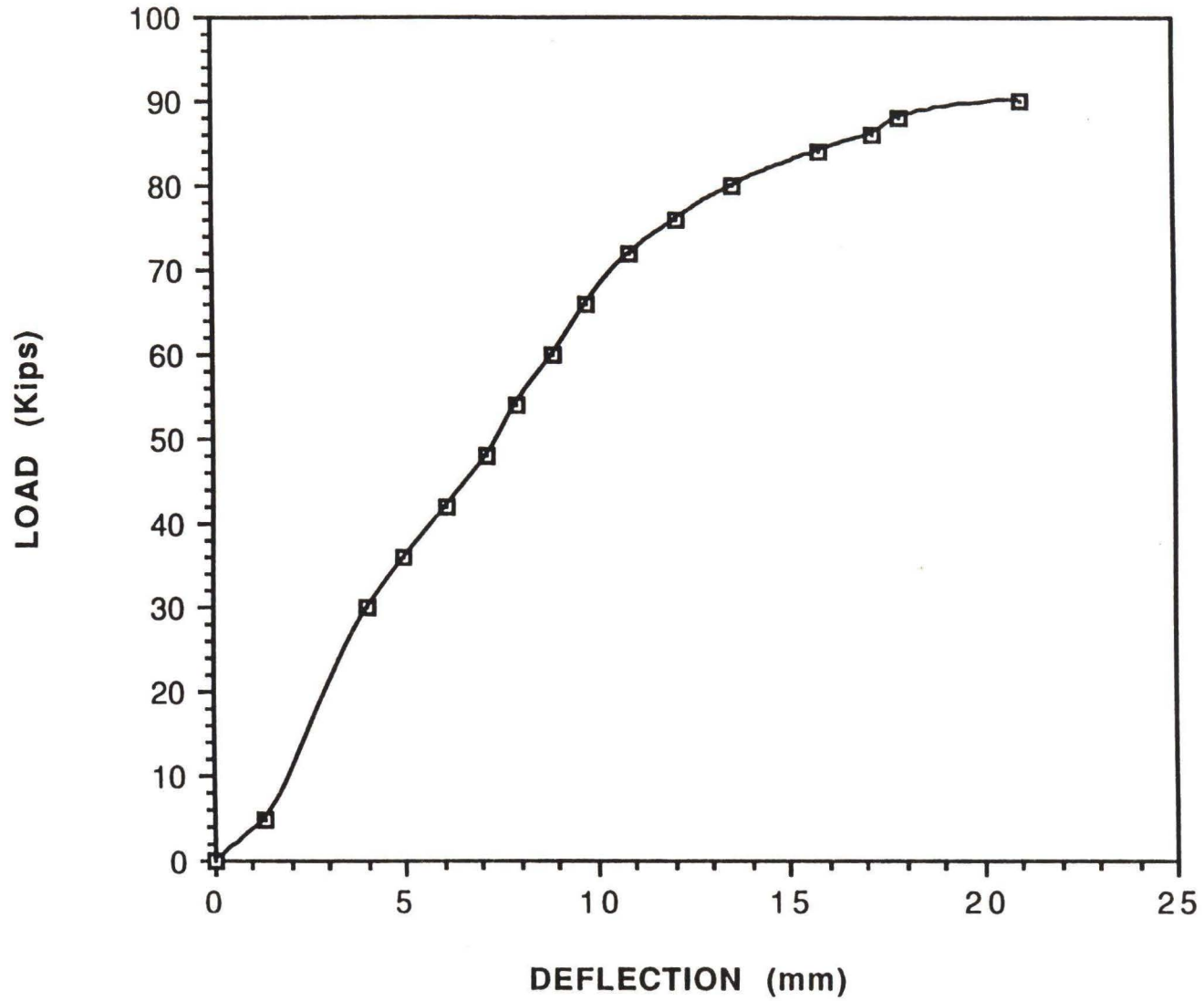
Fig. 5.35   Load versus deflection during ultimate load test of the bridge

the number of specimens in each 'mix type - corrosion duration - test method' group.

5.6.1 Accelerated Corrosion

The tests were performed under constant voltage, with the specimens connected in parallel, as explained in section 4.4. However, it is felt that individual circuits with three governing power parameters viz., constant current, constant voltage and constant power would have provided more comprehensive findings.

While preliminary studies in the laboratory and in the field at Treat Island (Reddy, 1986) do indicate that the three-week accelerated corrosion correlates reasonably well with a twenty five year marine exposure, additional studies are essential for determining more reliable correlations.

5.6.2 Impact and Flexure Tests

The common observation in both the impact and flexure tests seem to be that the residual strengths in the beams varied inversely with the period of accelerated corrosion. While this was expected, the performance of regular and fly ash modified concrete in the two tests was not so predictable.

Since concrete tensile properties are a function of their compressive strengths (f_t is proportional to $\sqrt{f'_c}$), and since fly ash concrete has greater compressive strength, one would expect fly ash concrete to have greater tensile strength as well. However, the tests indicated that normal concrete possesses greater tensile strength. The possible explanations could be:

a) Marine exposure of fly ash concrete tends to alter the material properties.

b) The relationship between tensile and compressive strengths of concrete may not be valid in the case of fly ash modified concrete.

Further studies need to be performed to analyze this aspect of these tests.

5.6.3 Fracture Mechanics Tests

While the AE monitoring and acoustic data analysis of the fracture mechanics tests reported here were carried out by the author, the fracture mechanics tests themselves were conducted by Mr. S.K.Lee, a fellow graduate student, as part of a Sea Grant funded research project. Whereas that study analyzed in depth the fracture mechanics behavior of different concrete mixes with and without entrained air, after subjecting a part of the specimens to accelerated durability testing, one interesting result from those studies seemed to mirror closely one of the conclusions of this study -   *The relationship between compressive strength and tensile strength do not hold good for fly ash modified concrete irrespective of whether they were subjected to durability testing or otherwise* '. Fig. 5.36 illustrates this. The modulus of rupture decreases with the increasing percentages of fly ash,
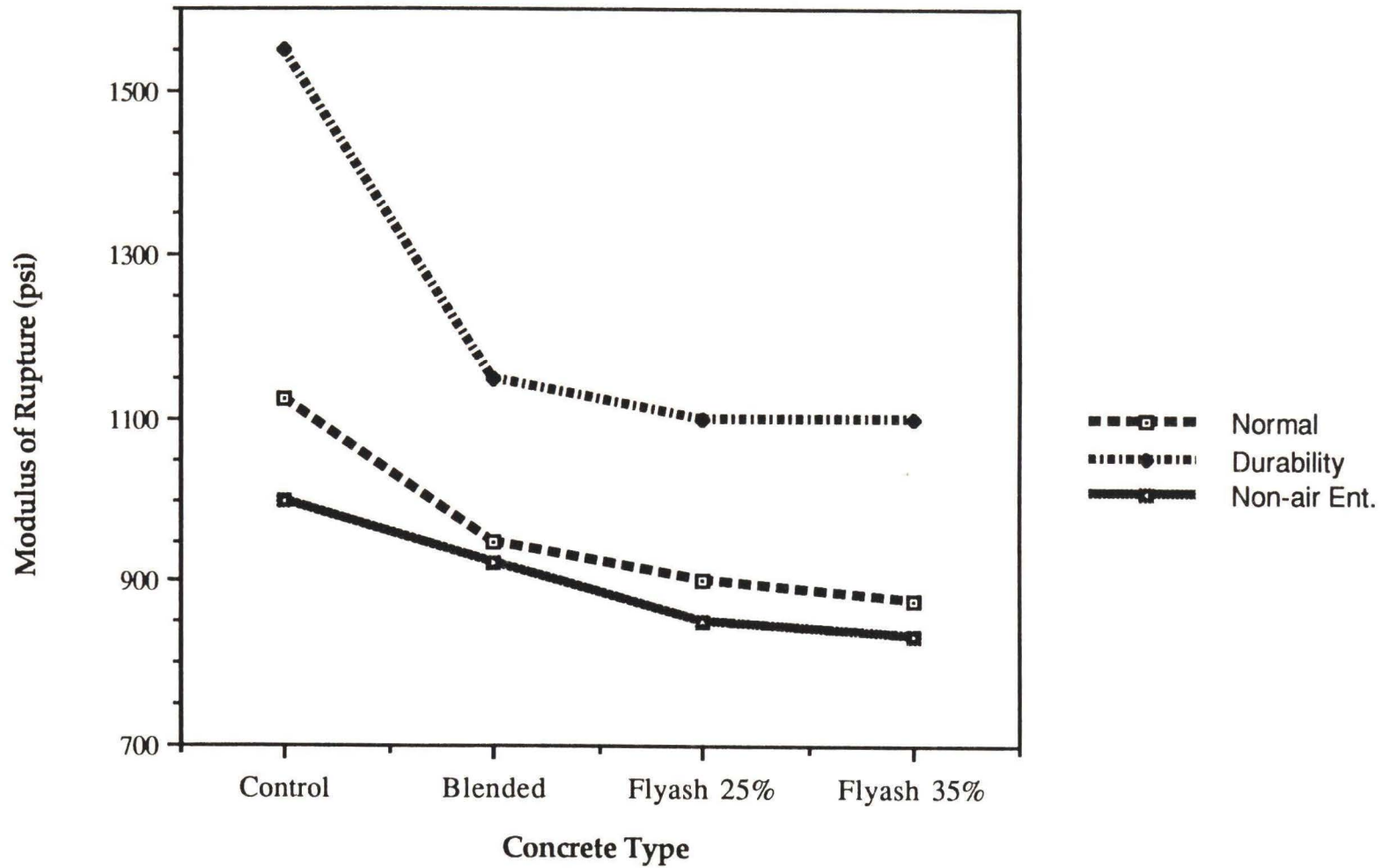
Fig. 5.36 Modulus of rupture for various concrete mixes (Lee, 1990)

regardless of whether they are 'air entrained and normally cured', 'air entrained and durability tested' or 'non-air entrained and normally cured' specimens.

5.6.4 Remaining Life Prediction

The Miner concept of cumulative damage assumes that the total damage in a specimen or a structure cannot exceed unity. In other words, when a specimen completely loses its strength, its damage is 1. As noted earlier, for both flexure and impact tests, the strength varies inversely with corrosion period and cumulative AE counts.

Fig. 5.37a is a plot of the strengths in flexure and impact, for both fly ash and normal concrete versus corrosion period. Logarithmic extrapolation indicates that in flexure, the fly ash beams would face a complete loss in strength, in 4 weeks and 4 days, while the normal concrete beams would lose their strength completely in 11 weeks and 5 days. In impact, on the other hand, the fly ash specimens would encounter complete strength loss in 5 weeks and 6 days, whereas the normal beams would be reduced to zero strength in 4 weeks and 3 days of similar accelerated marine corrosion exposure.

Using the three-week laboratory accelerated corrosion and field exposure correlation model, one can predict the years of exposure required to

deplete the strength of a structure totally. Replacing the laboratory exposure time in the X-axis by the field exposure time, one can determine the residual strength of a structure at any given point in time. This would enable the determination of the serviceability of an old structure that has been continually in service.

In Fig. 5.37b, the corrosion period on the X-axis has been replaced by cumulative AE counts. The general similarity of the curves suggest the viability of using AE counts to determine strength loss. Furthermore, AE counts could be used to perform a similar analysis of remaining life prediction as explained above.
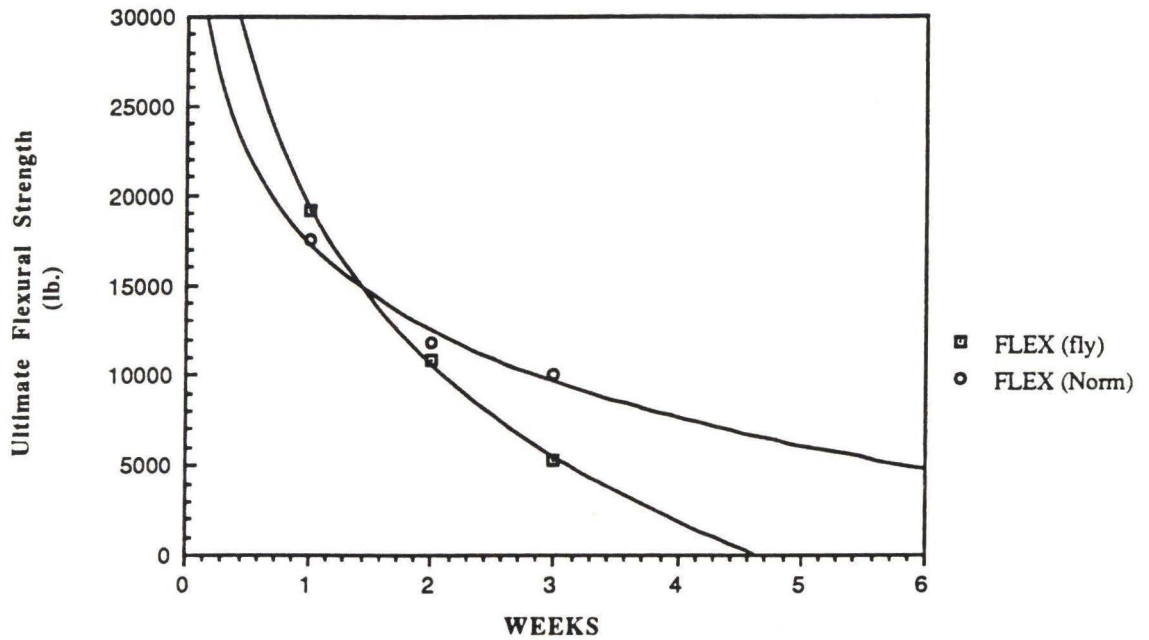
Fig. 5.37a(i) Interdependence of flexural strength and corrosion period
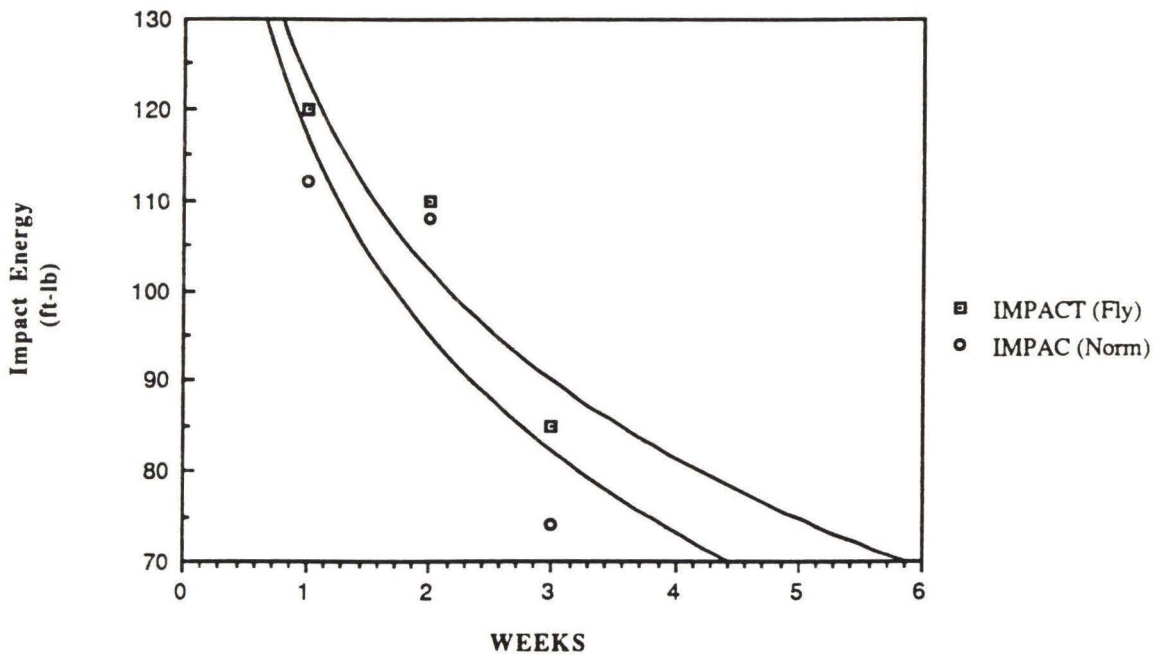
Fig. 5.37a(ii) Interdependence of impact energy and corrosion period
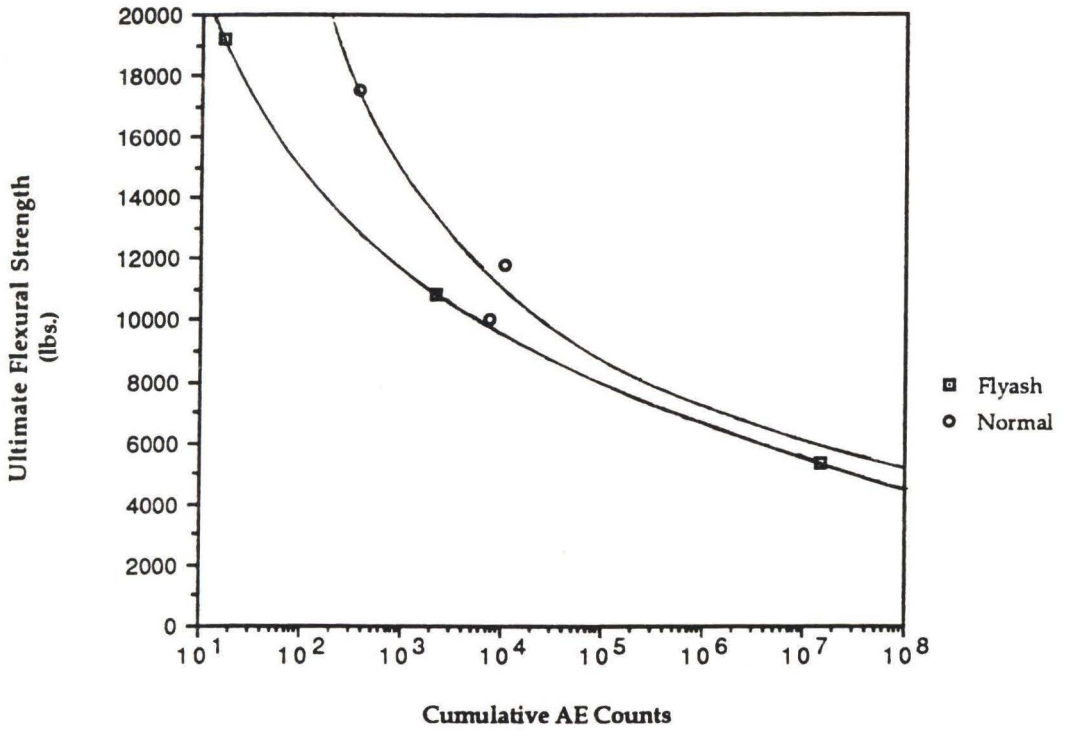
Fig. 5.37b(i) Interdependence of flexural strength and AE counts
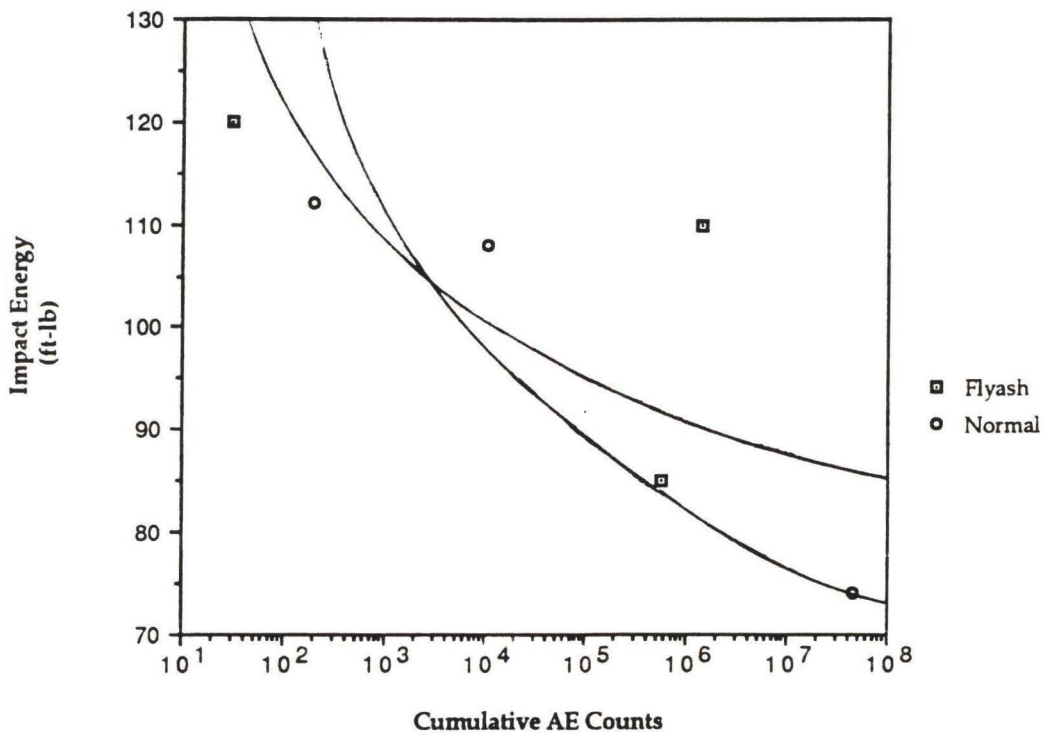
Fig. 5.37b(ii) Interdependence of impact energies and AE counts

Chapter 6

CONCLUSIONS

6.1 Summary

Most of the goals set at the outset of this research were achieved. Some of the expected results were verified and some new leads were identified. The major conclusions can be listed as follows:

1. Fly ash in concrete retards the rate of corrosion of the reinforcement.

2. Cumulative AE counts increase with increasing periods for both normal and fly ash concrete specimens.

3. While it is difficult to predict strength for a specific individual specimen based on its AE counts, over a large set of specimens, AE counts are indeed statistically reliable indicators of damage and strength retention.

4. Fly ash makes the concrete more brittle. Consequently fly ash concrete performed better in impact than in flexure. This makes a case for flyash being used in columns and other compression members, while it should be avoided for flexural members such as slabs, decks, and pavements. Beams seem to belong in the grey area, especially since the current trend leans heavily towards prestressing.

5. AE is a viable tool to study the fracture mechanics phenomenon.

6. AE plots clearly demarcate the three fracture process regions.

7. Normal concrete has a 24% larger slow crack growth period as compared to flyash concrete.

8. AE measurements indicated initiation of unstable crack propagation at 95% of maximum load.

6.2 Recommendations for further research

Studies of this nature intrinsically demand larger specimen sets. Moreover, amplitude studies should be pursued vigorously, especially for fracture mechanics experiments. Unfortunately, equipment malfunctions stymied efforts to pursue this avenue as part of this study. The on-line computer should have a larger memory of at least 40 megabytes to enable amplitude data to be recorded for a reasonable length of time. The current available memory is only about 11 megabytes.

The common plot patterns in the three-point beam bending tests and bridge tests suggest that the slope of the AE curve is an important factor in damage analysis. This would become especially important in studying existing structures in service, as on-line monitoring can be done for only a finite period of time to analyze and determine if remedial actions are called for. Hence, this aspect should be studied in greater detail.

REFERENCES

1. Joffo, A., "The Physics of Crystals", p. 50, McGraw Hill, New York, 1928.

2. Forster, F., and Scheil, E., "Zeitschrift fur Metallkunde", Vol. 9, pp. 245-247, 1936.

3. Miner, M.A., Journal of Applied Mechanics, JAMCA, Vol. 12, pp. A159-A164, 1945.

4. Kaiser, J., "Untersuchungen Uber das Auftreten Gerauschen beim Zugversuch", Ph. D. thesis, Technische Hochschule, Munich, 1950.

5. Rusch, H., "Physikalische Fragen der Betonprufung", p.178, Cement and Concrete Association, London, 1960.

6. Whitehurst, E.A., "Evaluation of Concrete Properties from Sonic Tests", ACI and Iowa State University Press, 1967.

7. Pollock, A.A., "Non-Destructive Testing: Views, Reviews, and Previews", Oxford University Press, 1969.

8. Green, A.T., "Stress Wave Emissions and the Fracture of Prestressed Concrete Reactor Vessel Materials", II Interamerican Conference on Materials Technology, Mexico City, 1970.

9. Hutton, P.H., and Ord, R.N., "Research Techniques in Non-Destructive Testing", Academic Press Inc., 1970.

10. Pickett, A.G., Reinhart, E.R., and Ying, S.P., "Acoustic Emission from Irradiated Steels", 8th Symposium on Non-Destructive Evaluation in Aerospace, Weapons Systems, and Nuclear Applications, San Antonio, 1971.

11. Pollock, A.A., and Stephens, R.W.B., Waveforms and Frequency Spectra of Acoustic Emissions", The Journal of the Acoutical Society of America, Vol. 50, No. 3 (Part 2), 1971.

12. Hardy, H.R., "Applications of Acoustic Emission Techniques to Rock Mechanics Research", ASTM Special Technical Publications 505, Philadelphia, 1972.

13. Achenback, J.D., "Wave Propogation in Solids", North Holland Publishing Co. Ltd., London, 1973.

14. Corle, R.R., "The Use of Acoustic Emission to Improve Motor Case Structural Reliability", American Institute of Aeronautics and Astronautics and Society of Automotive Engineers, 9th Propulsion Conference, Las Vegas, 1973.

15. Dunegan H.L., and Harris, D.O., "Experimental Techniques in Fracture Mechanics", Iowa State University Press & Society for Experimental Stress Analysis, 1973.

16. Jax, P., and Eisenblaetter, J., "Acoustic Emission Measurements during Plastic Deformation of Metals", Battelle Information, Frankfurt, 1973.

17. Drouillard, T.F., Liptai R.G., and Tatro, C.A., "Industrial Use of Acoustic Emission for Non-Destructive Testing", Poc. Symposium on Monitoring Structural Integrity by Acoustic Emission, Ft. Lauderdale, 1974.

18. Dunegan, H.L., "Quantitative Capabilities of Acoustic Emission for Predicting Structural Failure", Proc. of Second Materials/Design Forum, Port St. Lucie, 1974.

19. Kelly, M.P., Harris, D.O., and Pollock, A.A., "Detection and Location of Flaw Growth in Metallic and Composite Structures", Proc. Symposium on Monitoring Structural Integrity by Acoustic Emission, Ft. Lauderdale, 1974.

20. Prine, D.W., and Clark, R.N., "Inspection of Nuclear Reactor Welding by Acoustic Emission", Final Report, Gen. American Transportation Corp., IL., 1974-75.

21. Koerner, R.M., Lord Jr., A.E., and McCabe, W.M., "AE Behavior of Granular Soils", ASCE, Geotechnical Division, July 1976.

22. Koerner, R.M., Lord Jr., A.E., and McCabe, W.M., "AE Behavior of Cohesive Soils", ASCE, Geotechnical Division, August 1977.

23. Hardy, H.R., and Leighton, F.W., Editors: Proc. 1st Conference on Acoustic Emission/Microseismic Activity in Geologic Structures and Materials", Trans Tech Publications, Clausthal, Germany, 1977.

24. Robinson, G.S., "Methods of Detecting the Formation and Propogation of Microcracks in Concrete", The Structure of Concrete and its Behavior under Load, Cement and Concrete Association, London, 1977.

25. Koerner, R.M., Lord Jr., A.E, and McCabe, W.M., "AE Monitoring of Soil Stability", ASCE, Geotechnical Division, May 1978.

26. Hartbower, C.E., "Detection and Determination of Flaw Size by Acoustic Emission", AGARD Non-Destructive Inspection Practices, Vol. 1.

27. Hawkins, N.M., Kobayashi, A.S., and Fourney, M.E., "A Feasibility Study of Detecting Reinforcing Bar Debonding by Acoustic Emission Techniques", SESA Spring Meeting and Exposition, San Francisco,1979.

28. Portland Cement Association, "Design and Control of Concrete Mixtures", p. 52, 12th Edition, 1979.

29. Pollock, A.A., "Acoustic Emission Amplitude Distribution", International Advances in Non-Destructive Testing, Vol. 7, 1980.

30. Drnevich, V.O., and Gray, R.A., Editors:"Acoustic emissions in Geotechnical Engineering Practice", American Society for Testing Materials, ST 750, pp. 283-289, Detroit 1981.

31. Koerner, R.M., McCabe, W.M., and Baldiviesco, L.F., "AE Monitoring of Seepage", ASCE, Geotechnical Division, April 1981.

32. Hutton, P.H., Skorpic, J.R., and Kurtz, R.J., "Acoustic Emission for Continuous Surveillance of Various Commercial Structures", Proc. International Conference on New Trends in Non-Destructive Testing, Brussels, 1982.

33. "New Procedures in Non-Destructive Testing", Proceedings of the U.S.-German Workshop, Fraunhofer Institut, Saarbrucken, Germany, 1982.

34. Obert, L., "The Microseismic Method: Discovery and Early History", Proc First Conference on Acoustic Emission/Microseismic Activity in Geologic Structures and Materials, Trans Tech Publications, Clausthal, Germany, 1982.

35. Possa, G., "Acoustic Emission: Application to Nuclear Components", Proc. Int. Conference in New Trends in Non-Destructive Testing, Brussels, 1982.

36. Tripalin, A.S., Kuzmin, G.A., Eletskii, S.A., Kolomnets, Y.V., and Shikhman, V.M., "The Measurement of AE Parameters during Hydraulic Loading of the Novovorenezh AES Reactor Vessel VVER-1000", Energomashinostr, No. 3, U.S.S.R., 1982.

37. Dunn, S.E., Marshall, R.M., Hartt, W.H., and Young, J.D., "Acoustic Detection of Corrosion Cracking in Reinforced Concrete", Florida Sea Grant Report, Part 1, 1983.

38. Dunn, S.E., Babakanian, R., Ward, A.M., and Hartt, W.H., "Acoustic Detection of corrosion Cracking in Reinforced Concrete", Florida SEa Grant Report, Part 3, 1983.

39. Babakanian, R., "AE Testing of Prestressed Concrete in an Accelerated State of Corrosion", M.S. Thesis, Supervised by Dunn, S.E., Florida Atlantic University, 1984.

40. Koerner, R.M., Lord Jr., A.E, and Deutsch, W.L., "Determination of Prestress in Granular Soils using AE", ASCE, Journal of Geotechnical Engineering, March 1984.

41. Moskal, F.G., and Fageol, J.D., "Acoustic Emission Signal Processing Analog Unit for for Locating Flaws in Large Tanks", Rockwell International Corporation, 1984.

42. Getting, I.C., Roecken, C., and Spetzler, H., "Improved Acoustic Emission Locations", Journal of Non-Destructive Evaluation, Vol. 5, 1986.

43. Reddy, D.V., Hartt, W.H., and Dunn, S.E., "Effect of Marine Exposure upon Service Life of Reinforced Concrete", Final Report, Sea Grant No. R/C-D-10, 1986.

44. Titus, R.N.K., "Serviceability of Reinforced Concrete Beams Subjected to Accelerated Corrosion", M.S. Thesis, Supervised by Reddy, D.V., Florida Atlantic University, 1986.

45. Desnoyers, Jean-Francois, "Impact Behavior of Concrete Beams with Corroding Reinforcing Steel", M.S. Thesis, Supervised by Reddy, D.V., Florida Atlantic University, 1987.

46. Halmshaw, R., "Non-Destructive Testing", Edward Arnold Publishers, 1987.

47. Titus, R.N.K., Reddy, D.V., Dunn, S.E., and Hartt, W.H., "Acoustic Emission Crack Monitoring of Reinforced Concrete Beams in an Accelerated State of Corrosion and Prediction of Remaining Life", Proc. 4th European Conference on NDT, London, 1987.

48. Arockiasamy, M., and Reddy, D.V., "Static and Fatigue Behavior of Longitudinal Joints in Multi-Box Beam Bridge Prestressed Concrete Bridges", Florida Department of Transportation Project, 1987-88.

49. Reddy, D.V., Hartt, W.H., and Arockiasamy, M., "Strength and Durability of Flyash Modified Concrete in Coastal Construction", Sea Grant Project # R/C-D-15, 1987-89.

50. American Concrete Institute, "ACI Manual of Concrete Practice", p. 222 R.3, Part 1, 1989.

51. Bennett, J.E., and Mitchell, T.A., "Depolarization Testing of Cathodically Protected Reinforcing Steel in Concrete", NACE Conference, Paper No. 373, New Orleans, 1989.

52. Chhuy, S., Cannard, G., Robert, J.L., and Rossi, P., "Experimental Investigations on the Damage of Portland Cement Concrete Made with Natural Aggregates", Materials and Structures, 1989.

53. Murti, Vasu, "Strength and Durability of Fly Ash Modified Concrete in Coastal Construction", M.S. Thesis, Supervised by Reddy, D.V., Florida Atlantic University, 1989.

54. Reddy, D.V., and Sailappan, R.N., "Acoustic Emission as a NDE Tool - Certain Laboratory and Field Investigations", ASME Winter Annual Conference, San Francisco, 1989.

55. Rossi, P., Robert, J.L., Gervais, J.P., and Bruhat, D., Identification of Physical Mechanics Underlying Acoustic Emissions During the Cracking of Concrete", Materials and Structures, 1989.

56. Izumi, M., Mihashi, H., and Nomura, N., "Acoustic Emission Technique to Evaluate Fracture Mechanics Parameters of Concrete", 1990.

57. Lee, S.K., "Durability and Fracture Toughness of Fly Ash Concrete in the Marine Environment", Supervised by Reddy, D.V., Florida Atlantic University, 1990.

58. Liu, X., and Kannatey-Asibu, Jr., E, "Classification of AE Signals from Monitoring Martensite Formation from Welding", Welding Research Supplement, 1990.

59. Miller, R.K., "Tank Bottom Leak Detection in Above Ground Storage Tanks by Using Acoustic Emission", American Society for Non-destructive Testing, Inc., 1990.